NASA CR 120848
BOEING D3-8684

ACOUSTIC GRAZING FLOW IMPEDANCE USING WAVEGUIDE PRINCIPLES

BY
D. L. Armstrong

DECEMBER 12, 1971

THE BOEING COMPANY
WICHITA DIVISION • WICHITA, KANSAS, 67210

PREPARED FOR

NATIONAL AERONAUTICS AND SPACE ADMINISTRATION

NASA-LEWIS RESEARCH CENTER
CONTRACT NAS 3-14321
H. BLOOMER, PROJECT MANAGER

IG720368A

NOTICE

This report was prepared as an account of Government-sponsored work. Neither the United States, nor the National Aeronautics and Space Administration (NASA), nor any person acting on behalf of NASA:

A.) Makes any warranty or representation, expressed or implied, with respect to the accuracy, completeness, or usefulness of the information contained in this report, or that the use of any information, apparatus, method, or process disclosed in this report may not infringe privately-owned rights; or

B.) Assumes any liabilities with respect to the use of, or for damages resulting from the use of, any information, apparatus, method or process disclosed in this report.

As used above, "person acting on behalf of NASA" includes any employee or contractor of NASA, or employee of such contractor, to the extent that such employee or contractor of NASA or employee of such contractor prepares, disseminates, or provides access to any information pursuant to his employment or contract with NASA, or his employment with such contractor.

Requests for copies of this report should be referred to

National Aeronautics and Space Administration
Scientific and Technical Information Facility
P.O. Box 33
College Park, Md. 20740

NASA CR 120848
BOEING D3-8684

TOPICAL REPORT

ACOUSTIC GRAZING FLOW IMPEDANCE USING WAVEGUIDE PRINCIPLES

by
D. L. Armstrong

THE BOEING COMPANY
3801 SOUTH OLIVER
WICHITA, KANSAS 67210

Prepared For
NATIONAL AERONAUTICS AND SPACE ADMINISTRATION
December 12, 1971

CONTRACT NASA 3-14321

NASA-LEWIS RESEARCH CENTER
CLEVELAND, OHIO
H. BLOOMER, PROJECT MANAGER
V/STOL AND NOISE DIVISION

FOREWORD

The work described herein was done by The Boeing Company, Wichita Division, under NASA contract NAS 3-14321 with Mr. H. Bloomer, V/STOL and Noise Division, NASA - Lewis Research Center, as Project Manager.

ABSTRACT

A grazing flow apparatus has been designed to measure the impedance of acoustic materials when installed in environments that subject the material to grazing airflow. The design of the apparatus and the data analysis technique is based on the solution of the convected wave equation in an infinite length waveguide.

TABLE OF CONTENTS

LIST OF FIGURES

LIST OF FIGURES (CONT'D)

NOMENCLATURE

c	Speed of sound, in./sec (cm/sec)
C_x, S_x	Cosine and sine coefficients of x-component of pressure
C_y, S_y	Cosine and sine coefficients of y-component of pressure
f	Frequency, hertz
$f_{c.o.}$	Cut-off frequency, hertz
h	Duct height, in. (cm)
i	$\sqrt{-1}$
k	Wave number, ω/c, in.$^{-1}$ (cm^{-1})
k_x, k_y, k_z	Acoustic propagation constants in coordinate directions, in.$^{-1}$ (cm^{-1})
M	Mach number
m	Hard wall mode number in x-direction
n	Hard wall mode number in y-direction
p	Acoustic pressure, dyne/cm^2
t	Time, sec.
U	Freestream airflow velocity, in./sec (cm/sec)
v	RMS particle velocity, cm/sec
x, y, z	Duct coordinates, in. (cm)
X, Y, Z, T	Pressure components depending on coordinates x, y, z, and time, t.
α	Attenuation rate, dB/in (dB/cm)
Γ	Impedance function ζ/η
ζ	Normalized acoustic impedance
η	Frequency parameter, 2 hf/c
Θ	Boundary layer momentum thickness, in. (cm)
λ	Wavelength relative to fluid flow, in. (cm)
λ_m	Measured wavelength in duct, in. (cm)
μ	Real part of transverse propagation constant k_x
ξ	Particle displacement, in. (cm)
ρ	Air density, g/cm^3

NOMENCLATURE

σ	Attenuation parameter, imaginary part of axial propagation constant k_z
τ	Phase velocity parameter, real part of axial propagation constant k_z
ϕ_R	Phase rate, deg/in. (deg/cm)
X	Imaginary part of transverse propagation constant k_x
ω	Angular frequency, $2\pi f$, rad/sec.

1.0 SUMMARY

A grazing flow apparatus was designed and fabricated for the purpose of measuring the resistive and reactive acoustic impedance of materials as installed in the presence of grazing airflow. The design of the apparatus and the analysis of the data were based on the theory of sound propagation in a rectangular waveguide. The results of the testing indicate that the change in resistive and reactive impedance, as a function of grazing flow, is greater for the perforated sheet materials than that for the polyimide materials tested. In a general sense, the model predictions compare favorably to the data considering that facing sheet blockage due to the adhesive fillet between the core and the facing sheet and that the boundary layer effects on the impedance measurements have not been incorporated in the model predictions or the data analysis.

Based on the results of testing to date, there are several areas that warrant improvement which would expand the capability of the grazing flow facility. Recommended improvements are listed below:

- Increasing the acoustic transmission efficiency of the waveguide
- Increasing the frequency range
- Changing the boundary layer profile
- Using two simultaneously traversing microphones and cross-correlation techniques to obtain data
- Increasing the sound pressure level input

2.0 INTRODUCTION

2.1 Background

Two different methods have previously been used to measure grazing flow impedance. References 1, 2, 3, and 4 employed the two pressure method and Reference 5 employed a standing wave tub : mounted in the side of a rectangular flow duct.

The two pressure method of determining the complex impedance is based on measuring the sound pressure difference and phase difference across the resonator aperture. Binek (in Reference 4) states that under grazing flow conditions no phase measurements were taken indicating instrumentation problems. As a result, he assumed the reactive impedance to be a linear function of frequency, which is zero at the resonant frequency, and computed the corresponding phase angles at the frequencies of interest. However, the other investigators (References 1, 2, and 3) make no mention of such phase problems but they do make extensive use of the resonant frequency properties of a Helmholtz resonator in determining resistance, as well as reactance. The resonant frequency can be determined by measuring minimum pressures exterior or maximum pressures interior to the resonator without making phase measurements. The phase measurement, thus, appears to be an inherent weakness in the two pressure method of determining grazing flow impedances.

Feder (Reference 5) measured grazing flow impedance with a standing wave tube mounted in a flow duct wall by subtracting out the measured radiation impedance without the sample installed. However, the radiation impedance of a perforated sheet sample (assuming no hole-to-hole interaction) is $\frac{S}{OA}$ times the radiation impedance of one hole where S is the cross sectional area of one hole and OA is the open area of the sample. This can differ significantly from the radiation impedance of the open ended standing wave tube. Also, the effect of grazing flow on the radiation impedance needs to be incorporated. Therefore, an inherent limitation in the measuring technique becomes apparent.

The waveguide method of measuring grazing flow impedance, as developed in this document, also has several limitations. However, the major limitation appears to be in the magnitude of the standing wave inside the test section at higher Mach numbers, as indicated in the data scatter. This can be overcome by a redesign of the acoustic components of the apparatus.

2.2 Objective

The objective of this research effort was to develop a grazing flow apparatus in which both the resistive and reactive acoustic impedances of a material can be determined in the presence of a grazing airflow. From this information, more realistic mathematical impedance models can be developed.

2.3 Technical Approach

The design of the apparatus and the analysis of the data are based on the requirement for the propagation of the fundamental mode in the test section, one wall of which can be lined with an acoustic panel. This design requirement automatically limits the frequency range for the impedance measurements to those frequencies below the first cutoff frequency of the waveguide. At higher frequencies, the higher modes adversely affect the measurement of the attenuation rate and phase rate in the waveguide.

3.0 MATHEMATICAL MODEL

The geometry of the mathematical model consists of a semi-infinite rectangular waveguide (duct), the coordinates of which are given in Figure 1. It is assumed that the airflow in the waveguide is inviscid, nonturbulent, and has a steady state uniform velocity U along the duct z axis. Assume also that the acoustic impedance of the unlined walls of the duct is infinite and that the x = h wall has an acoustic impedance that is normally reacting, that is, its impedance is independent of the angle of incidence of the acoustic waves. An acoustic plane wave source is placed at z = 0 and its propagation in the waveguide will be investigated as a function of frequency, Mach number, duct size, sound pressure level, and acoustic lining impedance.

The acoustic wave equation for this flow condition is

$$c^2 \nabla^2 p = \left(\frac{\partial}{\partial} + U \frac{\partial}{\partial z} \right)^2 p \tag{1}$$

where p is the acoustic pressure and c is the speed of sound relative to the fluid flow. The geometry of the problem permits the wave equation to be solved by a separation of variables assuming a simple harmonic solution

$$p = XYZT \tag{2}$$

where

$$X = C_x \cos k_x x + S_x \sin k_x x \tag{3}$$

$$Y = C_y \cos k_y y + S_y \sin k_y y \tag{4}$$

$$Z = e^{-ik_z z} \tag{5}$$

$$T = e^{i\omega t} \tag{6}$$

C_x, S_x, C_y, S_y are constants determined by the boundary conditions at the duct walls, k_x, k_y, k_z are acoustic propagation constants in the coordinate directions, and $\omega = 2\pi f$ the angular frequency. The propagation constant k_z determines the phase velocity and attenuation rate in the duct and can be expressed as a function of k_x and k_y by substituting the assumed solution into the wave equation

$$k_z = \frac{-Mk + \sqrt{k^2 - (1-M^2)(k_x^2 + k_y^2)}}{1-M^2} \tag{7}$$

where $M = \frac{U}{c}$ is the Mach number of the flow and $k = \omega/c$.

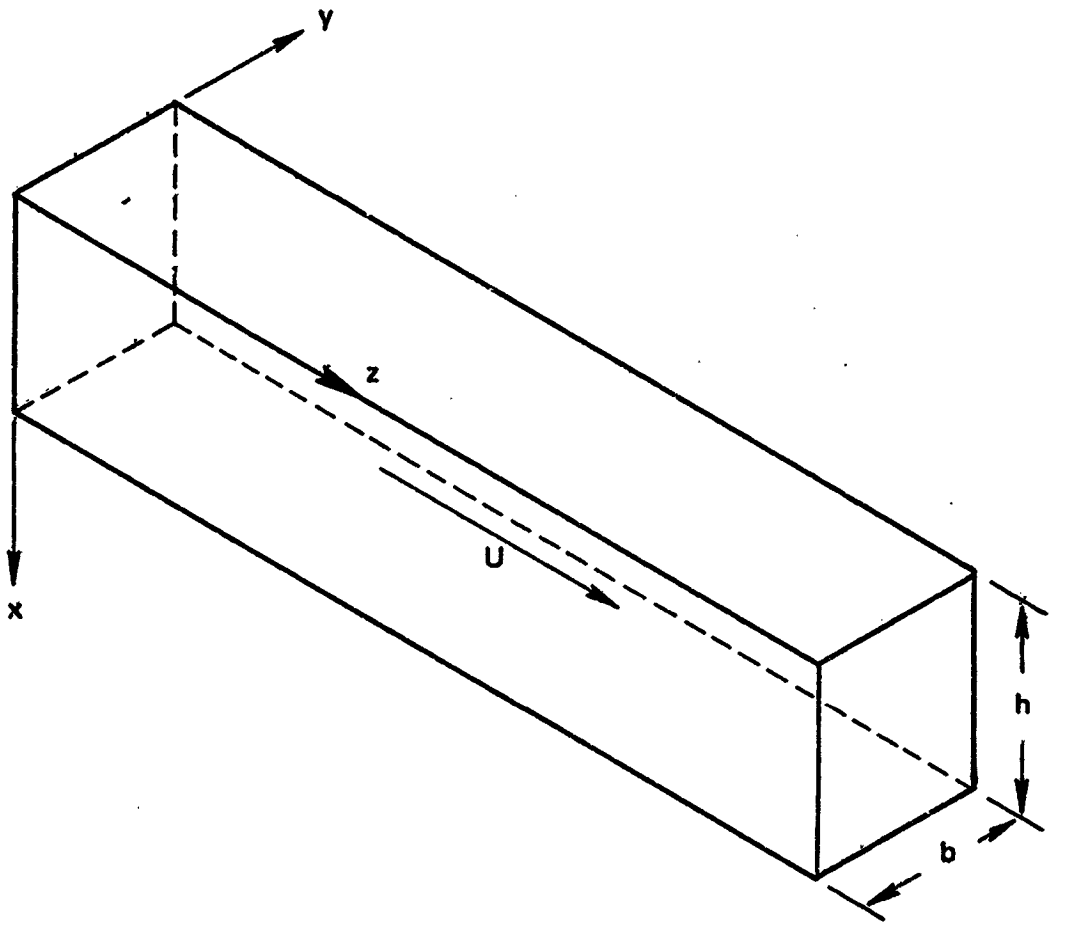

DUCT GEOMETRY
FIGURE 1

The boundary condition used to determine k_x and k_y is that of the continuity of particle displacement at the duct walls. Thus, at the wall let ξ_1 be the particle displacement in the fluid flow normal to the wall. The equation of motion is given by:

$$-\rho\left(\frac{\partial}{\partial t}+U\frac{\partial}{\partial z}\right)^2 \xi_1 = \text{grad } p \tag{8}$$

where ρ is the density of the fluid.

The hard wall boundary condition at $y = 0$, b and $x = 0$ is equivalent to the requirement that the gradient of the pressure vanish. Thus, S_x and S_y are zero and $k_y = \frac{n\pi}{b}$. In the present application, the frequency range usable is such that the $n = 1$ mode will be in cutoff. Therefore, the expression for k_z becomes

$$k_z = \frac{-Mk + \sqrt{k^2 - (1-M^2)\,k_x^2}}{1-M^2} \tag{9}$$

If the $x = h$ wall is lined with an acoustic impedance ζ, normalized by the characteristic acoustic impedance of the fluid ρc, then the relationship between pressure and particle velocity at the lined wall is

$$\rho c\zeta = \frac{p}{\frac{\partial \xi_2}{\partial t}} \tag{10}$$

where ξ_2 is the particle displacement in the lining material. Assuming simple harmonic motions

$$\rho c\zeta = \frac{p}{i\omega\xi_2}$$

or

$$\xi_2 = \frac{p}{i\omega\rho c\zeta} \tag{11}$$

The boundary condition is the equivalence of ξ_1 and ξ_2 at the soft wall. The equation of motion now becomes

$$-\rho\left(\frac{\partial}{\partial t}+U\frac{\partial}{\partial z}\right)^2 \frac{p}{i\omega\rho c\zeta} = \frac{\partial p}{\partial x}$$

or

$$-\rho\,(i\omega - iUk_z)^2 \frac{p}{i\omega\rho c\zeta} = \frac{\partial p}{\partial x}$$

or

$$\frac{ik}{\zeta}\left(1-M\frac{k_z}{k}\right)^2 p = -\frac{\partial p}{\partial x} \tag{12}$$

Using the assumed solution, this becomes

$$\frac{ik}{\zeta}\left(1-M\frac{k_z}{k}\right)^2 = k_x \tan(hk_x) \tag{13}$$

Since k_z is a complex quantity, it can be represented as

$$k_z = k(\tau - i\sigma) \tag{14}$$

The transverse propagation constant k_x is a complex quantity and is represented by

$$k_x = \frac{\pi}{h}(\mu + ix) \tag{16}$$

This representation is used so that the final results will be compatible with Cremer's (Reference 6) at $M \doteq 0$. Direct substitution and rearrangement yields

$$\frac{\zeta}{\eta} = (1 - M(\tau - i\sigma))^2 \frac{\operatorname{ctnh}(-i\pi(\mu + ix))}{\mu + ix} \tag{17}$$

where $\eta = \frac{2\pi f}{c}$ is the frequency parameter.

The quantities μ and X are computed from the measured propagation constant k_z by using a Newton-Raphson iteration technique on Equation 9 after the real (τ) and imaginary (σ) parts have been separated. Thus, all the parameters necessary to determine ζ in Equation 17 have been established.

4.0 METHOD OF SOLUTION APPLICATION

The upper limit of the usable frequency range is determined by the lowest cutoff frequency of the waveguide. This cut off frequency depends on the Mach number and duct size according to Equation 7 at the frequency at which the radical vanishes. For a square duct with hard walls $k_x = \frac{m\pi}{h}$, $k_y = \frac{n\pi}{h}$ and the cutoff frequency is

$$f_{c.o.} = \frac{c}{4}\sqrt{(1-M^2)(m^2+n^2)} \tag{18}$$

for the 2 inch duct height of the test section. Figure 2 shows the cutoff frequency for the first five modes. The usable frequency range is determined by the (1,0) or (0,1) mode curve.

The impedance of the waveguide wall, as sensed by the wave traveling down the duct, is given by Equation 17. The quantities measured in the duct are the real and imaginary parts of the axial propagation constant k_z. From Equation (5), the component of the pressure variation down the waveguide is

$$Z = e^{-ik_z z}$$

or

$$Z = e^{-ik(\tau - i\sigma)z} \tag{19}$$

The phase of the pressure in the duct repeats every 2π radians for one wavelength in the duct λ_m. Thus

$$k\tau = \frac{2\pi}{\lambda m}$$

or

$$\tau = \frac{\lambda}{\lambda m} \tag{20}$$

The attenuation in the duct per unit length is $e^{-k\sigma}$ or in terms of dB/in.

$$\text{dB/in.} = 8.68\, k\sigma \tag{21}$$

Therefore, by measuring the wavelength and the attenuation rate in the duct, Equations 20 and 21 determine all the required parameters since μ and X in Equation 17 are determined by σ and τ from Equation 9. The explicit expressions are as follows:

$$\tau = \frac{-M}{1-M^2} + \frac{1}{\sqrt{2(1-M^2)}}\left(\left(\left(\frac{1}{1-M^2} - \left(\frac{\mu}{\eta}\right)^2 + \left(\frac{x}{\eta}\right)^2\right)^2 + 4\left(\frac{\mu}{\eta}\right)^2\left(\frac{x}{\eta}\right)^2\right)^{1/2} + \left(\frac{1}{1-M^2} - \left(\frac{\mu}{\eta}\right)^2 + \left(\frac{x}{\eta}\right)^2\right)\right)^{1/2} \tag{22}$$

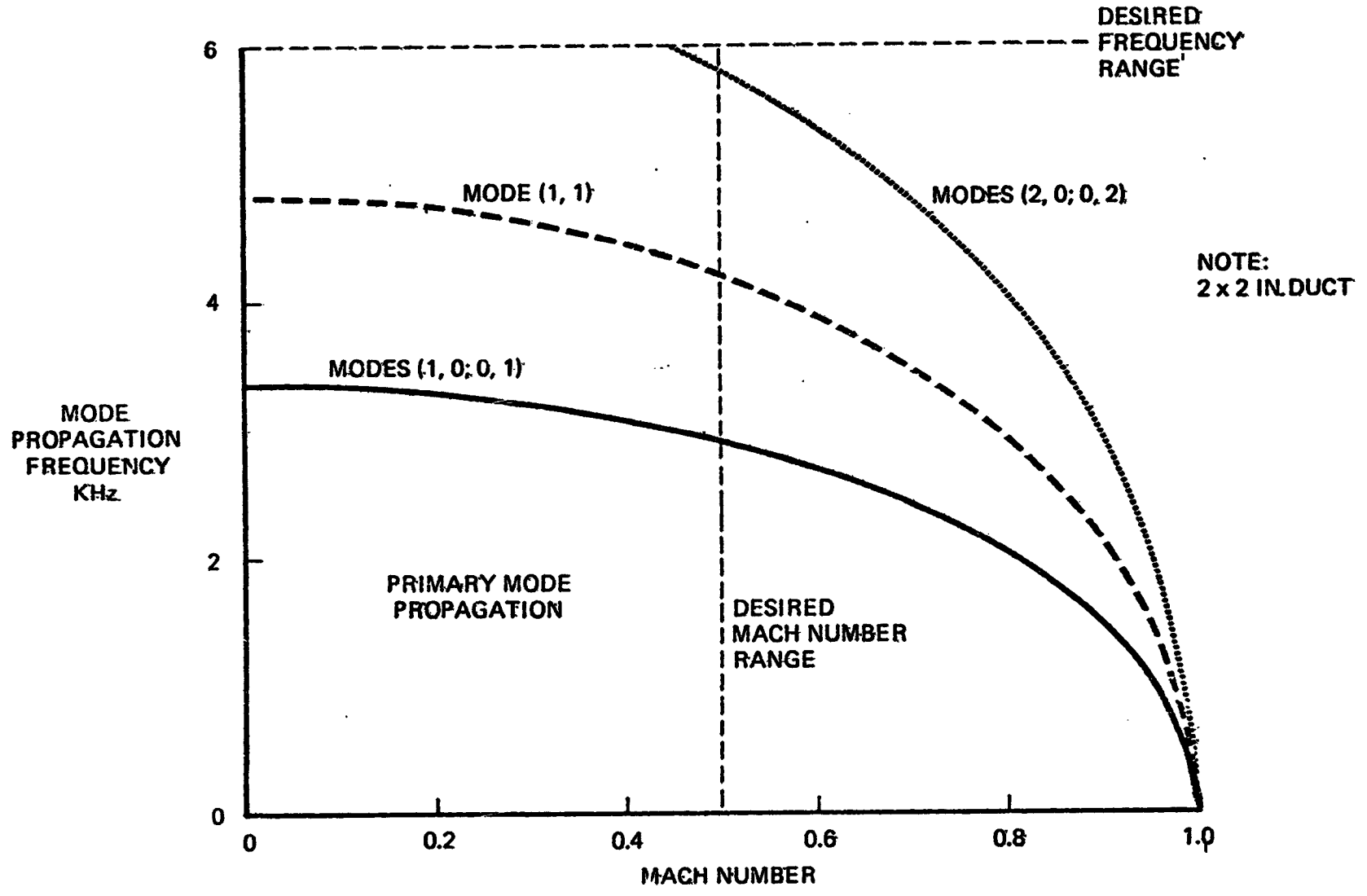

MODE PROPAGATION CHARACTERISTICS OF GRAZING FLOW TEST SECTION
FIGURE 2

$$\sigma = \frac{1}{\sqrt{1-M^2}}\left(\left(\frac{1}{1-M^2} - \left(\frac{\mu}{\eta}\right)^2 + \left(\frac{x}{\eta}\right)^2\right)^2 + 4\left(\frac{\mu}{\eta}\right)^2\left(\frac{x}{\eta}\right)^2\right)^{1/2} - \left(\frac{1}{1-M^2} - \left(\frac{\mu}{\eta}\right)^2 + \left(\frac{x}{\eta}\right)^2\right)^{1/2} \quad (23)$$

These equations can be solved for $\frac{\mu}{\eta}$ and $\frac{x}{\eta}$ and the results used in Equation 17 to compute the wall impedance.

The impedance data is plotted as a function of the discrete frequency sound pressure level (SPL) at the soft wall. This SPL is computed from the measured SPL on the opposite hard wall at the axial midpoint of the half wavelength section of data analyzed.

The RMS sound pressure at any location across the duct is given as:

$$p_x = p_0 \left(\cos^2(\pi\mu x/h) + \sinh^2(\pi x x/h)\right)^{1/2} \quad (24)$$

from which the RMS SPL at x = 2 inch is computed.

If the corresponding RMS particle velocities are desired, they can be computed from the following expression:

$$v = \frac{p_2}{|\zeta| \rho c} \quad (25)$$

5.0 GRAZING FLOW IMPEDANCE APPARATUS

The grazing flow impedance apparatus consists of an air plenum, a sound source, test section, and aerodynamic diffuser with an anechoic termination as shown in Figure 3.

The air plenum consists of a 36-inch diameter cylinder lined with acoustic insulation to minimize airflow noise, an electropneumatic sound generator and exponential horn that provides a uniform discrete frequency sound wave into the test section.

A detailed view of the test section is shown in Figure 4 and consists of a 2 x 2 inch cross section, the top wall of which accommodates a 16 inch test panel. Two microphones are mounted opposite the test panel, one of which can traverse the length of the test section. The stationary microphone located opposite the leading edge of the test panel is the reference microphone. The traversing microphone is initially aligned with the reference and during its traverse, in one-eighth inch increments, measures the relative amplitude and phase as a function of duct location. This information is recorded on a X - y - Y' plotter for on-line analysis and also punched on cards for digital computer processing.

The exponential horn attached to the downstream end of the test section serves as an aerodynamic diffuser and acoustic transformer. The flare cutoff frequency of the horn is 100 Hz and, therefore, has acceptable transmission properties in the 1000 – 3000 Hz frequency range that the impedance measurements are made. However, an aerodynamic analysis indicated that the flow will separate between 2 and 6 inches from the throat of the horn for a .2 to .5 Mach number range, thus, causing flow separation noise and mismatch in acoustic impedance resulting in reflected waves. The significance of these reflected waves depends upon both the Mach number and liner attenuation efficiency. Their effect on the measured data is quantitatively considered in Section 8.0

A portable anechoic chamber serves as an acoustic termination for the apparatus and provides an effective nonreflective termination in the test frequency range.

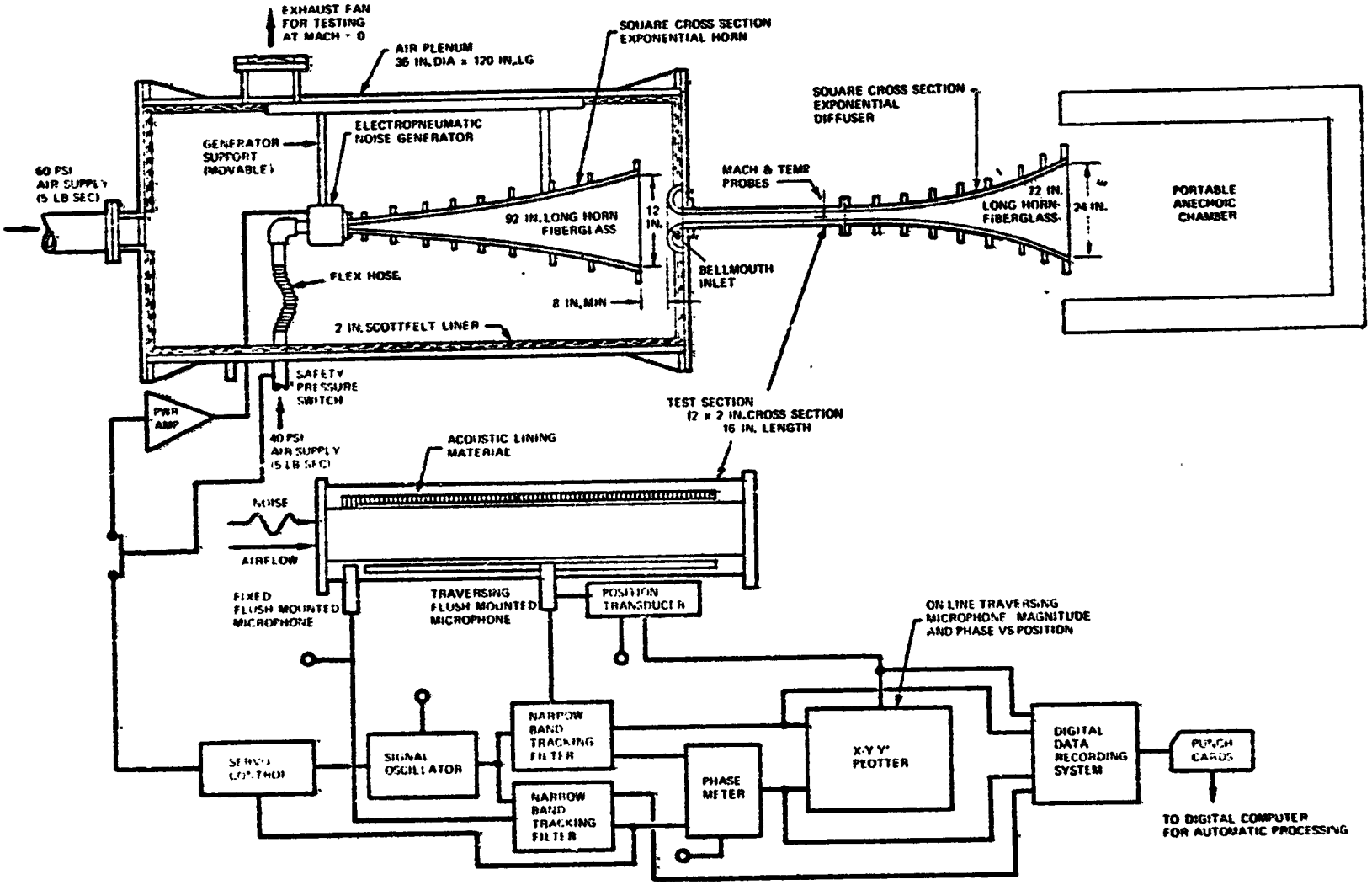

GRAZING FLOW APPARATUS INSTRUMENTATION
FIGURE 3

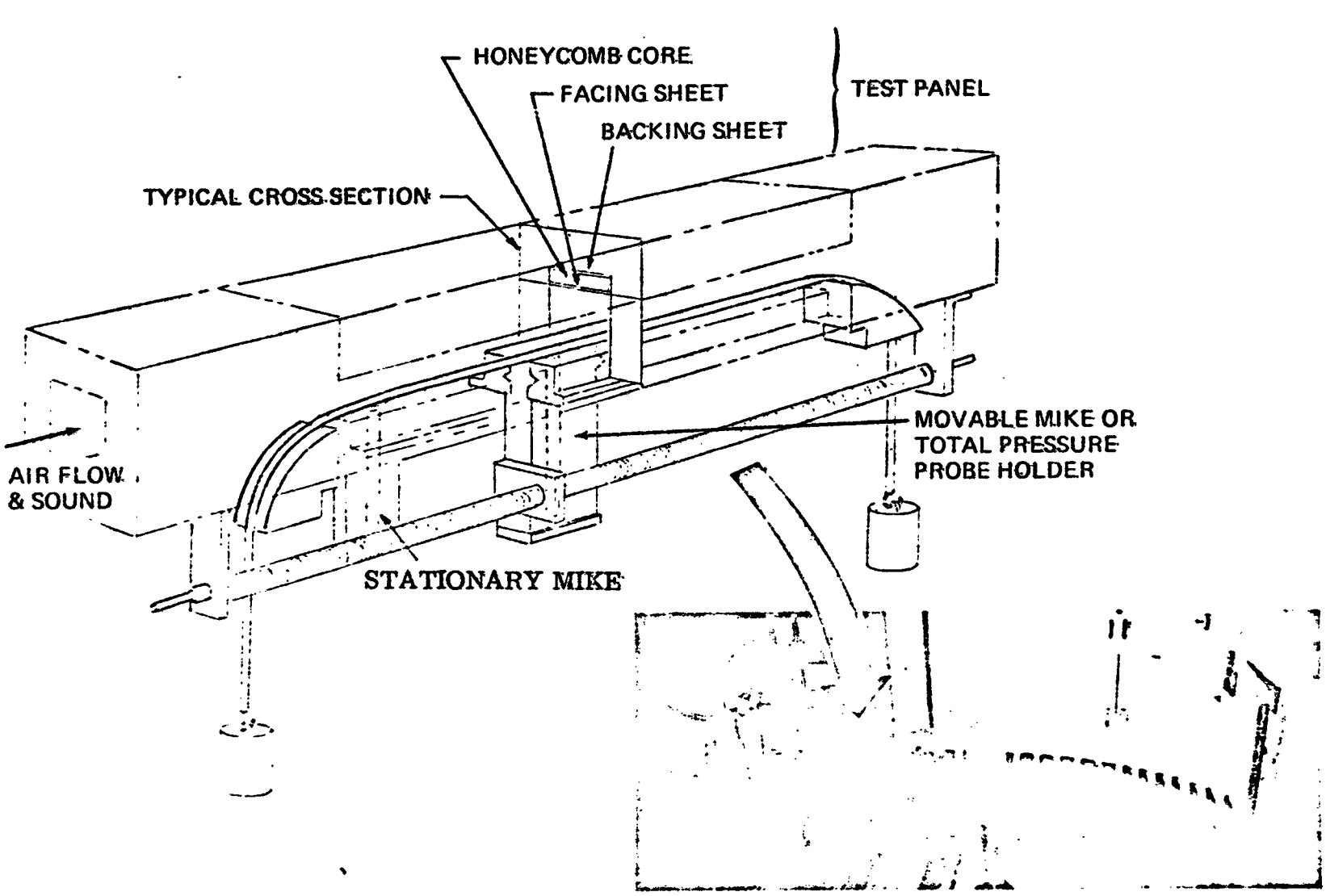

GRAZING FLOW IMPEDANCE TEST SECTION
FIGURE 4

6.0 BOUNDARY LAYER VELOCITY PROFILES

Typical boundary layer velocity profiles are given in Figures 5 and 6 for Mach numbers of .3 and .5 for two duct locations, at the leading edge of the panel and at 14 in. downstream. The momentum thickness Θ is indicated. These velocity profiles are indicative of all panels tested, both perforated sheet and polyimide.

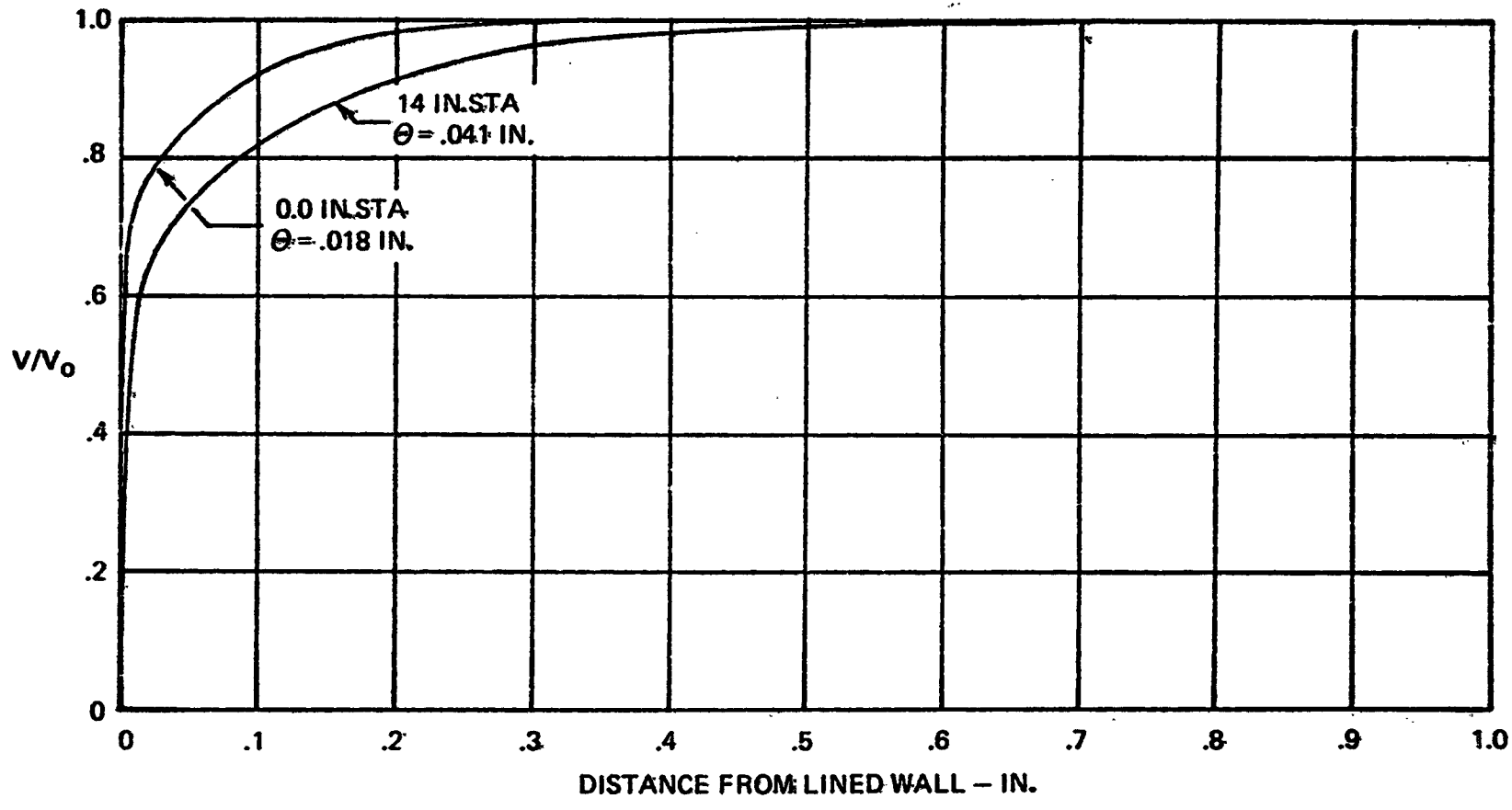

BOUNDARY LAYER VELOCITY PROFILES – M = 0.3
FIGURE 5

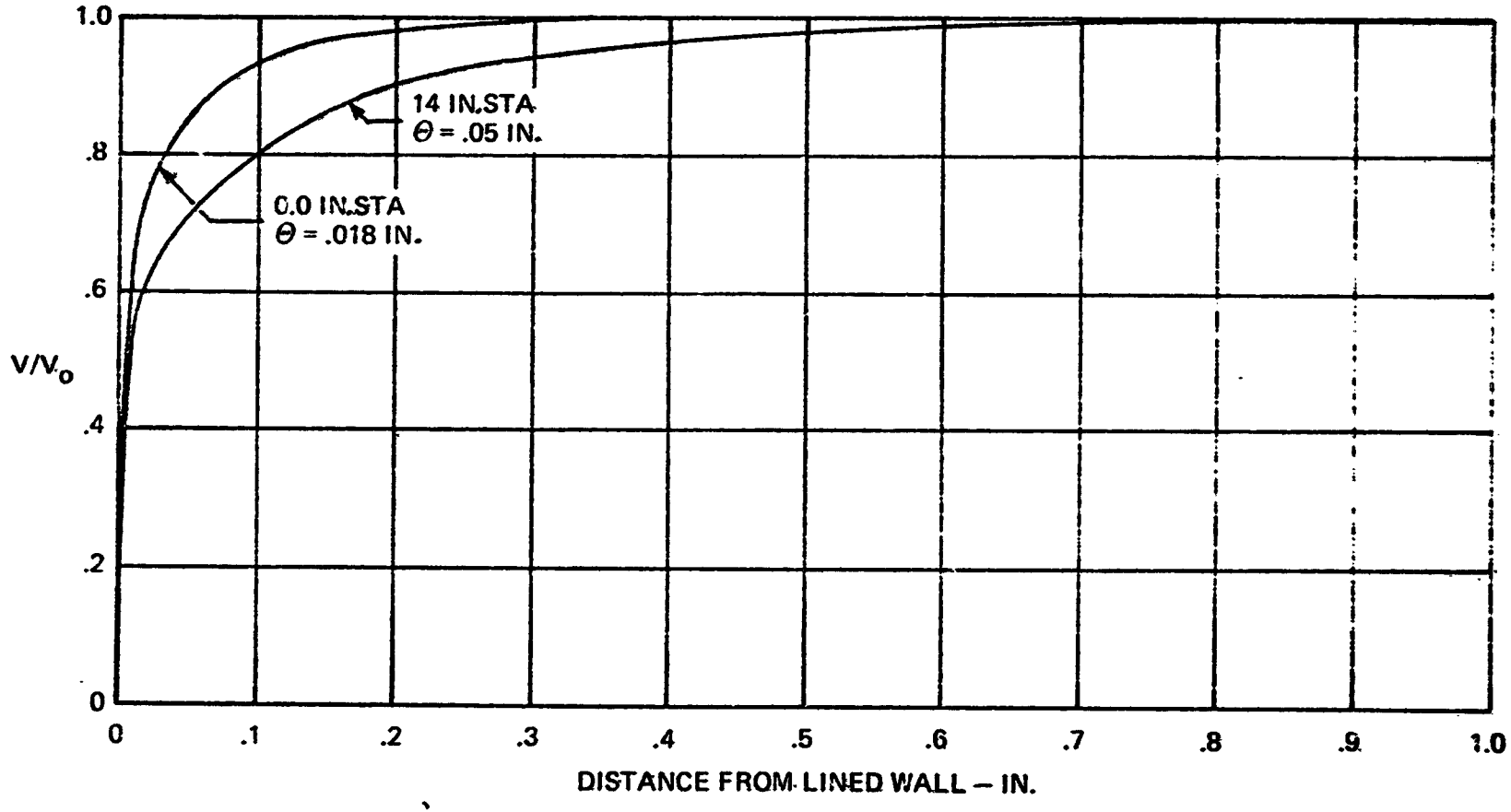

BOUNDARY LAYER VELOCITY PROFILES – M - 0.5
FIGURE 6

7.0 IMPEDANCE MODELS FOR PERFORATED SHEET AND POLYIMIDE

7.1 Perforated Sheet Impedance Model

The perforated sheet impedance model was developed by combining theoretical expressions for orifice impedance with measured flow resistance and standing wave tube impedance data. The effect of grazing flow on the impedance was derived from measurements of the DC flow resistance of the material subjected to the grazing flow by a method similar to that reported in Reference 5. The following equations represent the normalized resistance ($R/\rho c$) and reactance ($X/\rho c$) for the perforated sheet acoustic panel.

$$\frac{R}{\rho_c} = RVDC + ZJ + \frac{\pi}{2\sqrt{2}} \frac{VE}{c} \exp(SN)$$

$$\frac{X}{\rho_c} = \frac{.000469f}{OA\sqrt{T_T/519}} \left(t + .85d\,(1 - .7\sqrt{OA}) - .000012\,\frac{V}{OA}\right) - \cot(kL)$$

where

c	=	Speed of sound (cm/sec)
d	=	Perforate hole diameter (in)
f	=	Frequency (Hz)
k	=	$2\pi f/c$ (cm^{-1})
L	=	Panel core depth (cm)
M	=	Mach number
OA	=	Perforate open area
P_S	=	Static pressure (PSI)
t	=	Thickness of perforated sheet (in)
T_T	=	Total air temperature (^oR)
V	=	RMS total particle velocity (cm/sec)
V_{SPL}	=	RMS spectrum particle velocity (cm/sec)
V_{GF}	=	RMS grazing flow particle velocity (cm/sec)
Θ	=	Boundary layer momentum thickness (in)

and $$RVDC = \frac{.077t}{\frac{P_S}{14.7}\,OA}\,\frac{(T_T/519)^2}{\frac{T_T}{519} + .416}$$

$$ZJ = \frac{.0000383\,(T_T/519)^{.75}\sqrt{f}\,\left(\frac{t}{d} + 1 - OA\right)}{OA\sqrt{\frac{P_S}{14.7}\left(\frac{T_T}{519} + .416\right)}}$$

$$E = 1.0251\left(\frac{1}{(OA)^2} - 1\right)\left(\frac{1}{(OA)^{.1}}\right)\exp(-.5072t/d)$$

$$SN = -1.8\left(2.54\,df\,(OA)/V\right)^2$$

The RMS total particle velocity is obtained by

$$V = \sqrt{V_{SPL}^2 + V_{GF}^2}$$

Where $$V_{GF} = \frac{.25\,(XKK)\,cM^2}{\frac{RVDC}{2} + \sqrt{\left(\frac{RVDC}{2}\right)^2 + \frac{XKK}{2}\,E\,M^2}}$$

and $$XKK = \begin{cases} 0 & \text{if } \Theta = 0 \\ .05 + .11\,d/\Theta & \text{if } \Theta \neq 0 \end{cases}$$

7.2 Polyimide Impedance Model

The polyimide impedance model was developed empirically from DC flow resistance and standing wave impedance tube data. The grazing flow contribution was determined as that for the perforated sheet model. The following equations represent the normalized resistance ($R/\rho c$) and reactance ($X/\rho c$) for the polyimide acoustic panel.

$$\frac{R}{\rho c} = (RVDC + .305\,AN^2 f + 2.86\,\rho N^2 V)/\rho c$$

$$\frac{X}{\rho c} = (.549\,\rho N^{1.5} f - (5.12)\,10^{-5}\,\rho N^3 fV)/\rho c - \cot(kL)$$

Where $$A = (1.115)\,10^{-5}\,\frac{T_S^{1.5}}{T_S + 216}$$

$$RVDC = 4640\,AN^{1.333}$$

N = Number of plies

T_S = Static temperature (^oR)

The RMS total particle velocity is obtained by

$$V = \sqrt{V_{SPL}^2 + V_{GF}^2}$$

With

$$V_{GF} = \frac{.05\ cM^2}{\frac{RVDC}{\rho c} + \sqrt{\left(\frac{RVDC}{\rho c}\right)^2 + .71\ N^2\ M^2}}$$

8.0 DATA SUMMARY

Typical grazing flow impedance data for 2.7% open area (OA) perforated sheet will be discussed. Figure 7 shows the liner tuning characteristics as a function of Mach number for a constant 140 dB SPL input. As Mach number increases, the frequency of peak attenuation increases and the attenuation decreases indicating a decreasing reactive and increasing resistive impedance. Figure 8 shows the attenuation rates as a function of duct location for the peak frequency of attenuation. For a given Mach number, the attenuation rate can be determined for a certain duct location or it can be determined over a certain duct section. The data points are least square fitted by a straight line whose slope determines the attenuation rate. This attenuation rate is ascribed to the SPL at the section midpoint. The imaginary part of the axial propagation constant is defined by the attenuation rate according to Equation 21. Figure 9 shows the data for determining the wavelength in the duct as a function of Mach number. A relative phase change of 180^{o} indicates a half wavelength change. For a given Mach number, the phase rate can be determined for a certain duct location, or it can be determined over a certain duct section such as a 180^{o} phase change section (half wavelength). The data points are least square fitted by a straight line, which, when extended over 180^{o}, determines the half wavelength in the duct. The ratio of the wavelength relative to the fluid flow to the measured wavelength in the duct is the real part of the axial propagation constant.

This is a general representation of raw data as obtained from the grazing flow apparatus and is characteristics of all samples tested. As explained in Section 4.0, the data for each sample corresponding to Figures 8 and 9 are punched on cards for data processing. This raw data will not be presented due to its bulk. The processed raw data is presented in the Appendix in the form of test panel installed impedance, resistive and reactive. Table I lists the physical properties of the panels tested. Table II gives the flow resistance characteristics of the sample facing sheets in terms of zero particle velocity intercept and slope.

A summary of the data in the Appendix is given in Figures 10 through 13 for 0, .3, and .5 Mach numbers. The resistive and reactive impedances are plotted as a function of either percent open area (Figure 10) or number of plies (Figures 11, 12, and 13). A comparison of Figures 10 through 13 indicate that the grazing flow contribution to perforated sheet is greater than that for polyimide. This data represents the grazing flow contribution to the impedance at low input SPL particle velocities where the grazing flow particle velocity is dominant. The RMS particle velocity due to grazing flow cannot be determined from the data since sufficiently high input SPL's could not be produced to induce a particle velocity that dominates that produced by the grazing flow. If this could be done, a transition would appear in the data from constant resistance to a resistance dependent on the input SPL induced particle velocity, and this transition would define the grazing flow particle velocity.

The summary chart for the perforated sheet panels is given in Figure 10. The characteristic increase in resistance and decrease in reactance with increasing Mach number is indicated for all the samples tested.

Three different sets of polyimide panels were tested. The first set (Sample Nos. 6 through 9) were fabricated from layers of glass fiber cloth impregnated with polyimide resin. The layers were oriented at 0^{o}, 22.5^{o}, 45^{o}, 67.5^{o}, etc. These panels were

post-cured, that is, they were heat treated in air for an extra period of time at a higher temperature than the standard precured panels.

The second set (Sample Nos. 10, 12, 14, and 16) and the third set (Sample Nos. 11, 13, 15, and 17) differ in construction only in their core depths, 0.86 in. and 1.4 in., respectively. These panels are of the standard precured type with a weave orientation of 0^{o}, 15^{o} right, 0^{o} and 15^{o} left, etc.

The summary charts for the polyimide panels are given in Figures 11, 12, and 13, respectively, for the three sets of panels defined above. The unusual behavior of the 16 ply panel, as shown in Figure 11, was possibly due to air leakage caused by panel warpage that was not removed when installed in the grazing flow apparatus. However, the 4, 8, and 12 ply panels exhibit resistance values that are linear as a function of number of plies. The reactances are stronger functions of frequency than the resistances and, hence, show a greater variability since the reactances are plotted for different frequencies.

Figures 12 and 13 give the summary charts for the precured polyimide panels with core depths of 0.86 in. and 1.4 in., respectively. By comparing the two sets of curves, it will be seen that the resistive characteristics are again generally linear as to the number of plies. However, the slopes of the resistance curves are different for the precured and post-cured panels.

It should be mentioned that the blockage due to the adhesive fillet between the core and facing sheet affects the impedance properties of the polyimide panels. This blockage is very likely to vary from panel to panel, resulting in a certain amount of variability of measured impedance and, thus, affecting the general linear trends of the data as a function of the number of plies.

In the Data Appendix the first and second half wavelength duct section data are plotted as open and solid symbols. At zero Mach number, the two half wavelength sections exhibit data that have the same trends as a function of SPL. At the higher Mach numbers, the second section resistance data generally indicate the higher value. This could be indicative of the dependence of the panel impedance on the boundary layer profile that varies with duct length. At this time, panel impedance correlation with boundary layer properties is not possible.

The impedance model predictions are plotted as solid lines for 1 KHz and dotted lines for 2 KHz. For example, sample 1 at zero Mach number indicates that the predicted resistive impedance values are lower than the measured values at low SPL's but show better agreement above 130 dB's. The abscissa represents the SPL of the sinusoidal signal at the panel surface and not the total RMS SPL of the entire spectrum. Thus, at low input sinusoidal levels, the background noise spectrum induces an RMS particle velocity that controls the resistive impedance. The reactive impedance appears to be less affected by the background noise. This background noise could have been included in the impedance computations if it had been known as a function of panel location. Upon comparing the other predictions and data, it becomes apparent that generally the zero Mach comparisons are better than those at .3 or .5 Mach number. This is understandable

since the data includes the boundary layer effect and the impedance model does not. The momentum thickness used for .3 and .5 Mach numbers were .028 and .034 in., respectively.

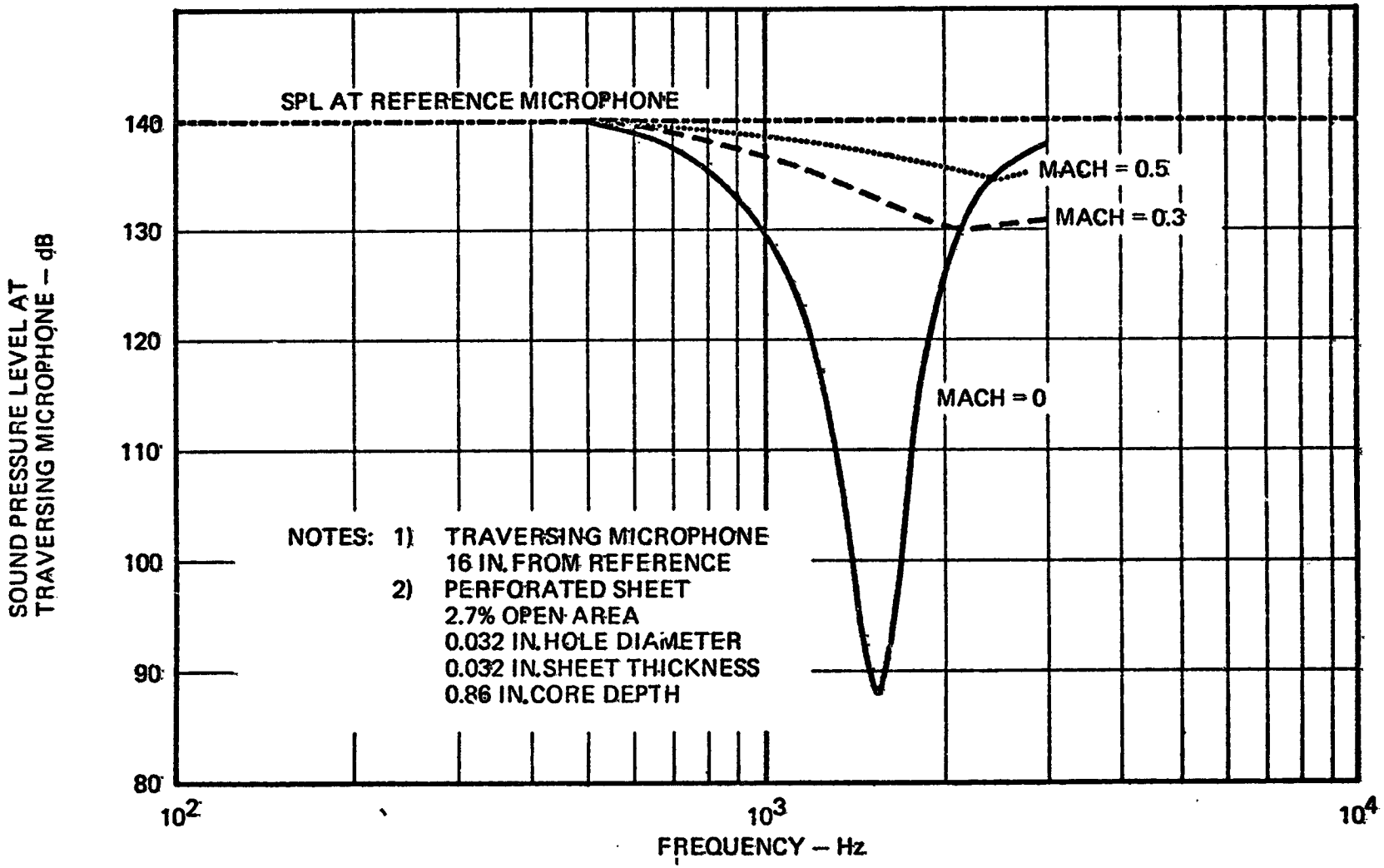

GRAZING FLOW IMPEDANCE TEST RESULTS – TUNING CHARACTERISTICS
FIGURE 7

NOTES: 1) FREQUENCIES ARE FOR PEAK ATTENUATION AT SPECIFIED MACH NUMBER
2) PERFORATED SHEET
2.7% OPEN AREA
0.032 IN. HOLE DIAMETER
0.032 IN. SHEET THICKNESS
0.86 IN. CORE DEPTH

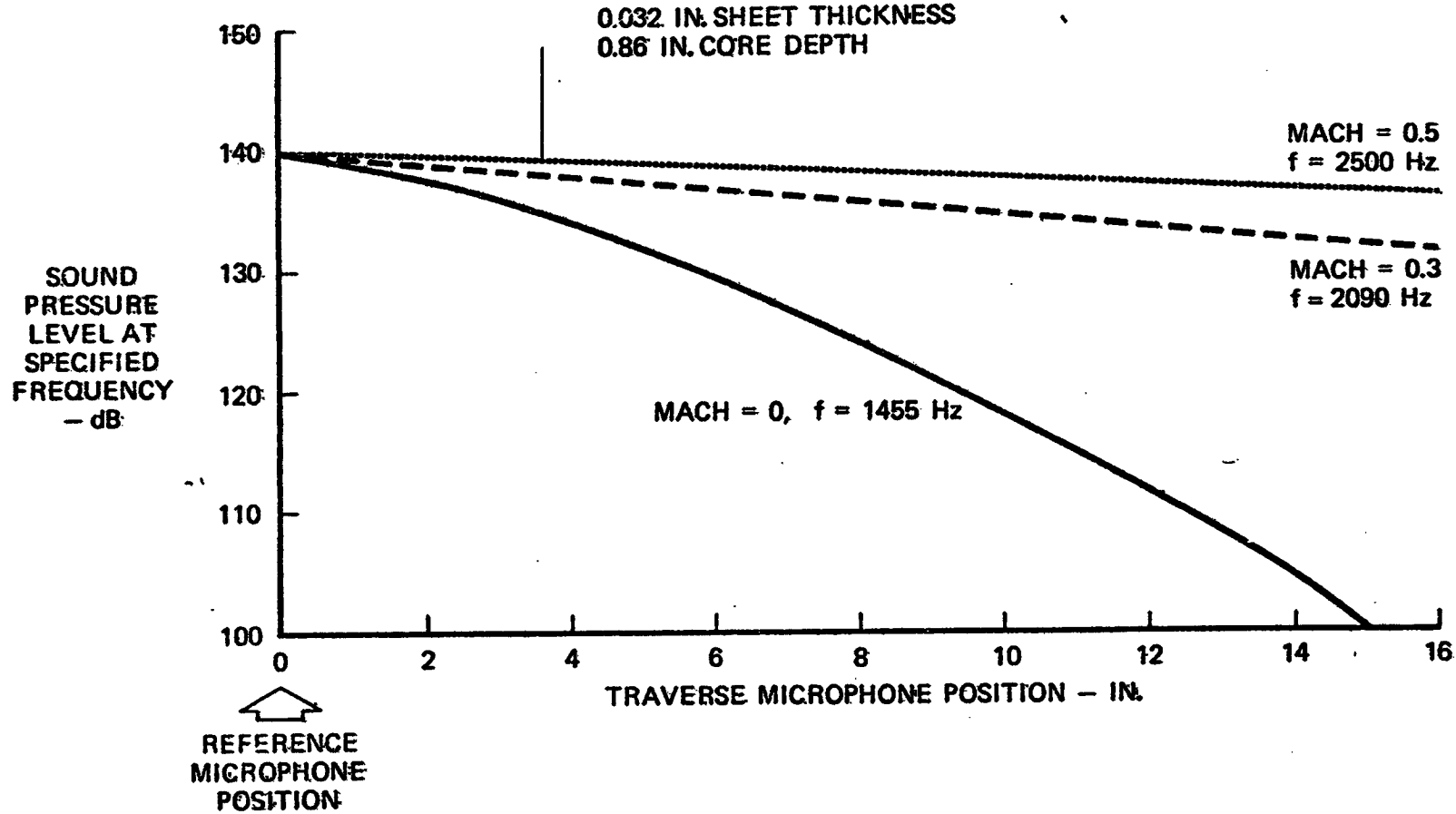

GRAZING FLOW IMPEDANCE RESULTS – ATTENUATION RATES
FIGURE 8

NOTES: 1) FREQUENCY = 2000 Hz
2) PERFORATED SHEET
2.7% OPEN AREA
0.032 IN. HOLE DIAMETER
0.032 IN. SHEET THICKNESS
0.86 IN. CORE DEPTH

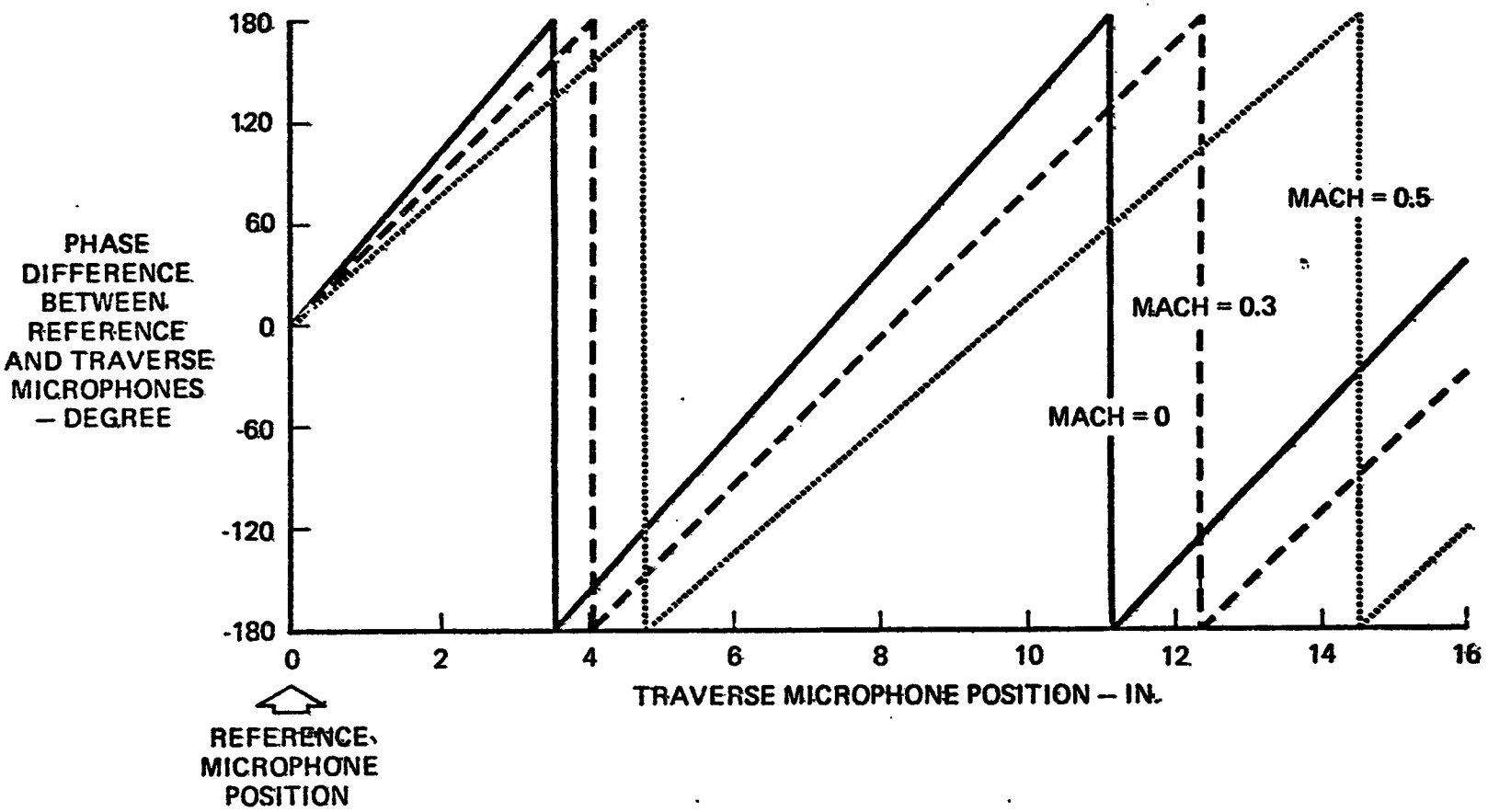

GRAZING FLOW IMPEDANCE TEST RESULTS – RELATIVE PHASE
FIGURE 9

TABLE I

TEST PANEL SPECIMEN DESCRIPTION

PERFORATED PLATE

Sample No.	Percent Open Area	Hole Diameter (In.)	Thickness (In.)	Core Depth (In.)
1	2.7	.032	.032	.86
2	4.4	.059	.030	.86
3	6.1	.039	.032	.86
4	10.4	.038	.032	.86
5	9.9	.1	.030	.86

POLYIMIDE

Sample No.	Plies	Core Depth (In.)
6	4	.86
7	8	.86
8	12	.86
9	16	.86
10	6	.86
11	6	1.4
12	9	.86
13	9	1.4
14	12	.86
15	12	1.4
16	15	.86
17	15	1.4

TABLE II

FACING SHEET FLOW RESISTANCES

Sample No.	Zero Velocity Intercept (Rayls)	Slope (Rayl . sec/cm)
1	2.75	1.55
2	1.58	.71
3	1.22	.30
4	.71	.10
5	.7	.14
6	6.	.135
7	12.5	.525
8	25.	1.15
9	34.1	2.09
10 - 11	9.3	.293
12 - 13	15.7	.663
14 - 15	30.	1.15
16 - 17	40.	1.77

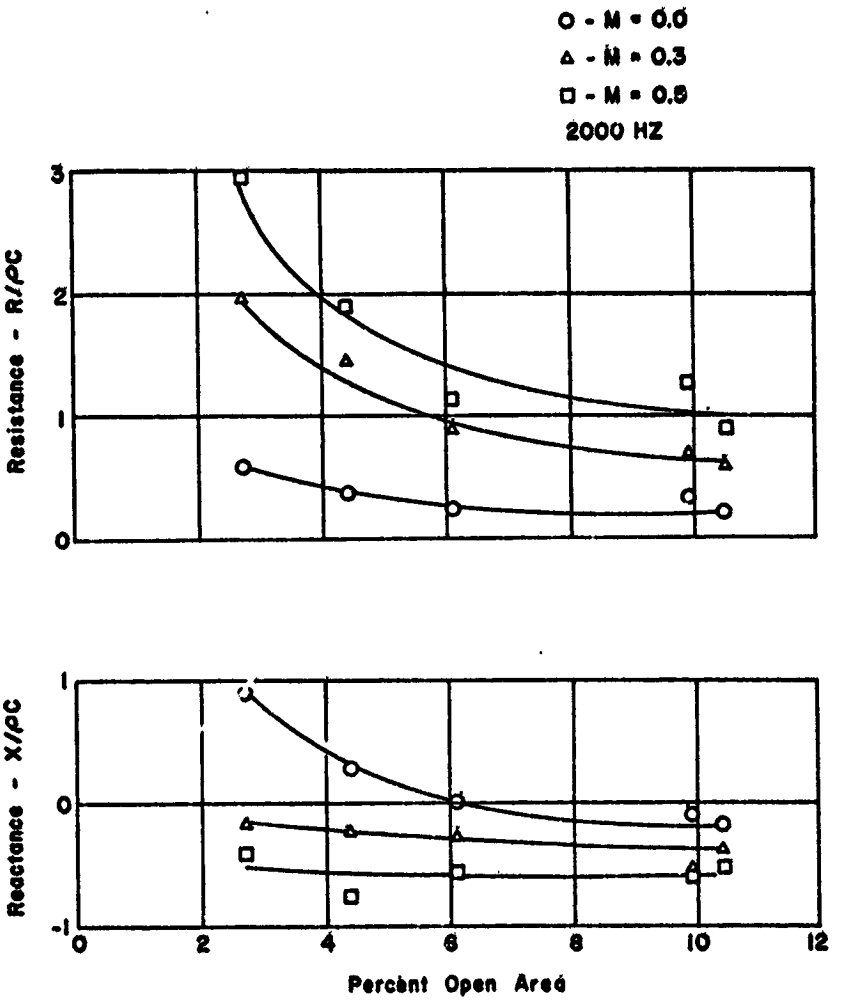

GRAZING FLOW RESISTANCE AND REACTANCE TRENDS
FOR PERFORATED SHEET SAMPLES
FIGURE 10

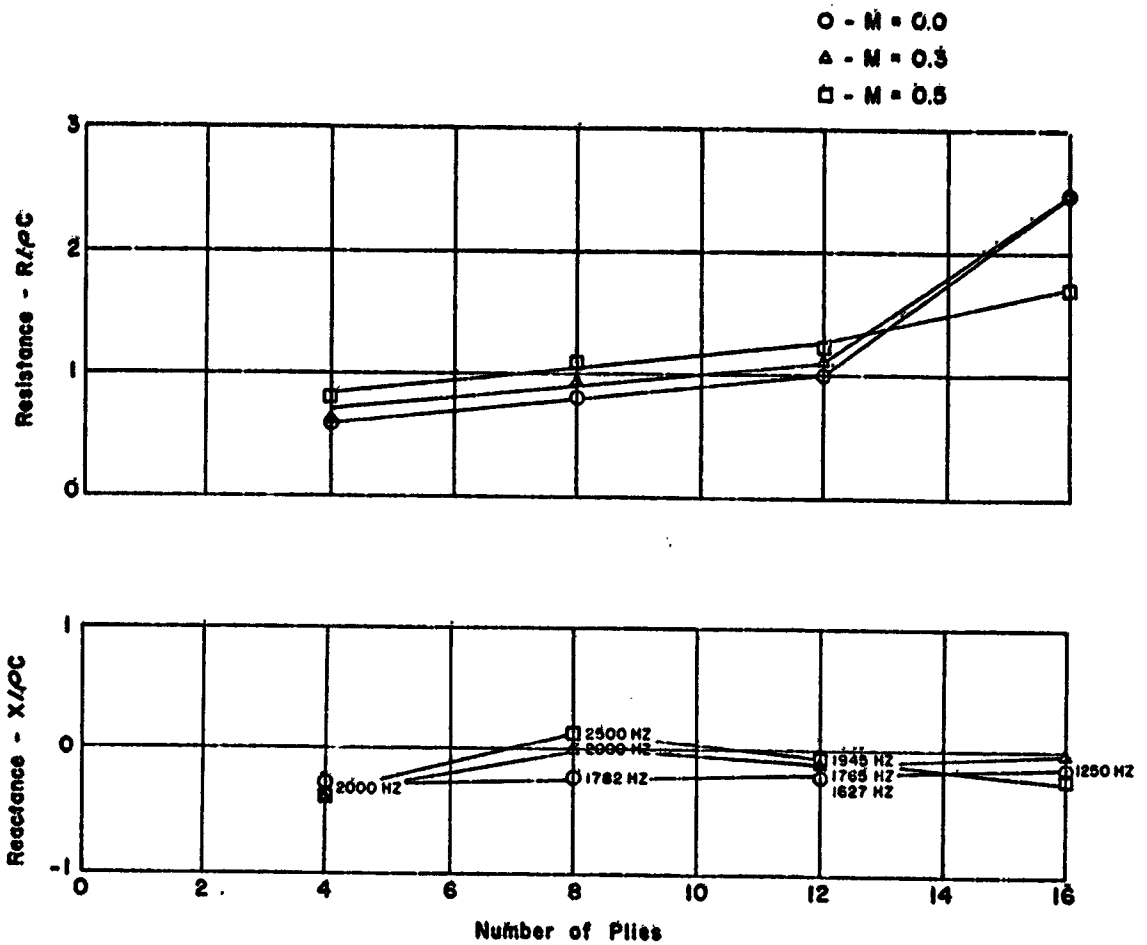

GRAZING FLOW RESISTANCE AND REACTANCE TRENDS FOR POSTCURED POLYIMIDE SAMPLES (0.86 IN. CORE DEPTH)
FIGURE 11

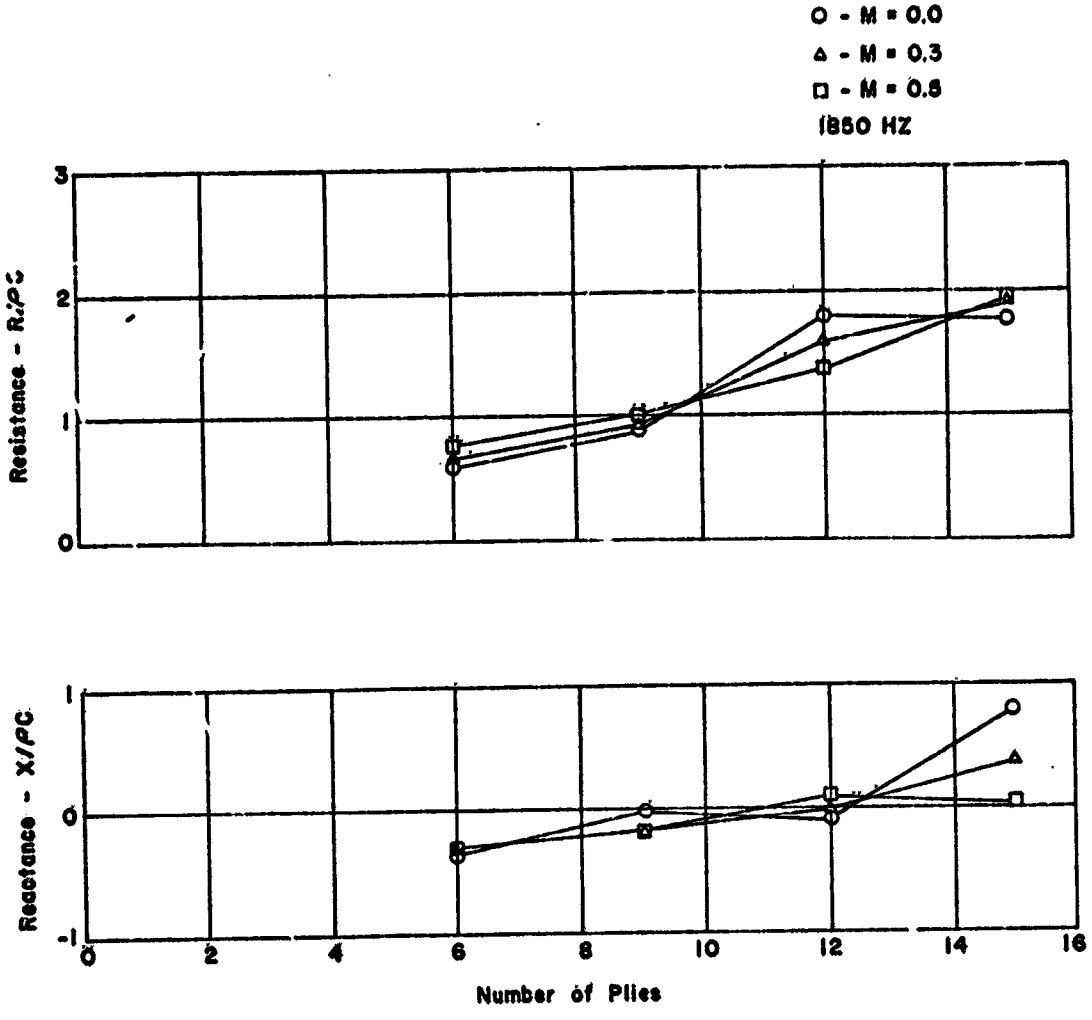

GRAZING FLOW RESISTANCE AND REACTANCE TRENDS FOR PRECURED POLYIMIDE SAMPLES (0.86 IN. CORE DEPTH)
FIGURE 12

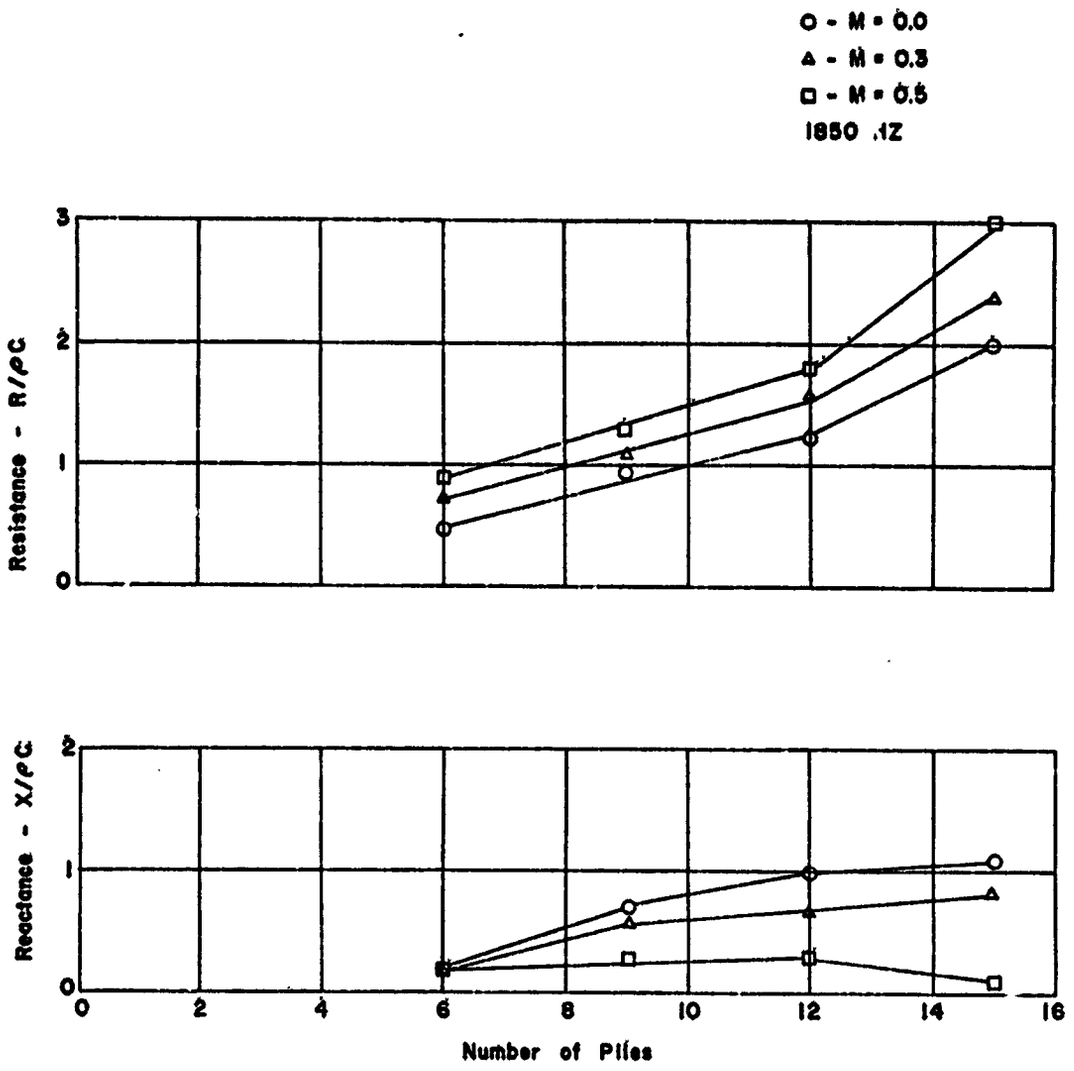

GRAZING FLOW RESISTANCE AND REACTANCE TRENDS FOR PRECURED POLYIMIDE SAMPLES (1.4 IN. CORE DEPTH)
FIGURE 13

9.0 RELATIVE ERROR OF IMPEDANCE MEASUREMENTS

A statistical error analysis of the impedance measurements should be based on many impedances values for the range of parameters involved (frequency, SPL, Mach number, impedance, etc.). This information is not available at this time. However, a relative estimate of the error can be calculated based on the standard estimate of the error between the data and the least square straight line fit to the data.

The expression for the impedance is given in Equation 17 as a function of Mach number and the transverse propagation parameters μ and χ. Assuming that the Mach number is constant, the change in the impedance relative to μ and χ can be obtained. However, these quantities are not measured directly and, therefore, must be expressed in terms of the measured attenuation rate and phase rate. The axial propagation constant is given by

$$k_z = k(\tau - i\sigma)$$

where σ and τ are known functions of μ and χ. The quantity τ is computed from the measured wavelength in the duct as

$$\tau = \frac{\lambda}{\lambda_m}$$

where $\lambda = c/f$ is the calculated wavelength and $\lambda_m = 360^0/\phi_R$ is the measured wavelength as related to the measured phase rate ϕ_R. The quantity σ is related to the measured attenuation rate α (dB/in) by

$$\sigma = \frac{\alpha c}{54.6 f}$$

Thus, if the impedance is expressed as

$$\frac{\zeta}{\eta} = \Gamma(\mu, \chi)$$

the change in impedance relative to μ and χ is

$$d\Gamma = \frac{\partial \Gamma}{\partial \mu} d\mu + \frac{\partial \Gamma}{\partial \chi} d\chi$$

But, since $\sigma = F(\mu, \chi)$

and $\tau = G(\mu, \chi)$

where F and G are given by Equations 22 and 23.

Therefore, $$d\sigma = \frac{\partial F}{\partial \mu} d\mu + \frac{\partial F}{\partial \chi} d\chi$$

and $$d\tau = \frac{\partial G}{\partial \mu} d\mu + \frac{\partial G}{\partial \chi} d\chi$$

Solving for $d\mu$ and $d\chi$

$$d\mu = \left(\frac{\partial G}{\partial \chi} d\sigma - \frac{\partial F}{\partial \chi} d\tau\right) \Big/ J$$

and

$$dx = \left(\frac{\partial F}{\partial \mu} d\tau - \frac{\partial G}{\partial \mu} d\sigma \right) \Big/ J$$

Where $J = \frac{\partial F}{\partial \mu} \frac{\partial G}{\partial x} - \frac{\partial F}{\partial x} \frac{\partial G}{\partial \mu}$

The relationship between $d\sigma$ and $d\tau$ to the standard estimate of the error (SE) for the measured values of phase and attenuation can be obtained by considering the change in phase rate and attenuation rate due to rotating the least square straight line fit to the data about the beginning of the section ($\frac{\lambda m}{2}$ length) by the amount of the standard error at the end of that section. Thus,

$$d\sigma_1 = \frac{h}{27.3\eta} (\alpha - \alpha_{-SE}) = -\frac{2h(SE)}{27.3\eta} = -\frac{\tau(SE)}{27.3}$$

$$d\sigma_2 = \frac{h}{27.3\eta} (\alpha - \alpha_{-SE}) = \frac{2h(SE)}{27.3\eta} = \frac{\tau(SE)}{27.3}$$

and

$$d\tau_1 = \frac{\lambda}{360} (\phi - \phi_{-SE}) = -\frac{\lambda(SE)}{180\lambda_m} = -\frac{\tau(SE)}{180}$$

$$d\tau_2 = \frac{\lambda}{360} |\phi - \phi_{-SE}| = \frac{\tau(SE)}{180}$$

Substituting the above formulas into the expression for $d\Gamma$ yields the required expression for the error in terms of the standard estimate of the error of the measured values of attenuation and phase. The maximum values of $d\Gamma$ obtained from the four combinations of $d\tau$ and $d\sigma$ are used to represent the spread in impedance values. Generally, this variation was not larger than the symbol size used to plot the data and, therefore, is not presented in the data plots. The range of the relative estimate of the error is given in Figure 14 as a function of Mach number. This function increases with Mach number indicating the increasing influence of the standing waves on the data.

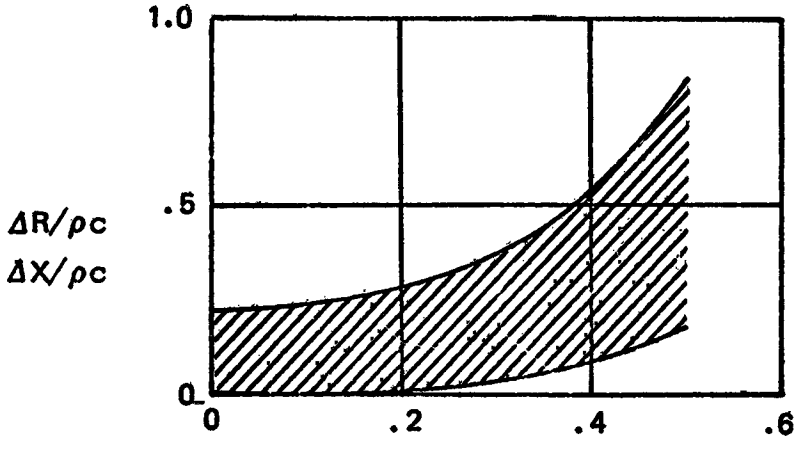

CALCULATED RANGE OF DEVIATIONS FOR PERFORATED SHEET AND POLYIMIDE IMPEDANCE MEASUREMENTS
FIGURE 14

10.0 CONCLUSIONS

Considering the inherent limitations of the grazing flow apparatus and the experience gained in its usage, several areas exist that require modification and improvement. They are:

- The waveguide apparatus, as it now exists, should be redesigned to reduce the standing wave component at higher Mach numbers which would reduce the variability of the impedance measurements. This can be done basically by improving the efficiency of the diffuser exponential horn by a redesign.

- The frequency range of the apparatus can be doubled by decreasing the duct height by a factor of two. However, the maximum usable Mach number could be further limited by fully developed pipe flow.

- The dependence of impedance on the boundary layer profile should be studied. This can be accomplished by introducing boundary layer trips of different degrees upstream of the test section. Boundary layer velocity profiles would be measured from which boundary layer momentum thickness and other flow properties could be correlated to acoustic impedance.

- The impedance measuring technique can be improved by using two simultaneously traversing microphones. A "Fast Fourier Transformer" (FFT) could be used to cross correlate the two signals to obtain the attenuation rate and phase velocity of the acoustic wave as a function of duct position. Coupling this FFT directly to a computer would make it possible to obtain directly impedance vs. duct position. In this case, it would be possible, if necessary, to average impedance over a certain duct length rather than straight line curve fitting data over half wave length duct sections as required by the present measurement technique. Also, as a by-product of using the FFT, the power spectral density of the entire acoustic spectrum would be available on demand at any duct location. Thus, by making these modifications, more information would be made available in a shorter period of time.

- A higher SPL source is needed to produce SPL's that induce particle velocities that dominate that due to grazing flow so that the grazing flow induced particle velocities can be determined.

The feasibility of using a waveguide method of determining the impedance of acoustic materials in a grazing flow environment has been proven. This method determines both the resistive and reactive impedances of the installed panel. Therefore, a realistic mathematical impedance model that considers Mach number, SPL, and frequency can be derived from this type of impedance measurement.

11.0 REFERENCES

1. Phillips, B. and Morgan, C. J., "Mechanical Absorption of Acoustic Oscillations in Simulated Rocket Combustion Chambers," NASA TN D-3792 (Jan. 1967)

2. Phillips, B., "Effects of High Value Wave Amplitude and Mean Flow on a Helmholtz Resonator," NASA TM X-1582 (May 1968)

3. Garrison, G. D., et al, "Suppression of Combustion Oscillations with Mechanical Damping Devices, Interim Report," PWA FR-3299 (8 Aug. 1969)

4. Binck, J. S., "Behavior of Acoustic Resistance of Typical Duct Liners in the Presence of Grazing Flow Measured by a Two Microphone Method," M. S. Thesis, University of Southampton (Oct. 1969)

5. Feder, E. and Dean III, L. W., "Analytical and Experimental Studies for Predicting Noise Attenuation in Acoustically Treated Ducts for Turbofan Engines," NASA CR-1373 (Sept. 1969)

6. Cremer, L., "Theorie der Luftschall — Dampfung im Rechtekkanal mit Schluckender Wand und das sich dabei Ergebende Hochste Dampfungsmass," Acoustica 3, 249 – 263 (1953).

7. Nelsen, M. D., et al, "Study and Development of Acoustic Treatment for Jet Engine Tailpipes," NASA CR-1853 (Nov. 1971)

APPENDIX

PRECEDING PAGE BLANK NOT FILMED

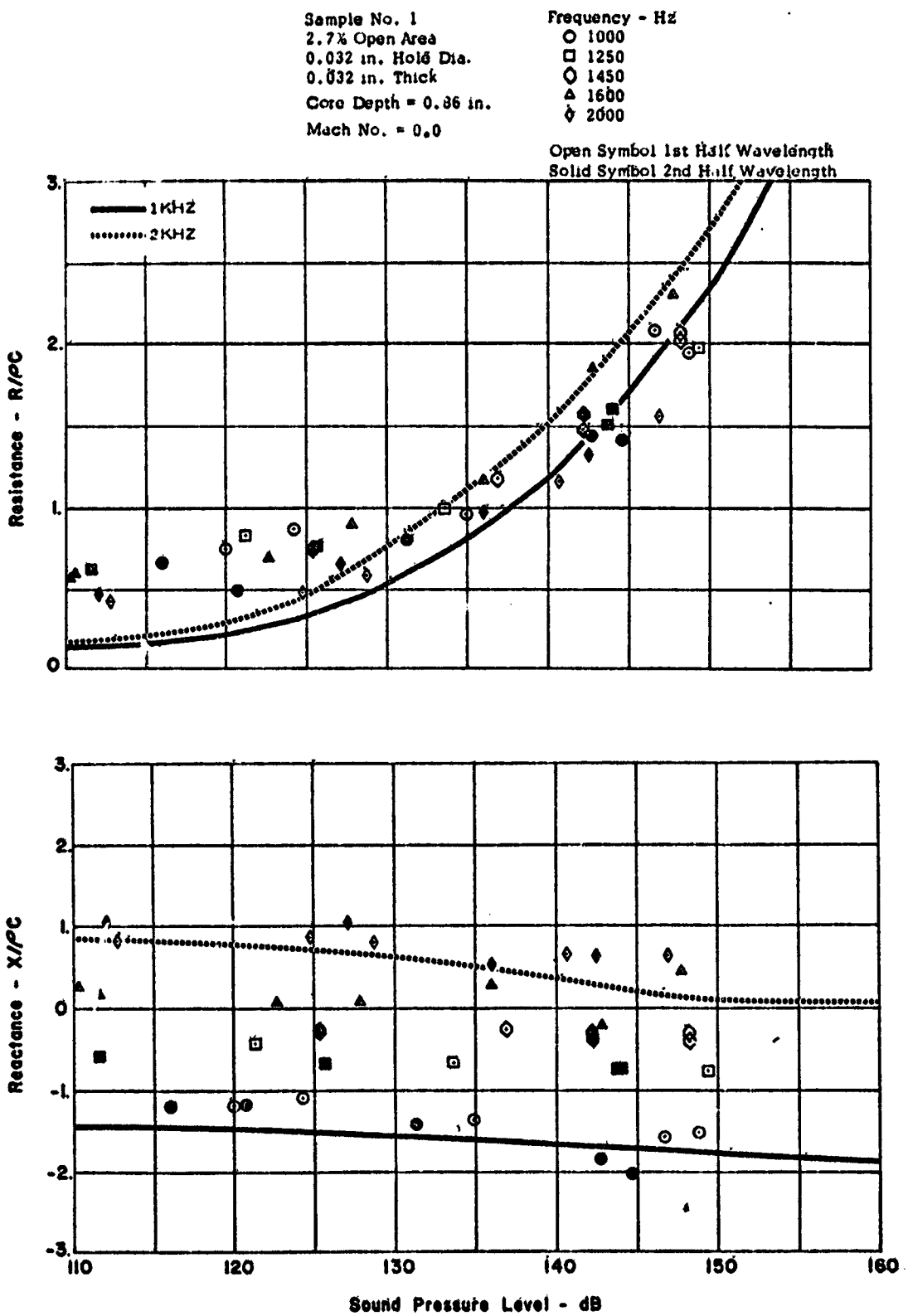

SAMPLE NO. 1, RESISTANCE AND REACTANCE DATA (0.0 MACH)
FIGURE 15

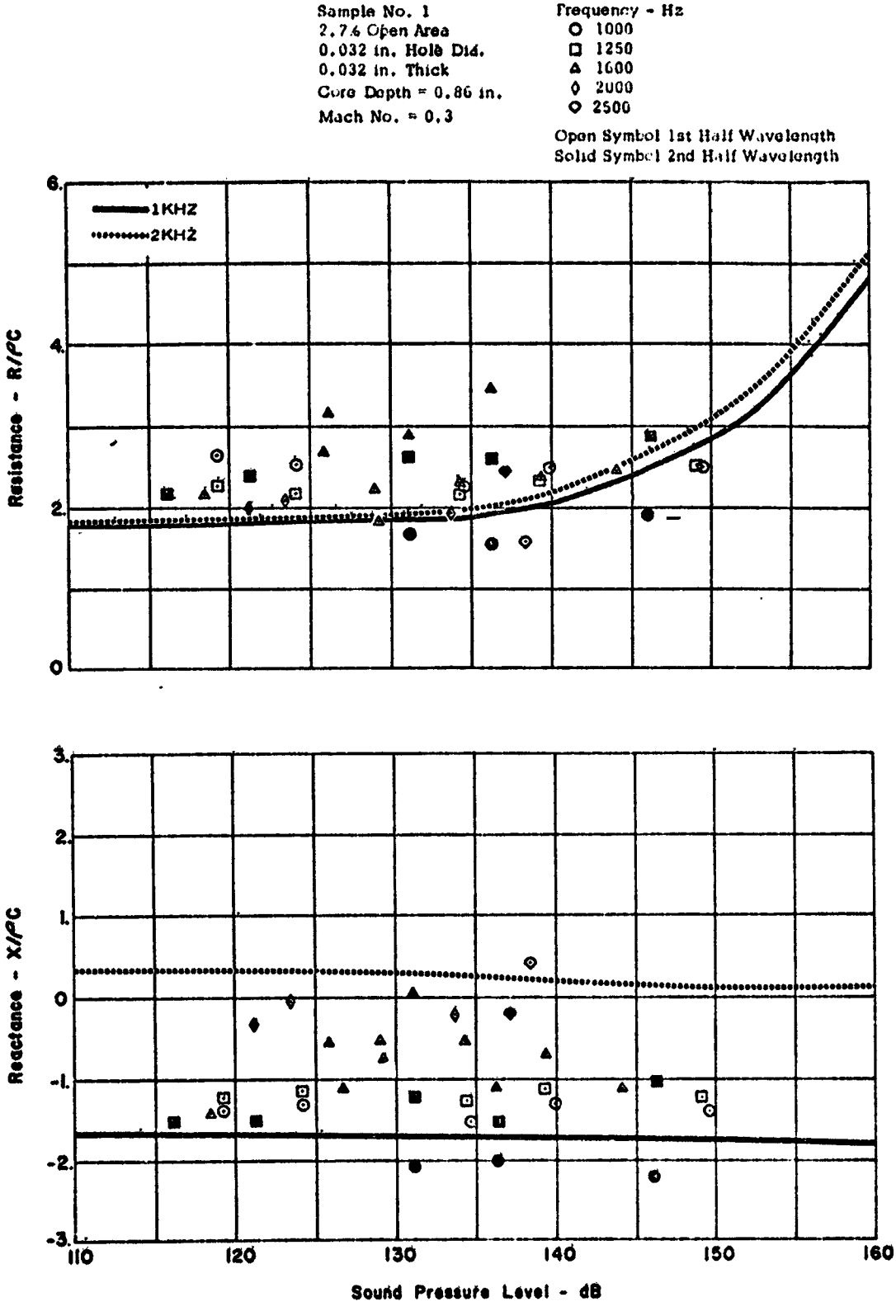

SAMPLE NO. 1, RESISTANCE AND REACTANCE DATA (0.3 MACH)
FIGURE 16

Sample No. 1
2.7% Open Area
0.032 in. Hole Dia.
0.032 in. Thick
Core Depth = 0.86 in.
Mach No. = 0.5

Frequency - Hz
□ 1250
△ 1600
◊ 2000

Open Symbol 1st Half Wavelength
Solid Symbol 2nd Half Wavelength

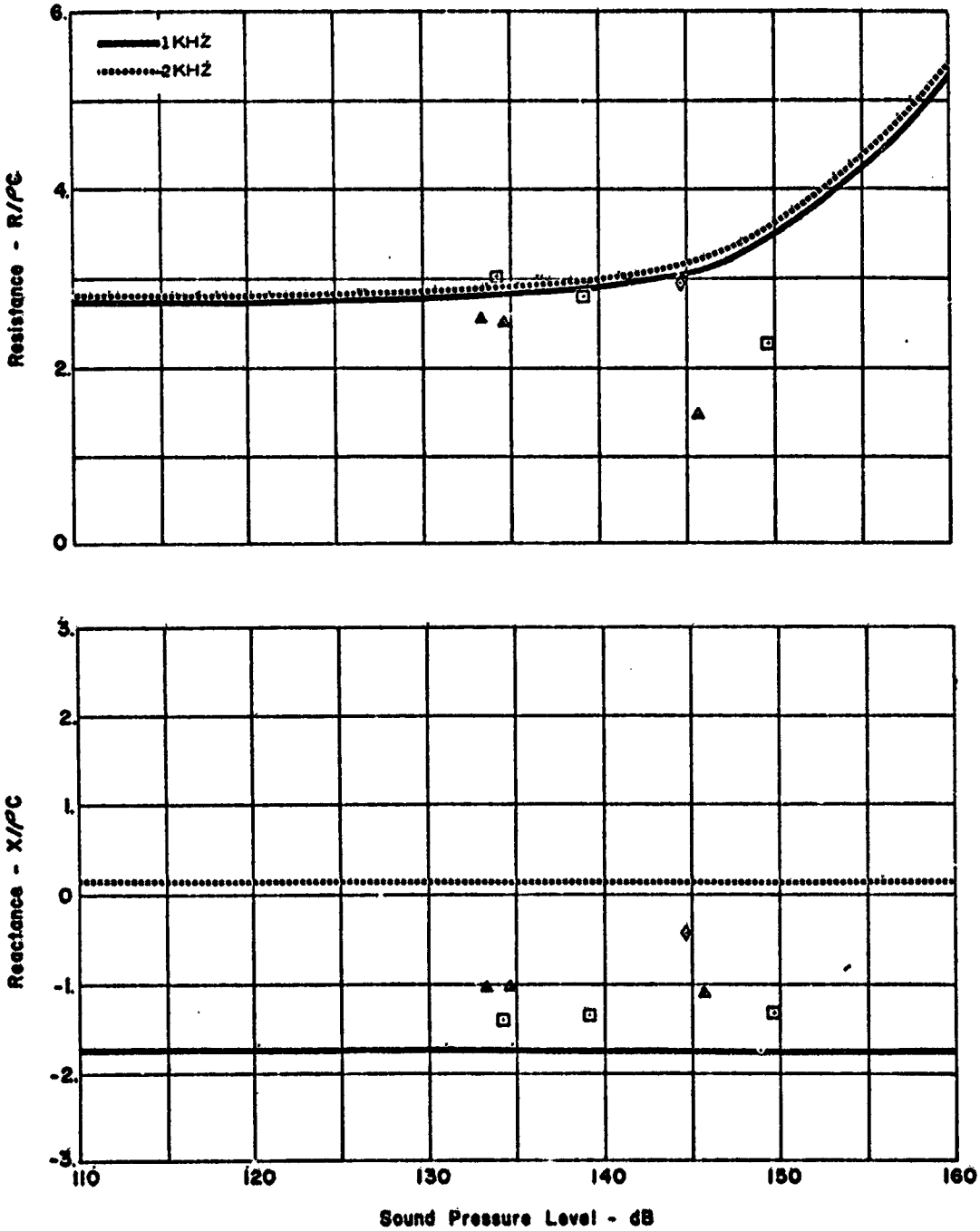

SAMPLE NO. 1, RESISTANCE AND REACTANCE DATA (0.5 MACH)
FIGURE 17

Sample No. 2
4.4% Open Area
0.059 in. Hole Dia.
0.030 in. Thick

Core Depth = 0.86 in.

Mach No. = 0.0

Frequency - Hz
Δ 1600
◊ 2000

Open Symbol 1st Half Wavelength
Solid Symbol 2nd Half Wavelength

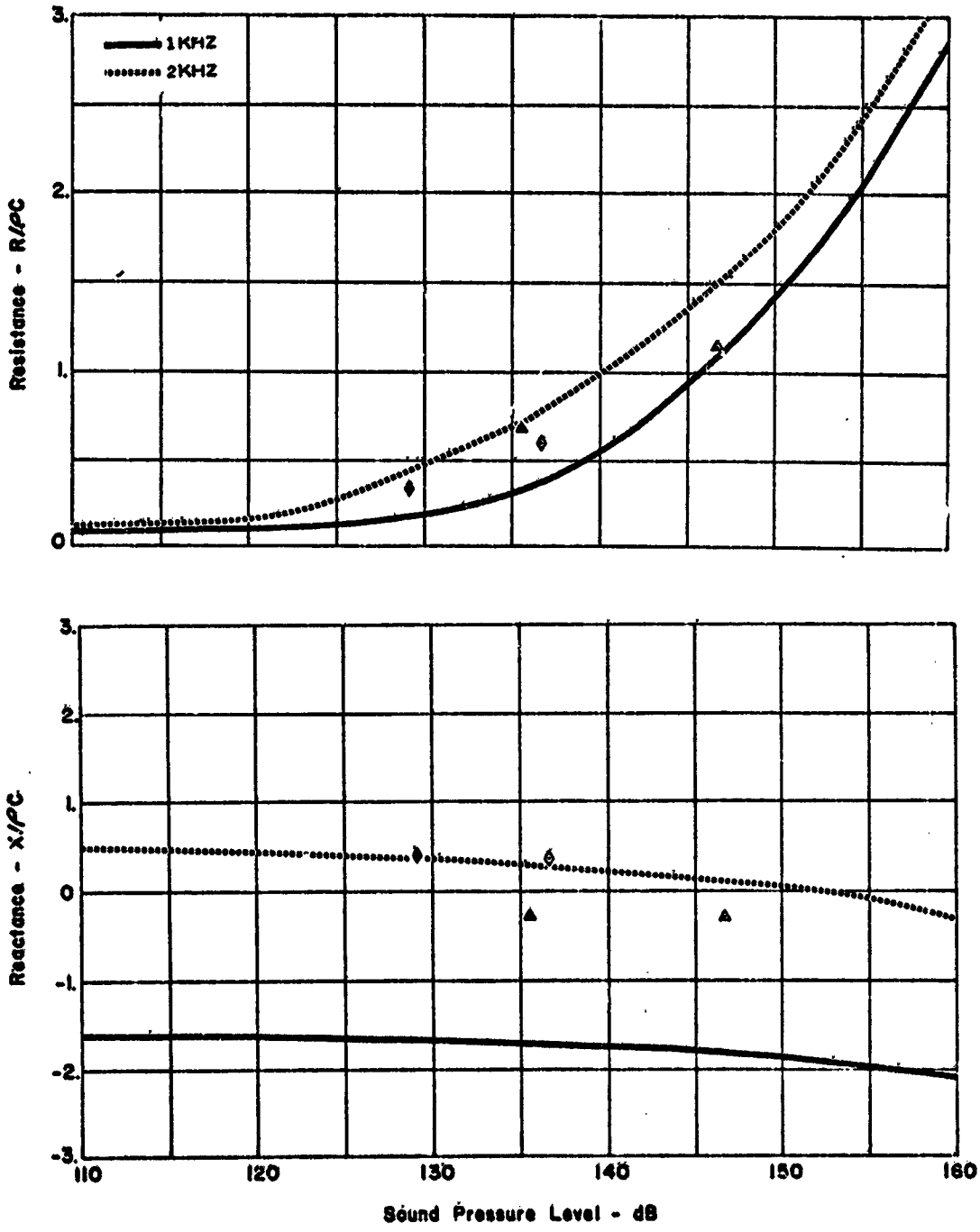

SAMPLE NO. 2, RESISTANCE AND REACTANCE DATA (0.0 MACH)
FIGURE 18

Sample No. 2
4.4% Open Area
0.059 in. Hole Dia.
0.030 in. Thick
Core Depth = 0.86 in.
Mach No. = 0.3

Frequency - Hz
○ 1000
□ 1250
△ 1600
◇ 2000

Open Symbol 1st Half Wavelength
Solid Symbol 2nd Half Wavelength

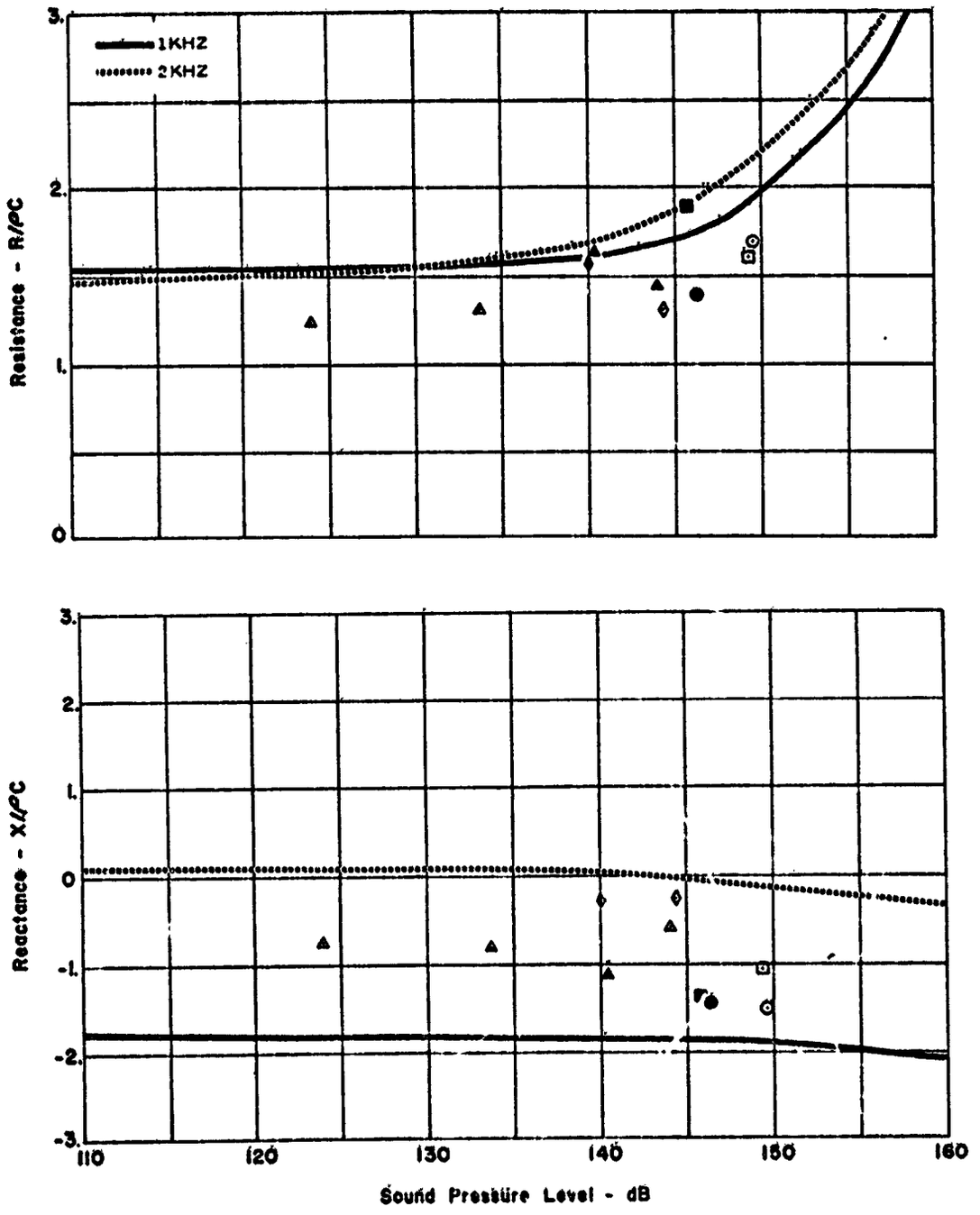

SAMPLE NO. 2, RESISTANCE AND REACTANCE DATA (0.3 MACH)
FIGURE 19

Sample No. 2
4.4% Open Area
0.059 in. Hole Dia.
0.030 in. Thick

Core Depth = 0.86 in.

Mach No. = 0.5

Frequency - Hz
- ○ 1000
- □ 1450
- △ 1600
- ◊ 2000

Open Symbol 1st Half Wavelength
Solid Symbol 2nd Half Wavelength

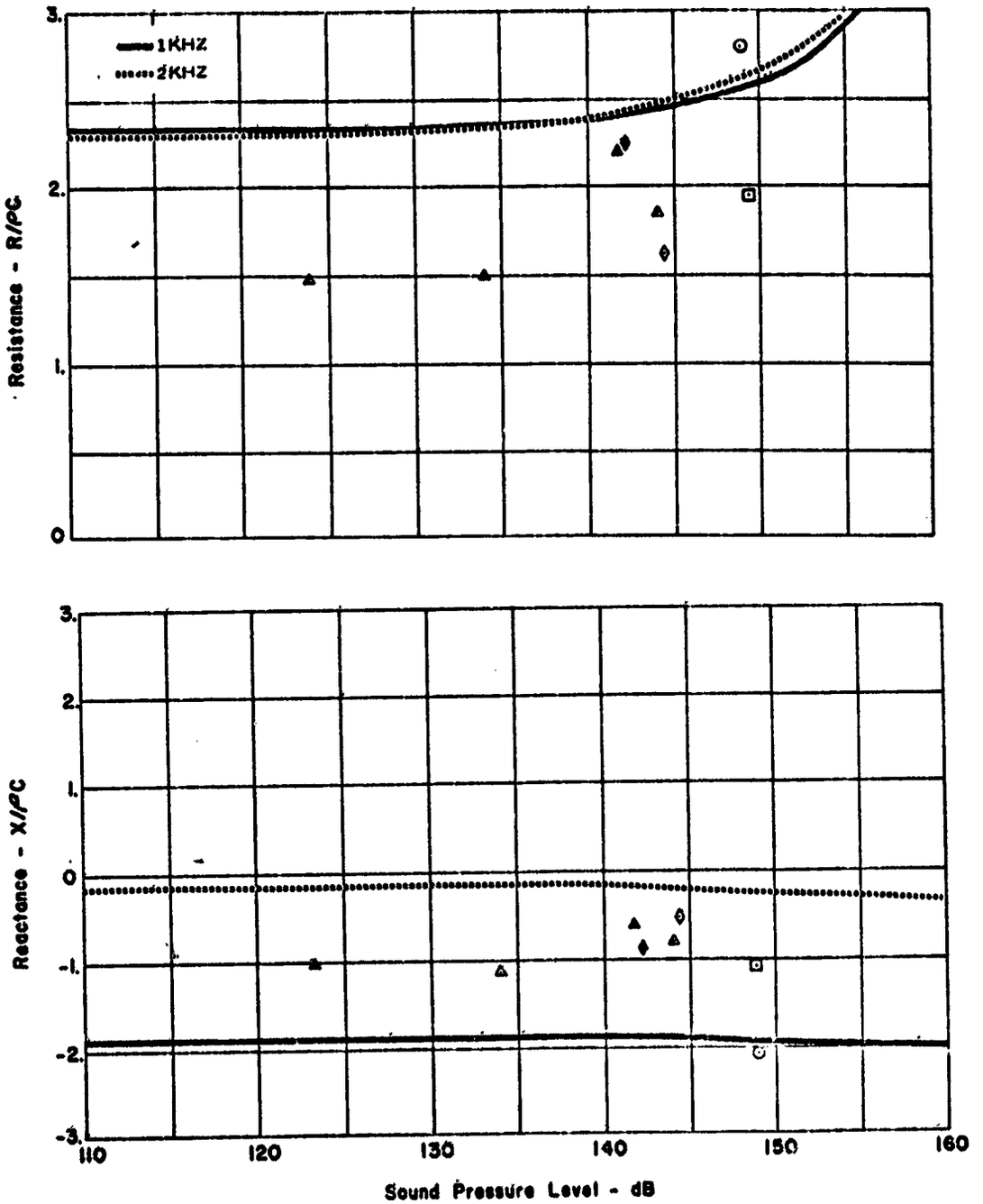

SAMPLE NO. 2, RESISTANCE AND REACTANCE DATA (0.5 MACH)
FIGURE 20

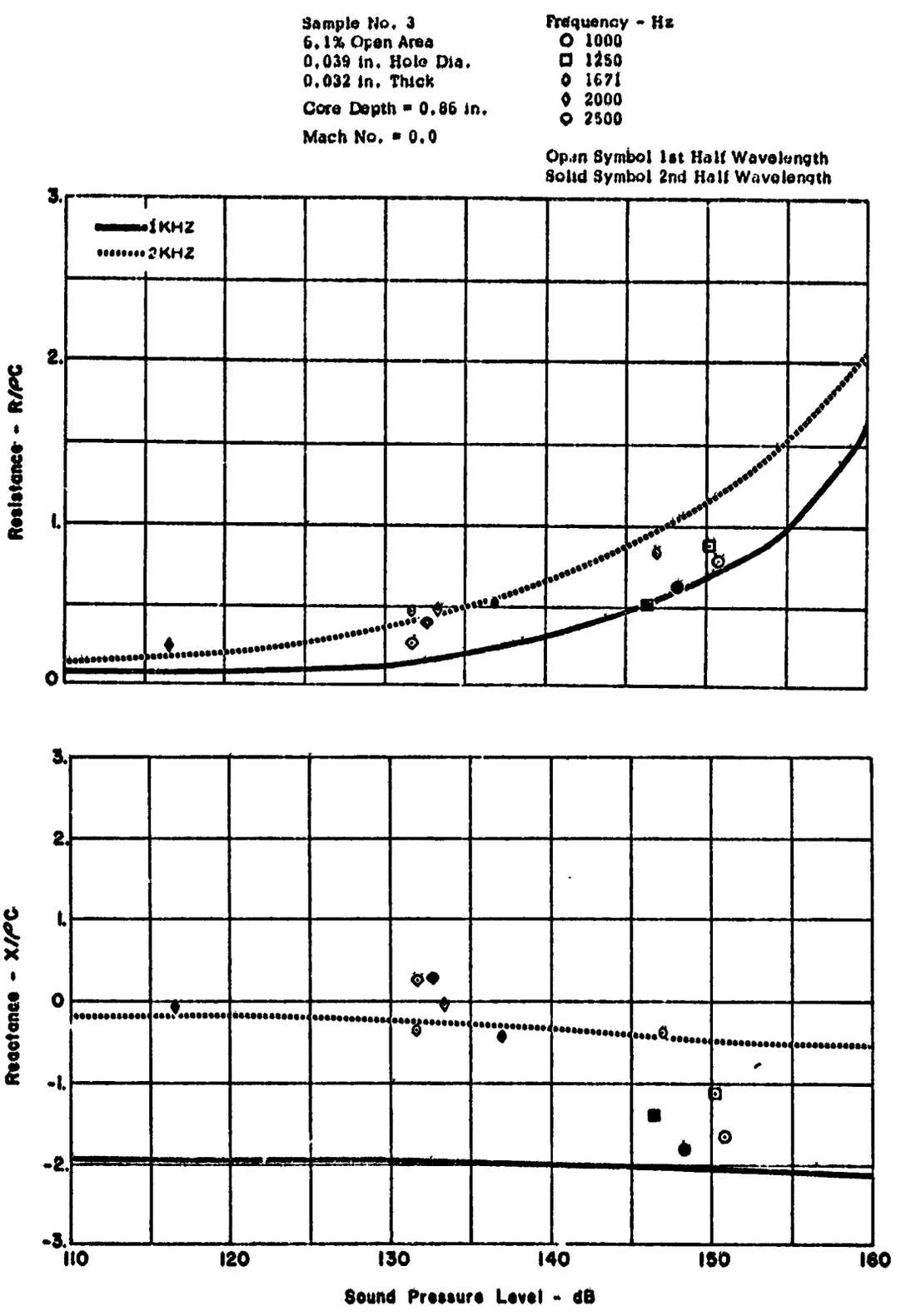

SAMPLE NO. 3, RESISTANCE AND REACTANCE DATA (0.0 MACH)
FIGURE 21

Sample No. 3
6.1% Open Area
0.039 in. Hole Dia.
0.032 in. Thick
Cavity Depth = 0.86 in.
Mach No. = 0.3

Frequency - Hz
□ 1250
◊ 2000
○ 2240

Open Symbol 1st Half Wavelength
Solid Symbol 2nd Half Wavelength

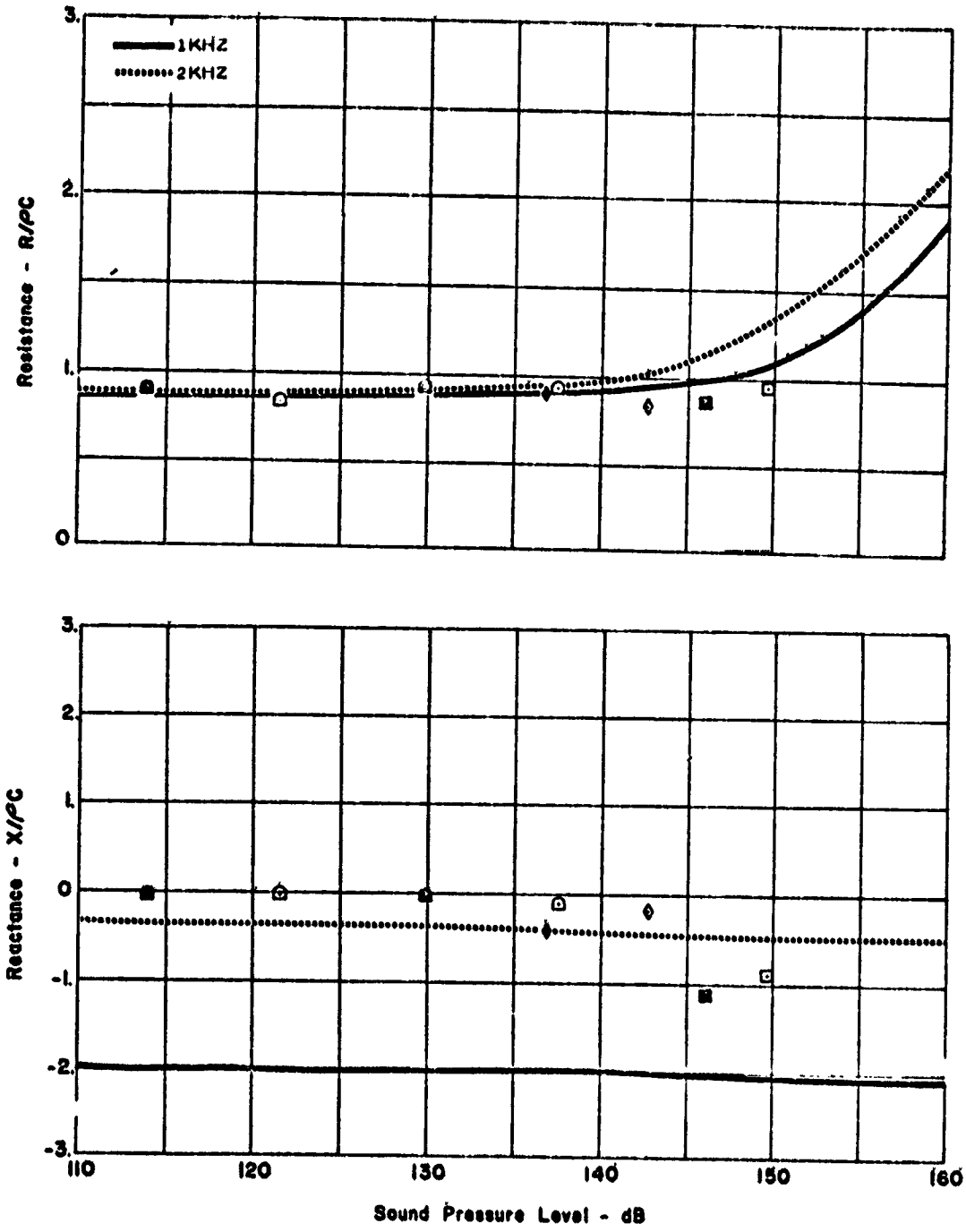

SAMPLE NO. 3, RESISTANCE AND REACTANCE DATA (0.3 MACH)
FIGURE 22

Sample No. 3
6.1% Open Area
0.039 in. Hole Dia.
0.032 in. Thick

Core Depth = 0.50 in.

Mach No. = 0.5

Frequency - Hz
◊ 2000
□ 2240
▷ 2582

Open Symbol 1st Half Wavelength
Solid Symbol 2nd Half Wavelength

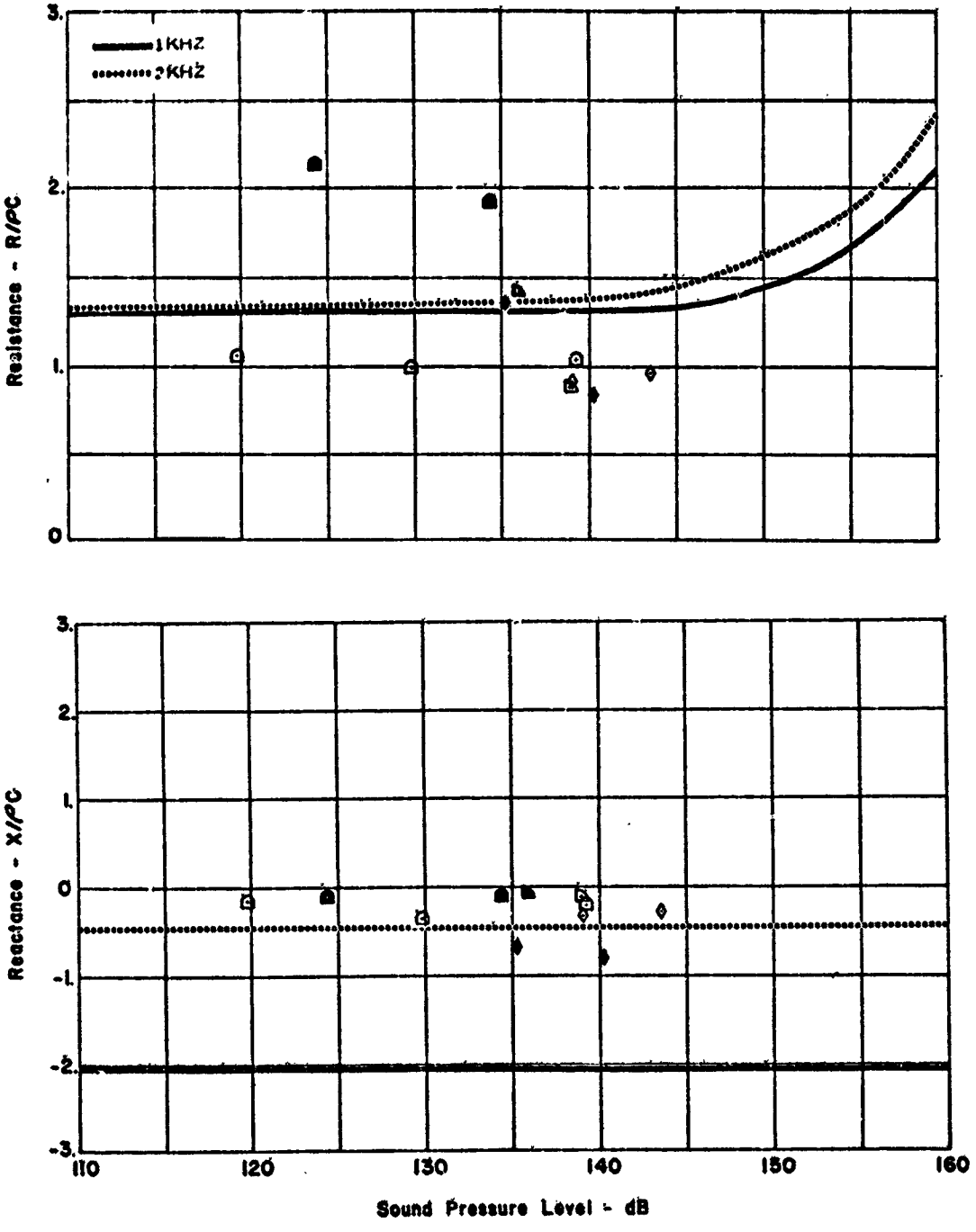

SAMPLE NO. 3, RESISTANCE AND REACTANCE DATA (0.5 MACH)
FIGURE 23

Sample No. 4
10.4% Open Area
0.038 in. Hole Dia.
0.032 in. Thick
Core Depth = 0.86 in.
Mach No. = 0.0

Frequency - Hz
D 2100

Open Symbol 1st Half Wavelength
Solid Symbol 2nd Half Wavelength

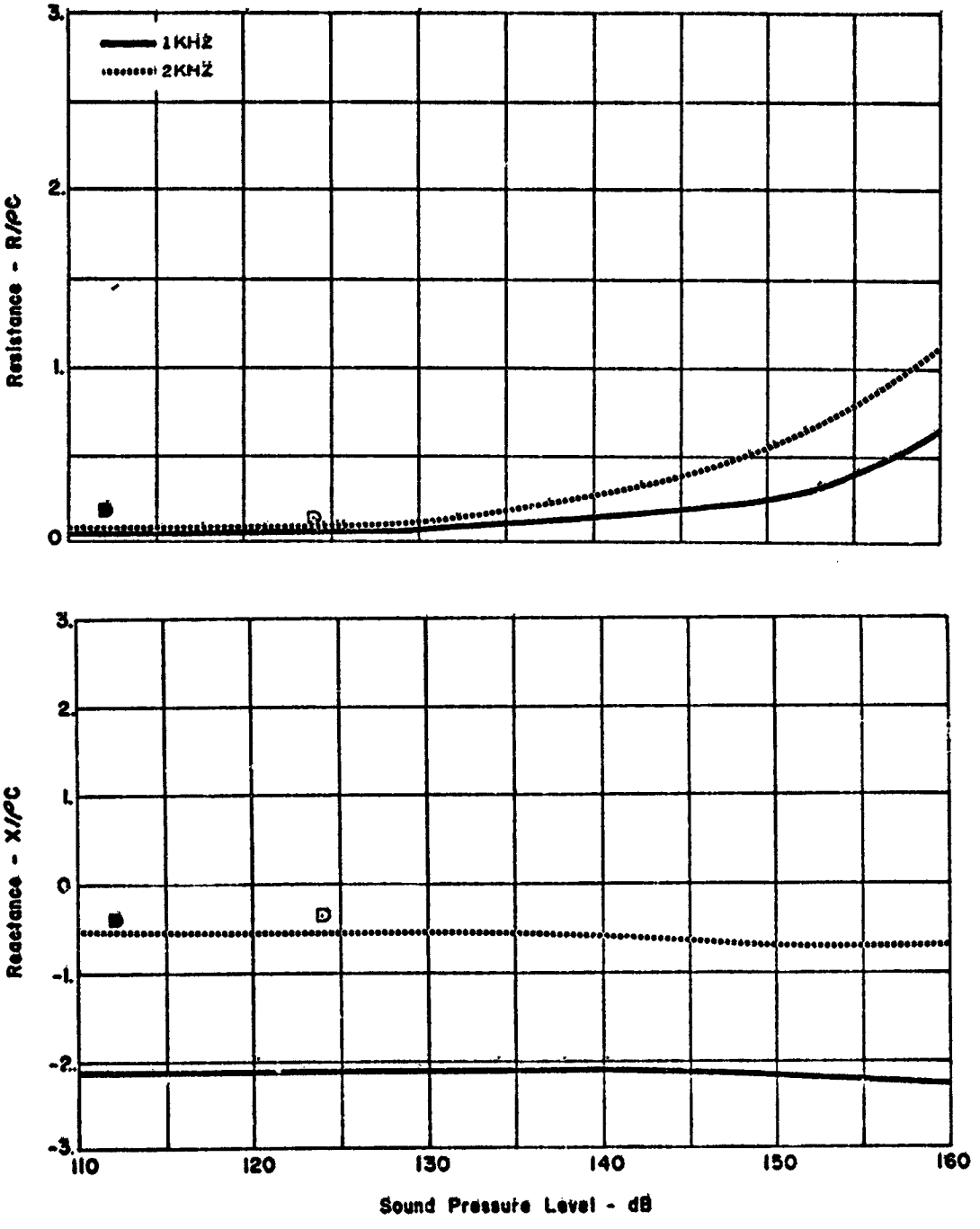

SAMPLE NO. 4, RESISTANCE AND REACTANCE DATA (0.0 MACH)
FIGURE 24

Sample No. 4
10.4% Open Area
0.038 in. Hole Dia.
0.032 in. Thick
Core Depth = 0.86 in.
Mach No. = 0.3

Frequency - Hz
D 2100

Open Symbol 1st Half Wavelength
Solid Symbol 2nd Half Wavelength

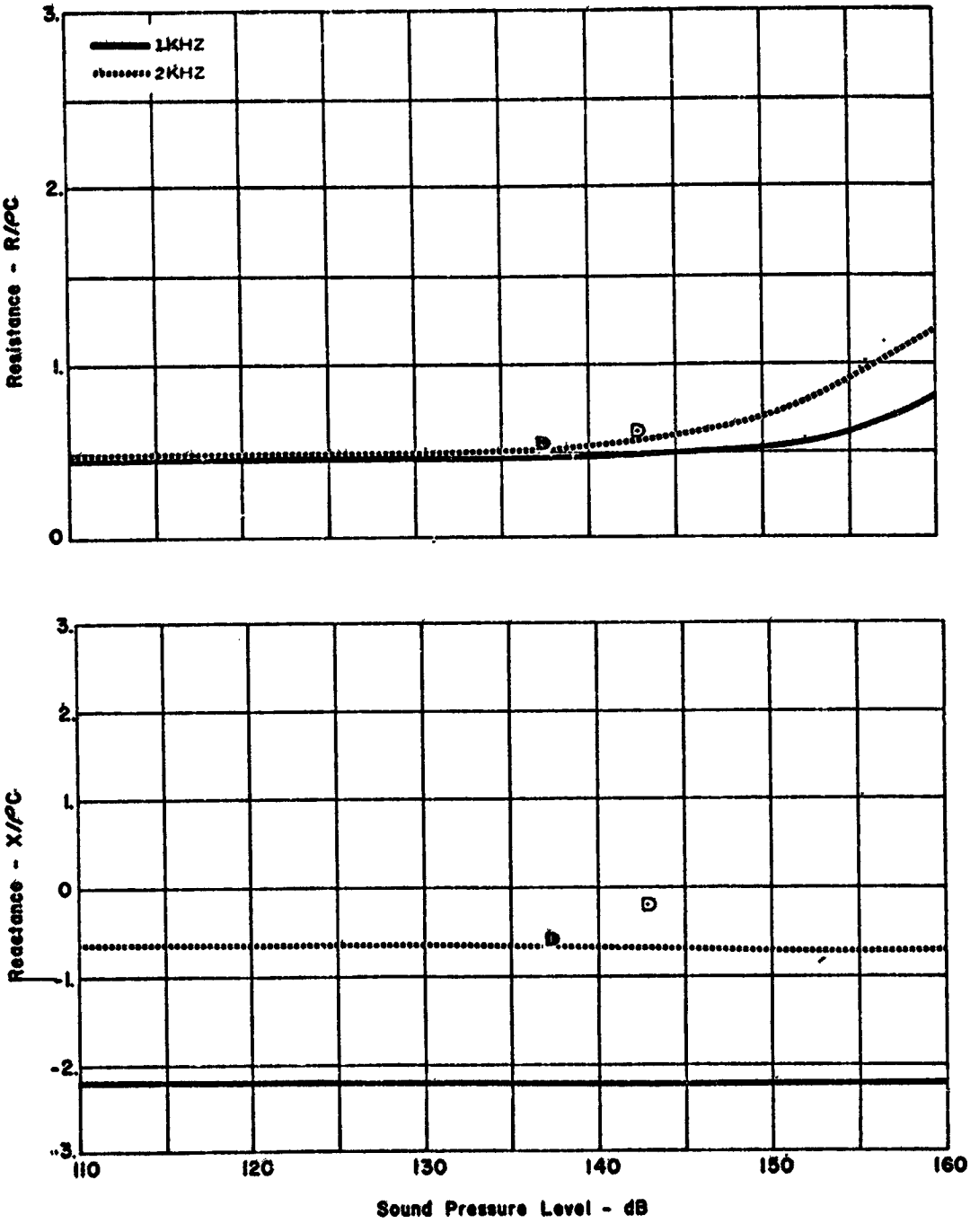

SAMPLE NO. 4, RESISTANCE AND REACTANCE DATA (0.3 MACH)
FIGURE 25

Sample No. 4
10.4% Open Area
0.038 in. Hole Dia.
0.032 in. Thick
Core Depth = 0.86 in.
Mach No. = 0.5

Frequency - Hz
D 2100

Open Symbol 1st Half Wavelength
Solid Symbol 2nd Half Wavelength

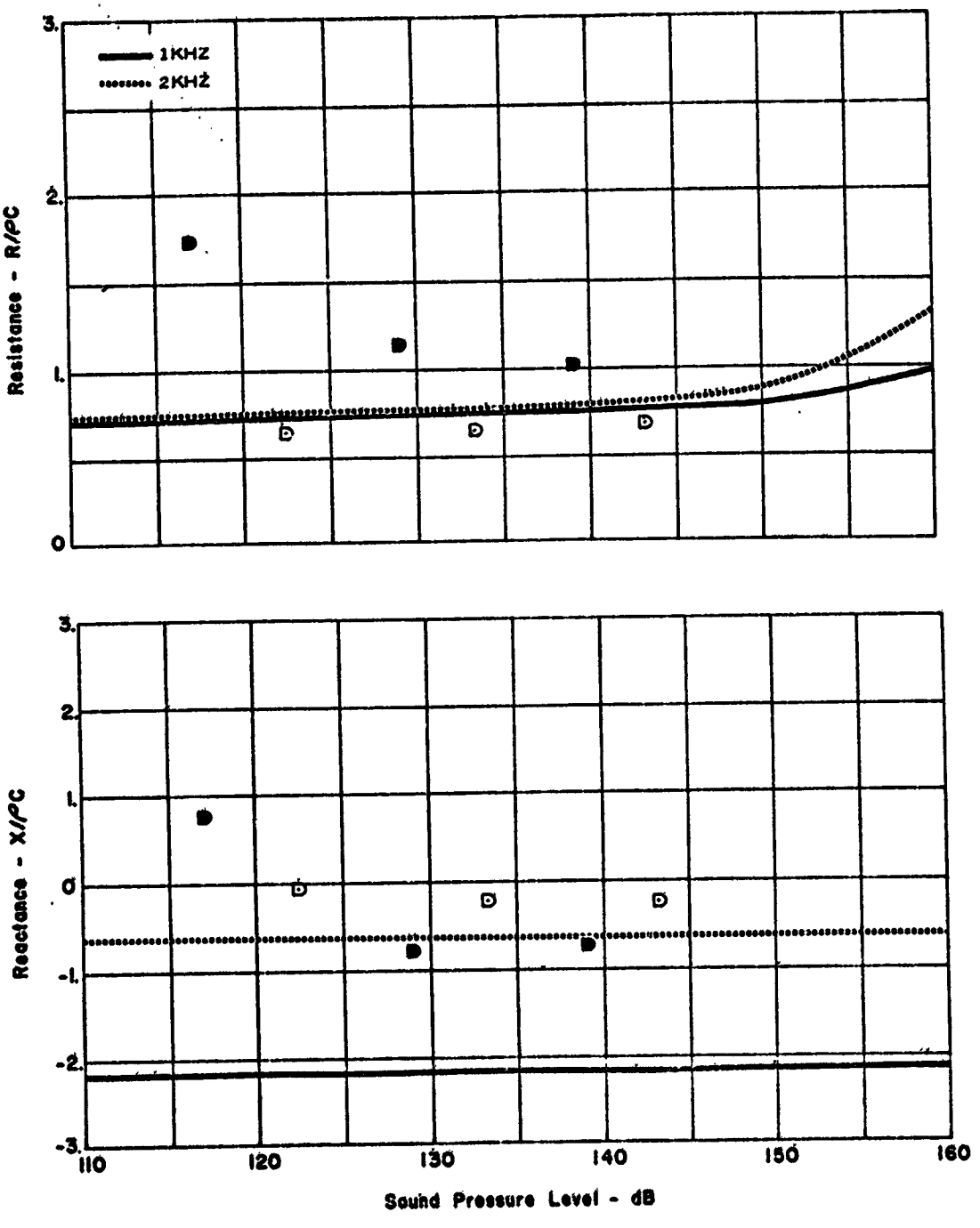

SAMPLE NO. 4, RESISTANCE AND REACTANCE DATA (0.5 MACH)
FIGURE 26

Sample No. 5
9.9% Open Area
0.1 in. Hole Dia.
0.03 in. Thick
Core Depth = 0.86 in.
Mach No. = 0.0

Frequency - Hz
◊ 2000

Open Symbol 1st Half Wavelength
Solid Symbol 2nd Half Wavelength

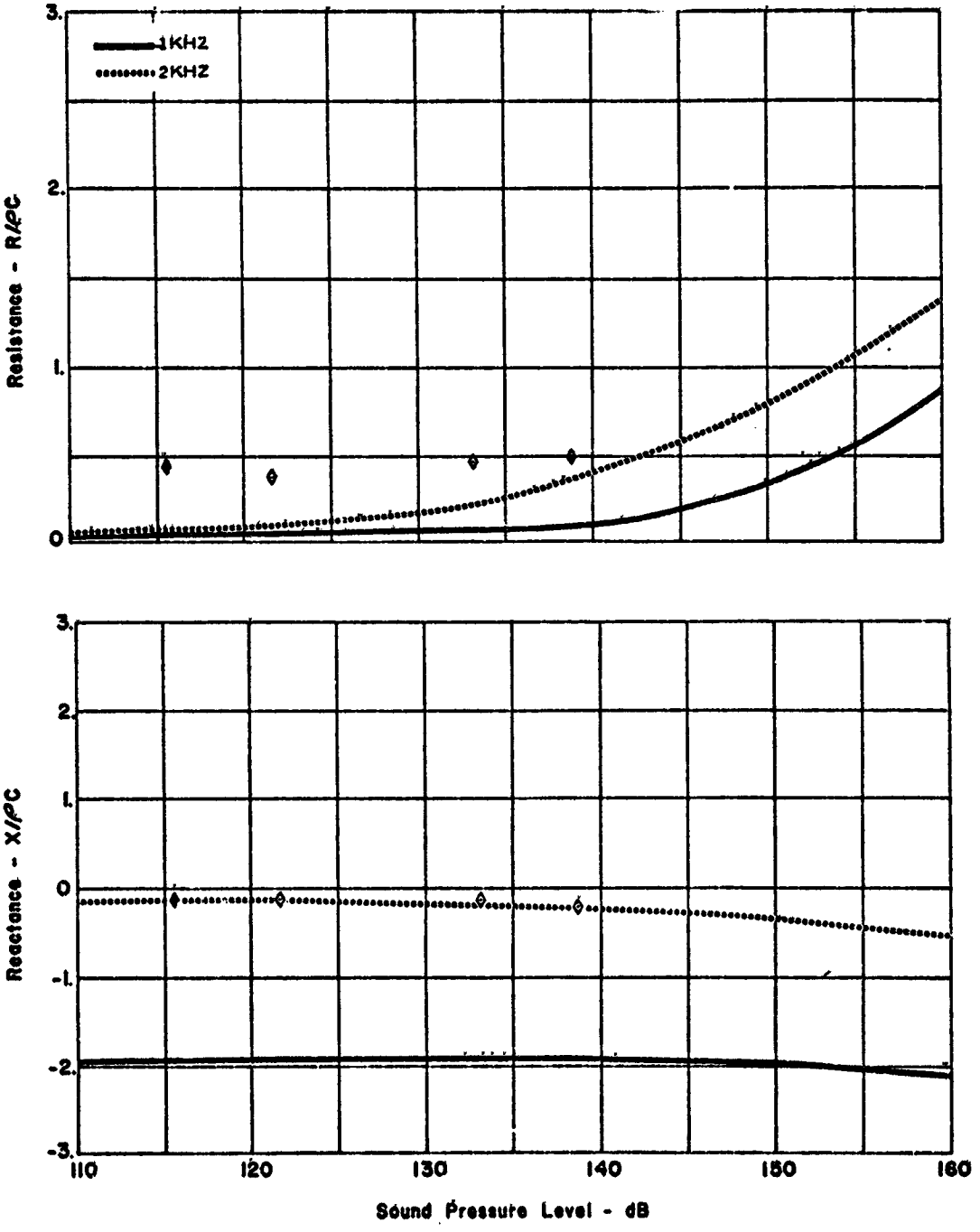

SAMPLE NO. 5, RESISTANCE AND REACTANCE DATA (0.0 MACH)
FIGURE 27

Sample No. 5
9.9% Open Area
0.1 in. Hole Dia.
0.03 in. Thick

Core Depth = 0.86 in.

Mach No. = 0.3

Frequency - Hz
◊ 2000

Open Symbol 1st Half Wavelength
Solid Symbol 2nd Half Wavelength

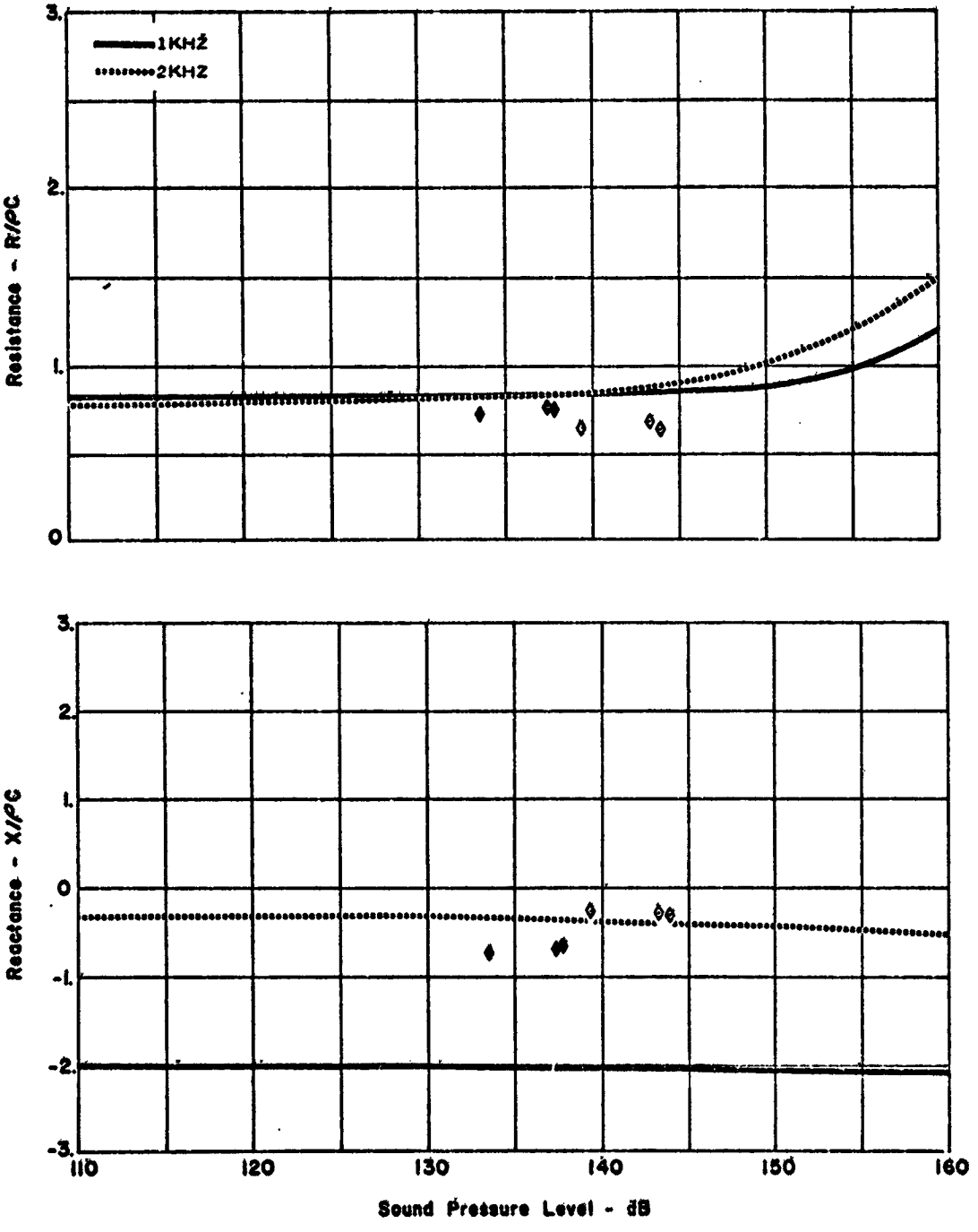

SAMPLE NO. 5, RESISTANCE AND REACTANCE DATA (0.3 MACH)
FIGURE 28

Sample No. 5
9.9% Open Area
0.1 in. Hole Dia.
0.03 in. Thick

Core Depth = 0.86 in.

Mach No. = 0.5

Frequency - Hz
◊ 2000

Open Symbol 1st Half Wavelength
Solid Symbol 2nd Half Wavelength

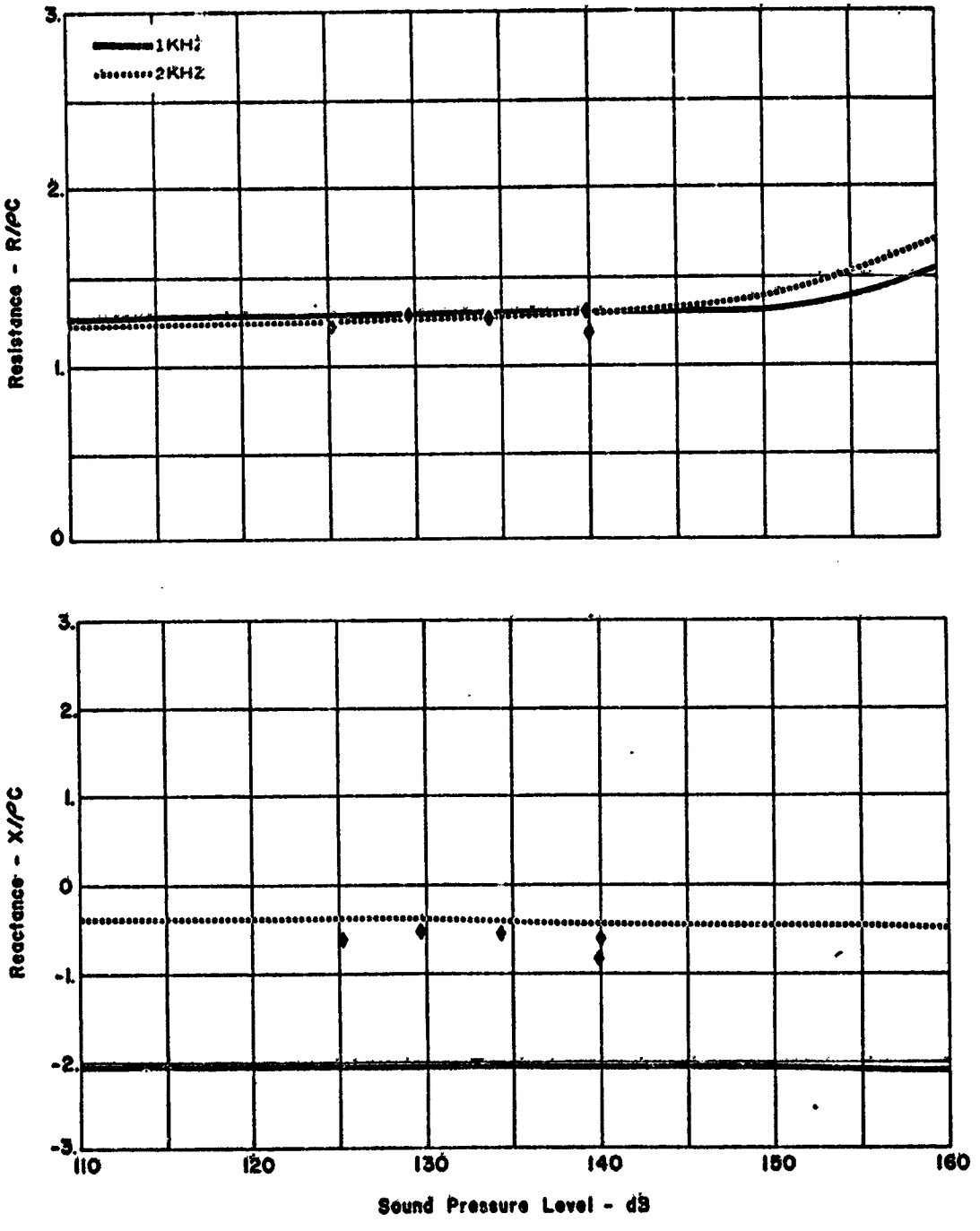

SAMPLE NO. 5, RESISTANCE AND REACTANCE DATA (0.5 MACH)
FIGURE 29

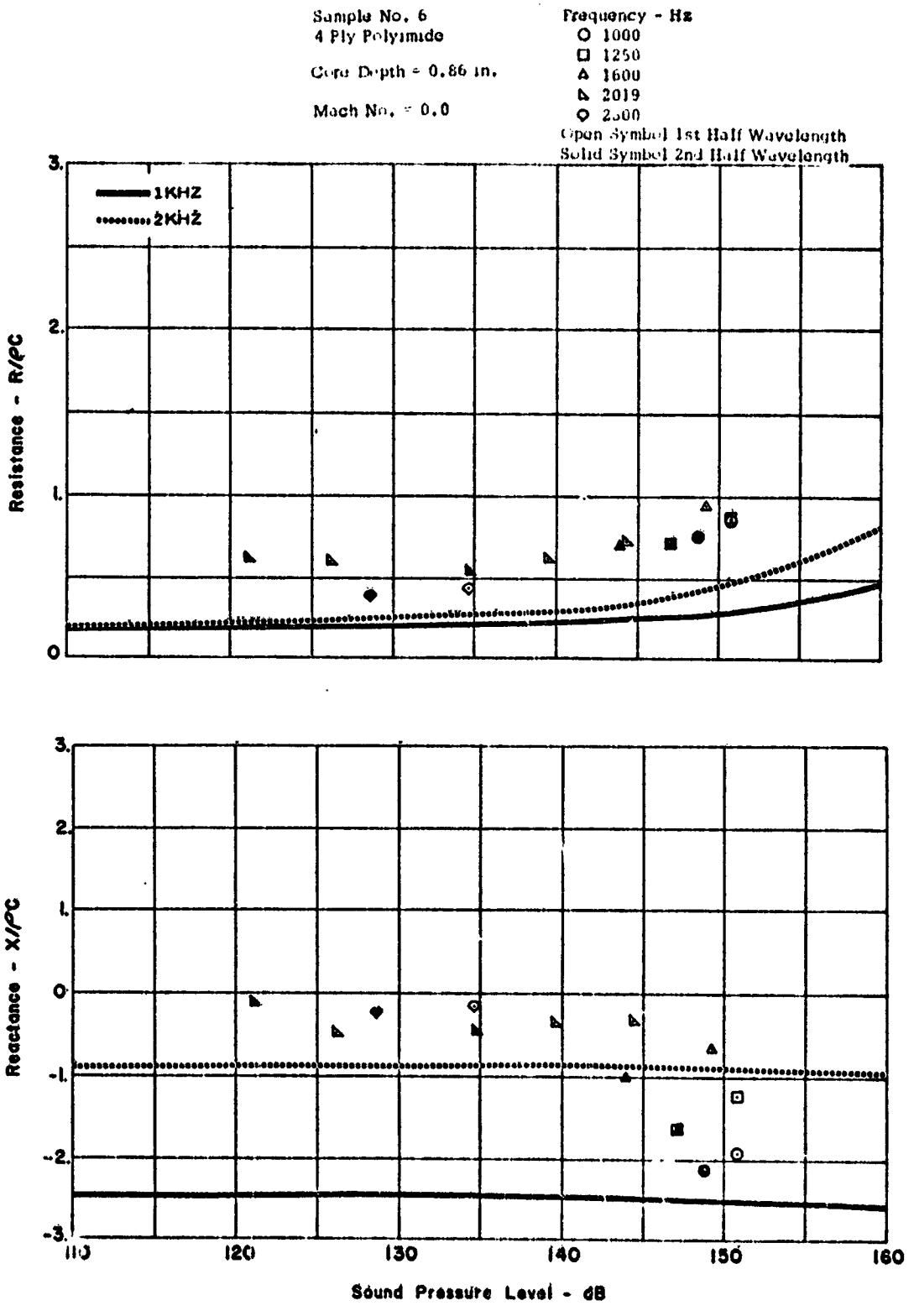

SAMPLE NO. 6, RESISTANCE AND REACTANCE DATA (0.0 MACH)
FIGURE 30

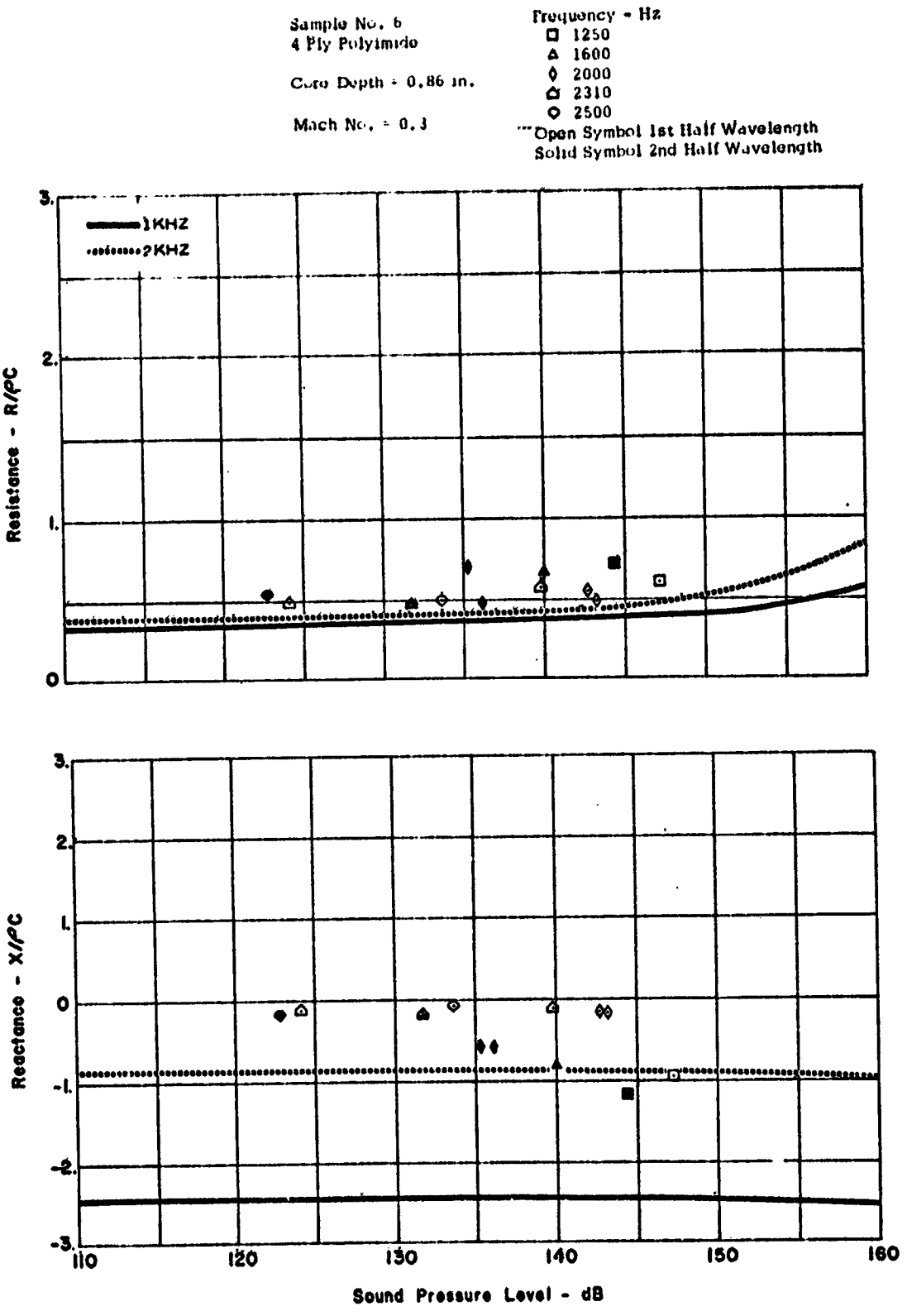

SAMPLE NO. 6, RESISTANCE AND REACTANCE DATA (0.3 MACH)
FIGURE 31

Sample No. 6
4 Ply Polyimide

Core Depth = 0.86 in.

Mach No. = 0.5

Frequency - Hz
□ 1250
△ 1600
◇ 2000
▽ 2416
Open Symbol 1st Half Wavelength
Solid Symbol 2nd Half Wavelength

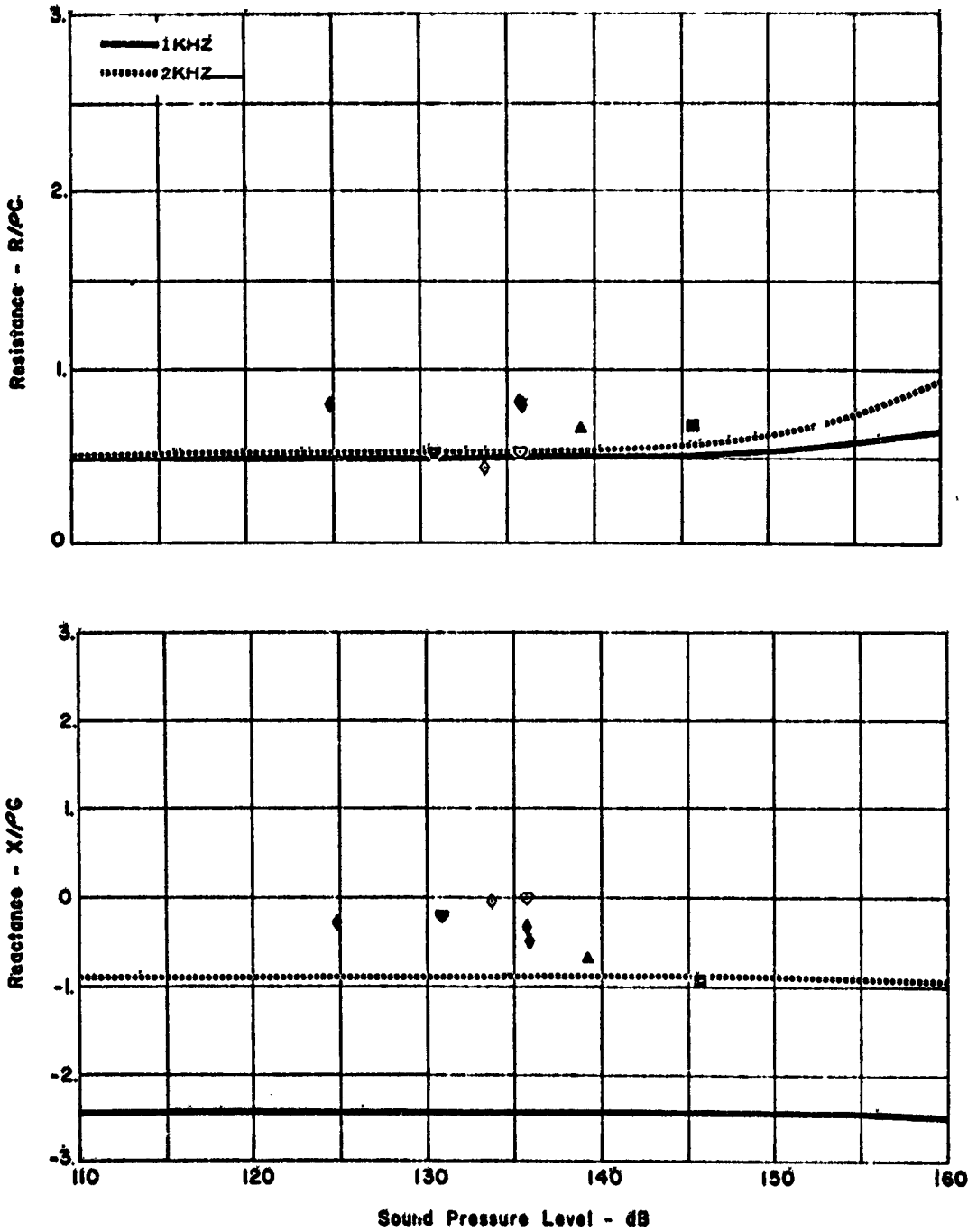

SAMPLE NO. 6, RESISTANCE AND REACTANCE DATA (0.5 MACH)
FIGURE 32

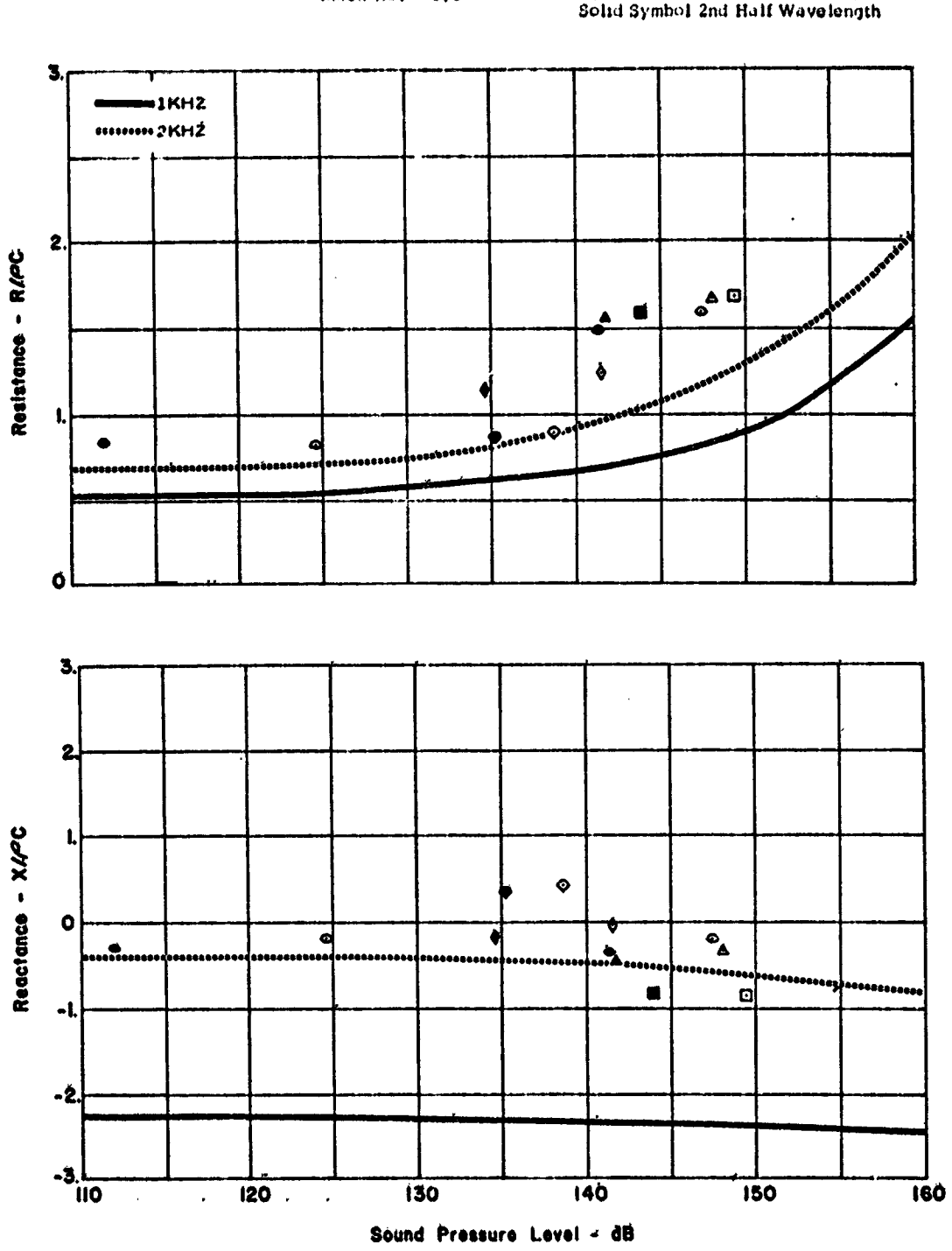

SAMPLE NO. 7, RESISTANCE AND REACTANCE DATA (0.0 MACH)
FIGURE 33

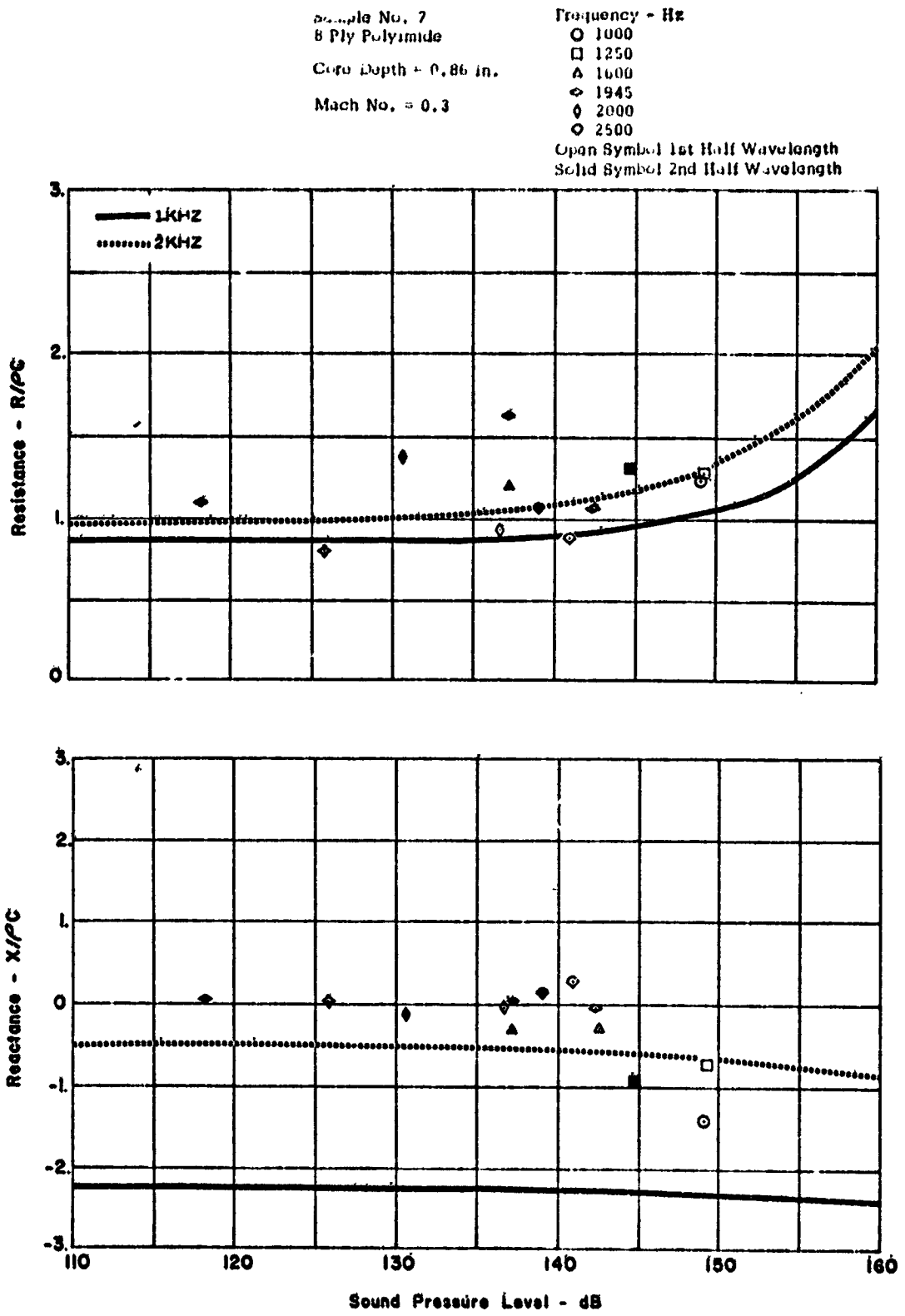

SAMPLE NO. 7, RESISTANCE AND REACTANCE DATA (0.3 MACH)
FIGURE 34

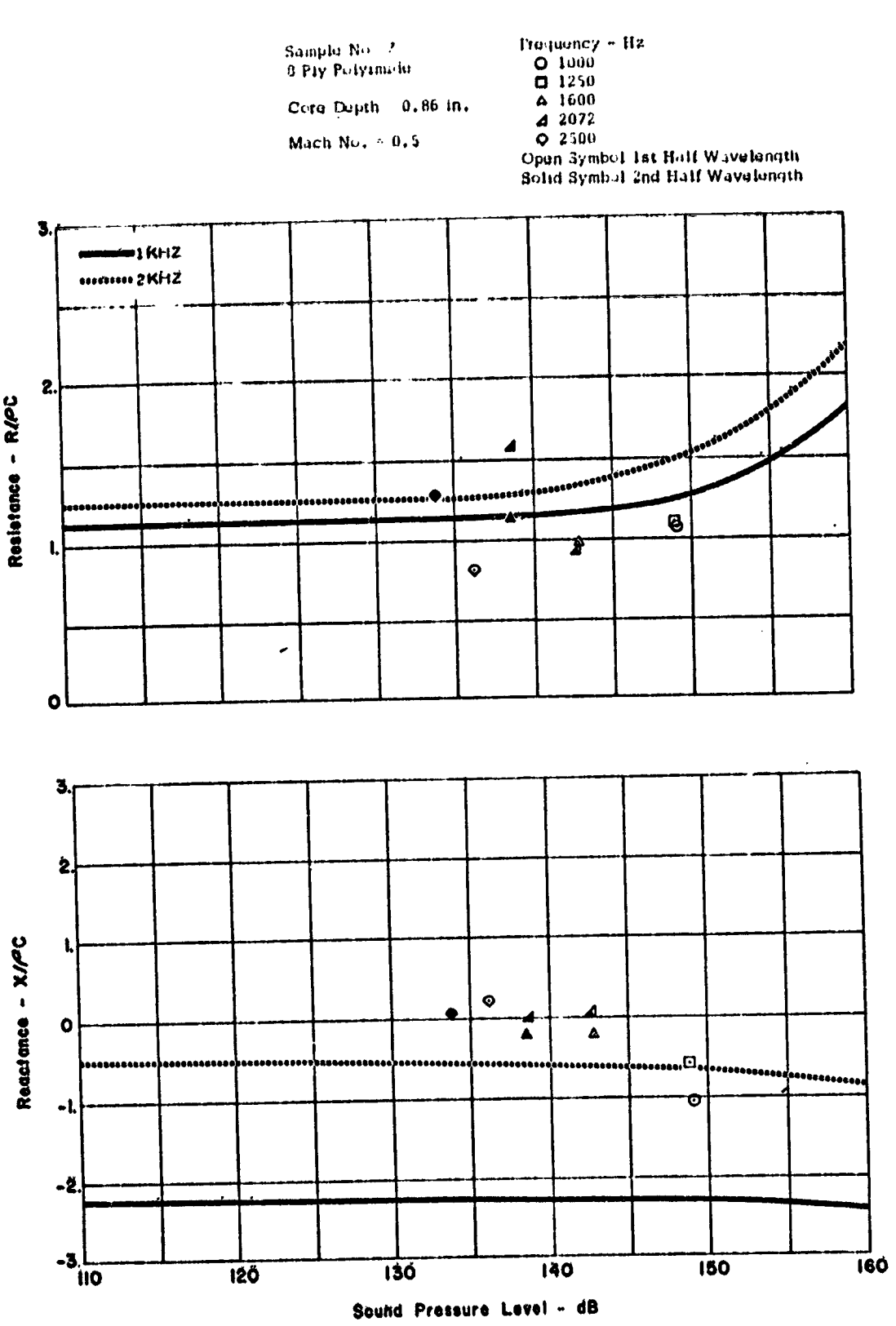

SAMPLE NO. 7, RESISTANCE AND REACTANCE DATA (0.5 MACH)
FIGURE 35

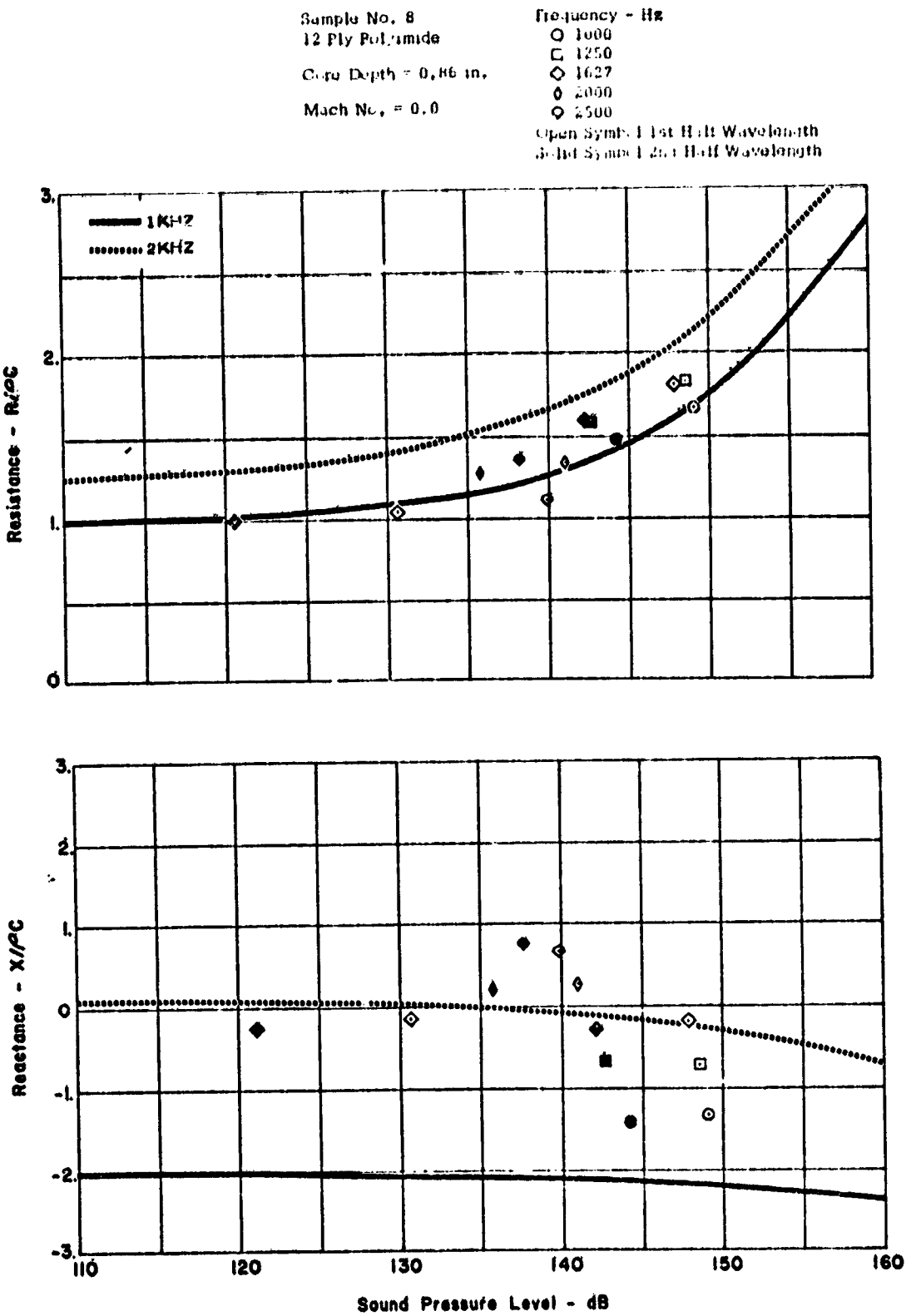

SAMPLE NO. 8, RESISTANCE AND REACTANCE DATA (0.0 MACH)
FIGURE 36

Sample No. 8
12 Ply Polyimide

Core Depth = 0.86 in.

Mach No. = 0.3

Frequency - Hz
▽ 1765
◊ 2000
○ 2500
Open Symbol 1st Half Wavelength
Solid Symbol 2nd Half Wavelength

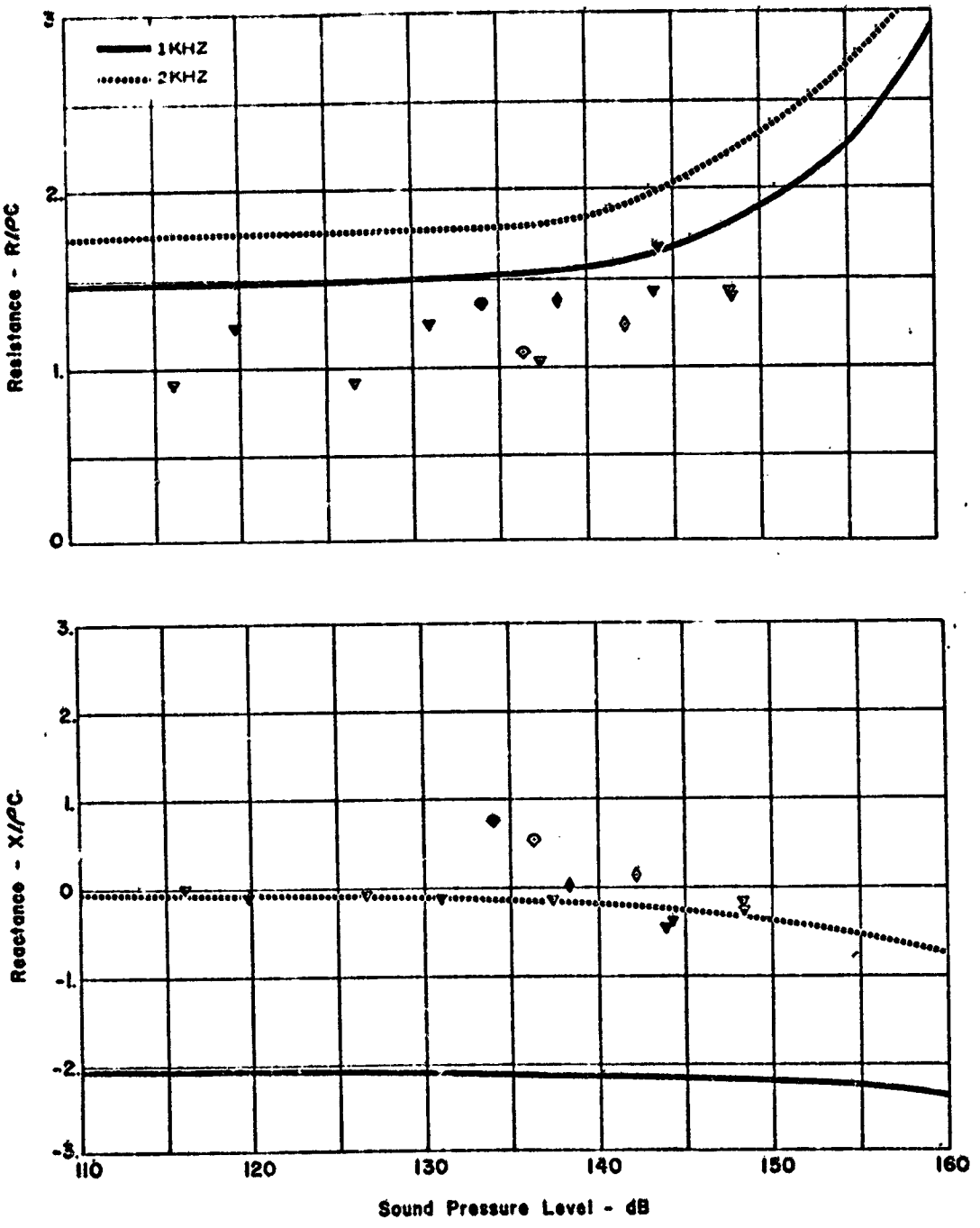

SAMPLE NO. 8, RESISTANCE AND REACTANCE DATA (0.3 MACH)
FIGURE 37

Sample No. 8
12 Ply Polyimide

Core Depth = 0.86 in.

Mach No. = 0.5

Frequency - Hz
△ 1600
◇ 1945
○ 2500
Open Symbol 1st Half Wavelength
Solid Symbol 2nd Half Wavelength

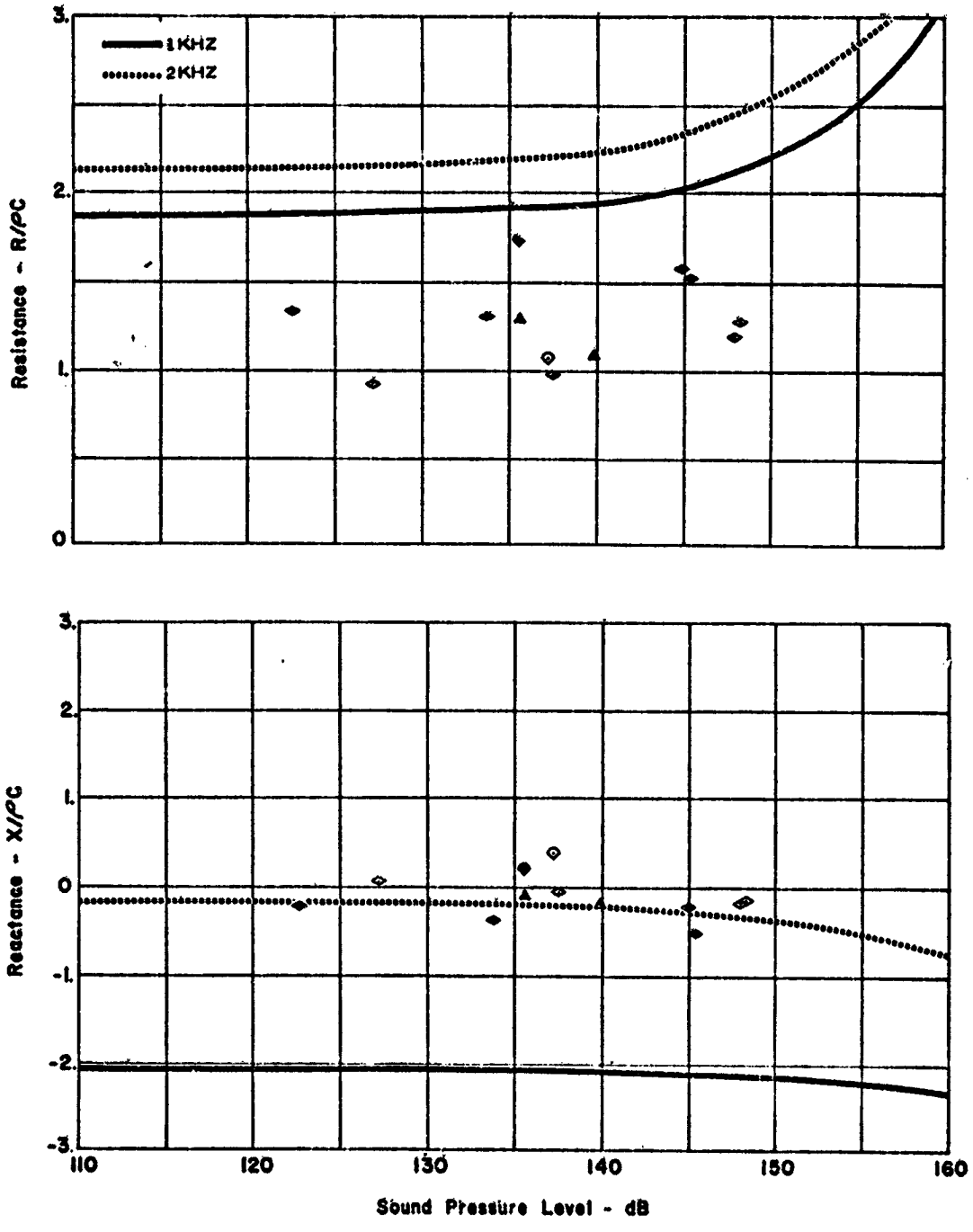

SAMPLE NO. 8, RESISTANCE AND REACTANCE DATA (0.5 MACH)
FIGURE 38

Sample No. 9
16 Ply Polyimide
Core Depth = 0.86 in.
Mach No. = 0.0

Frequency - Hz
□ 1250
△ 1600
Open Symbol 1st Half Wavelength
Solid Symbol 2nd Half Wavelength

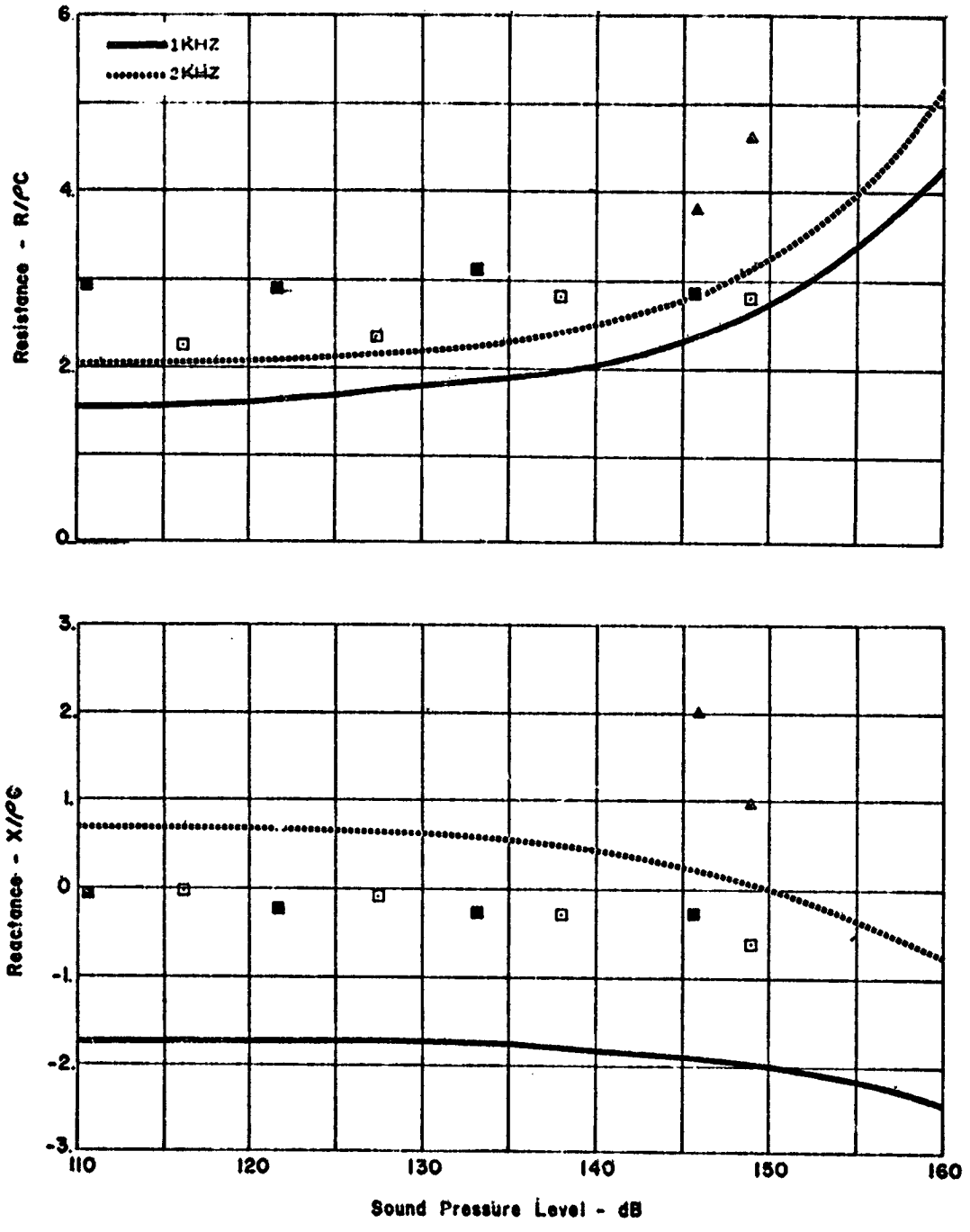

SAMPLE NO. 9, RESISTANCE AND REACTANCE DATA (0.0 MACH)
FIGURE 39

Sample No. 9
16 Ply Polyimide
Core Depth = 0.86 in.
Mach No. = 0.3

Frequency - Hz
□ 1250
△ 1600
Open Symbol 1st Half Wavelength
Solid Symbol 2nd Half Wavelength

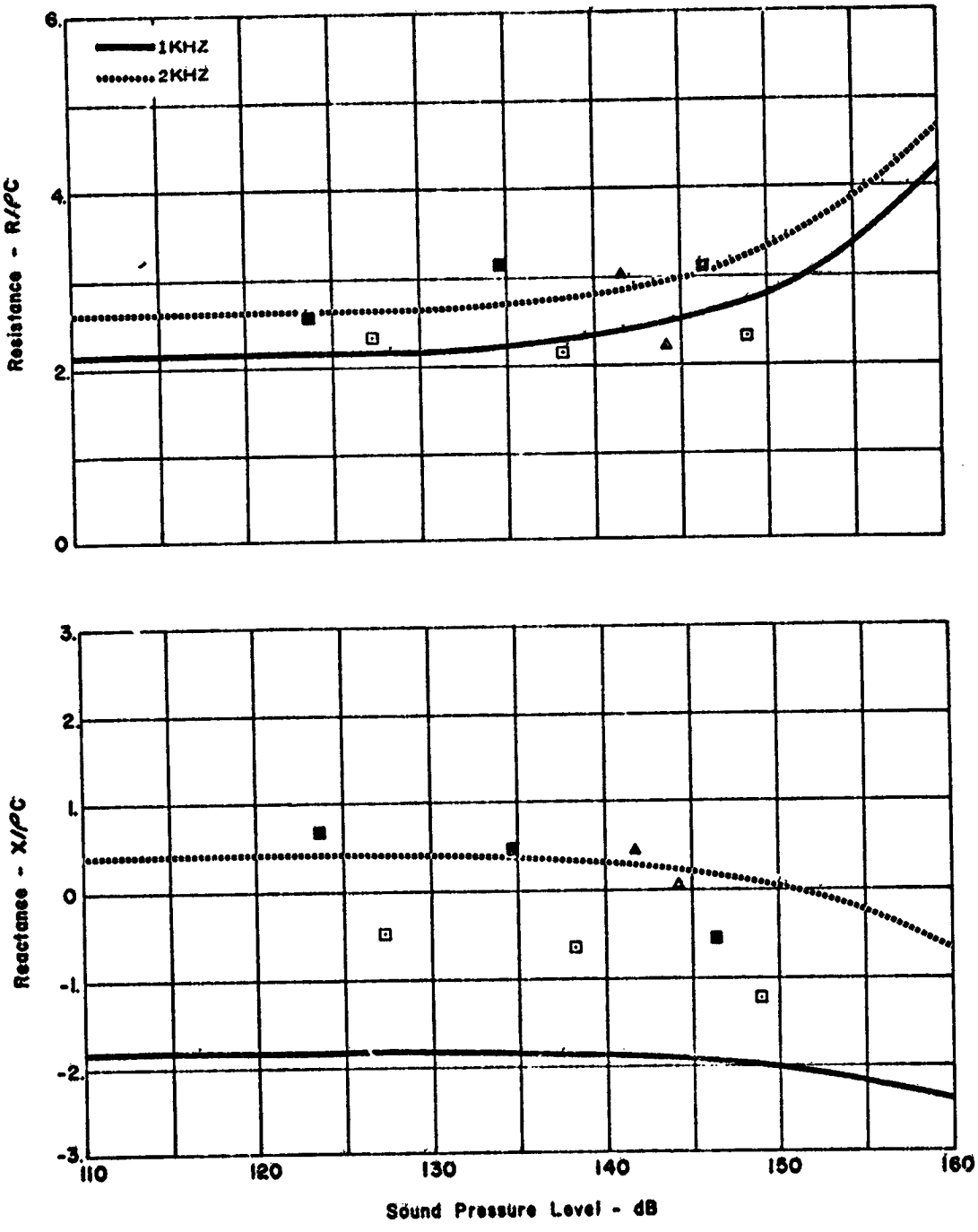

SAMPLE NO. 9, RESISTANCE AND REACTANCE DATA (0.3 MACH)
FIGURE 40

Sample No. 9
16 Ply Polyimide
Core Depth = 0.86 in.
Mach No. = 0.5

Frequency - Hz
□ 1250
△ 1600
◊ 2000
Open Symbol 1st Half Wavelength
Solid Symbol 2nd Half Wavelength

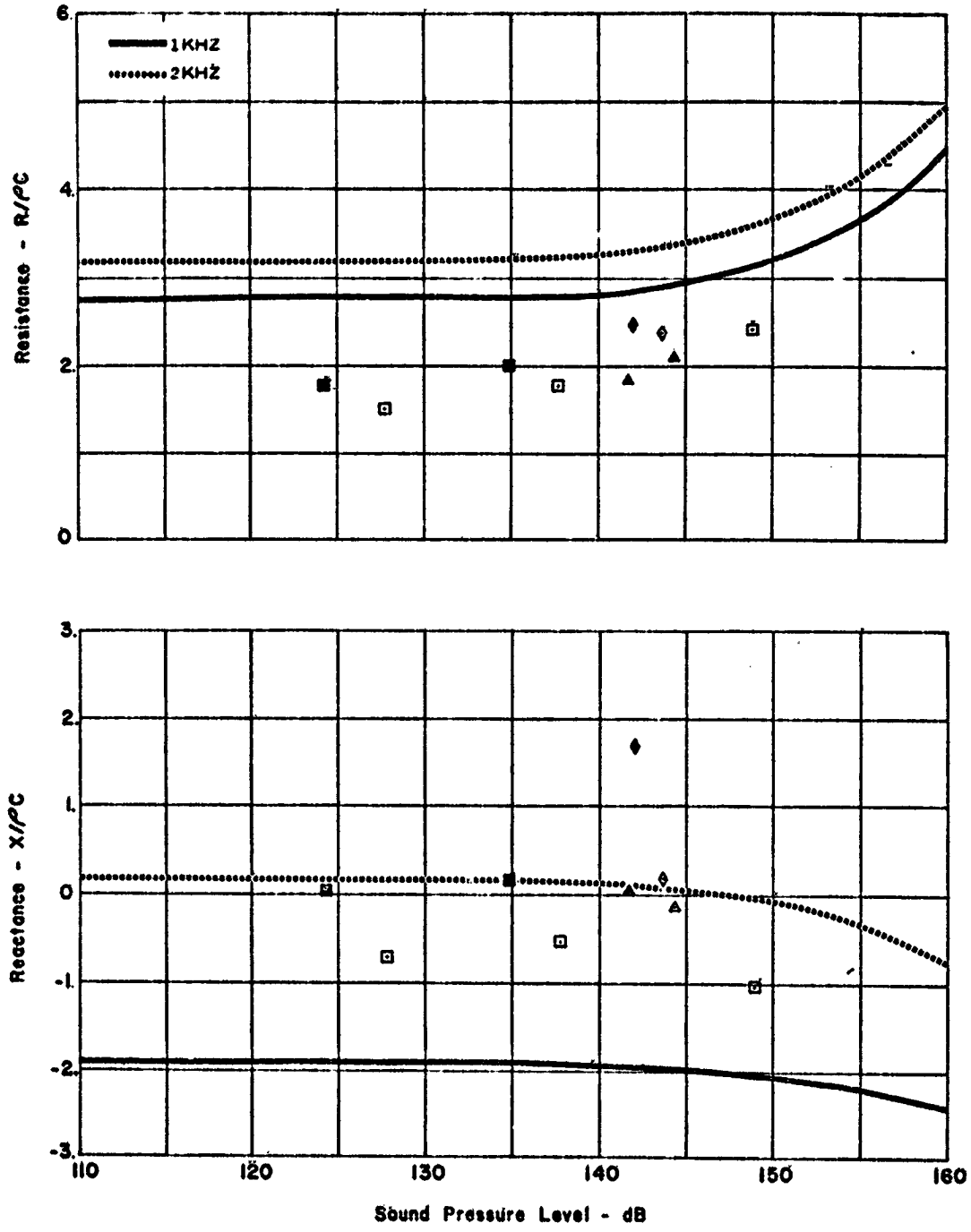

SAMPLE NO. 9, RESISTANCE AND REACTANCE DATA (0.5 MACH)
FIGURE 41

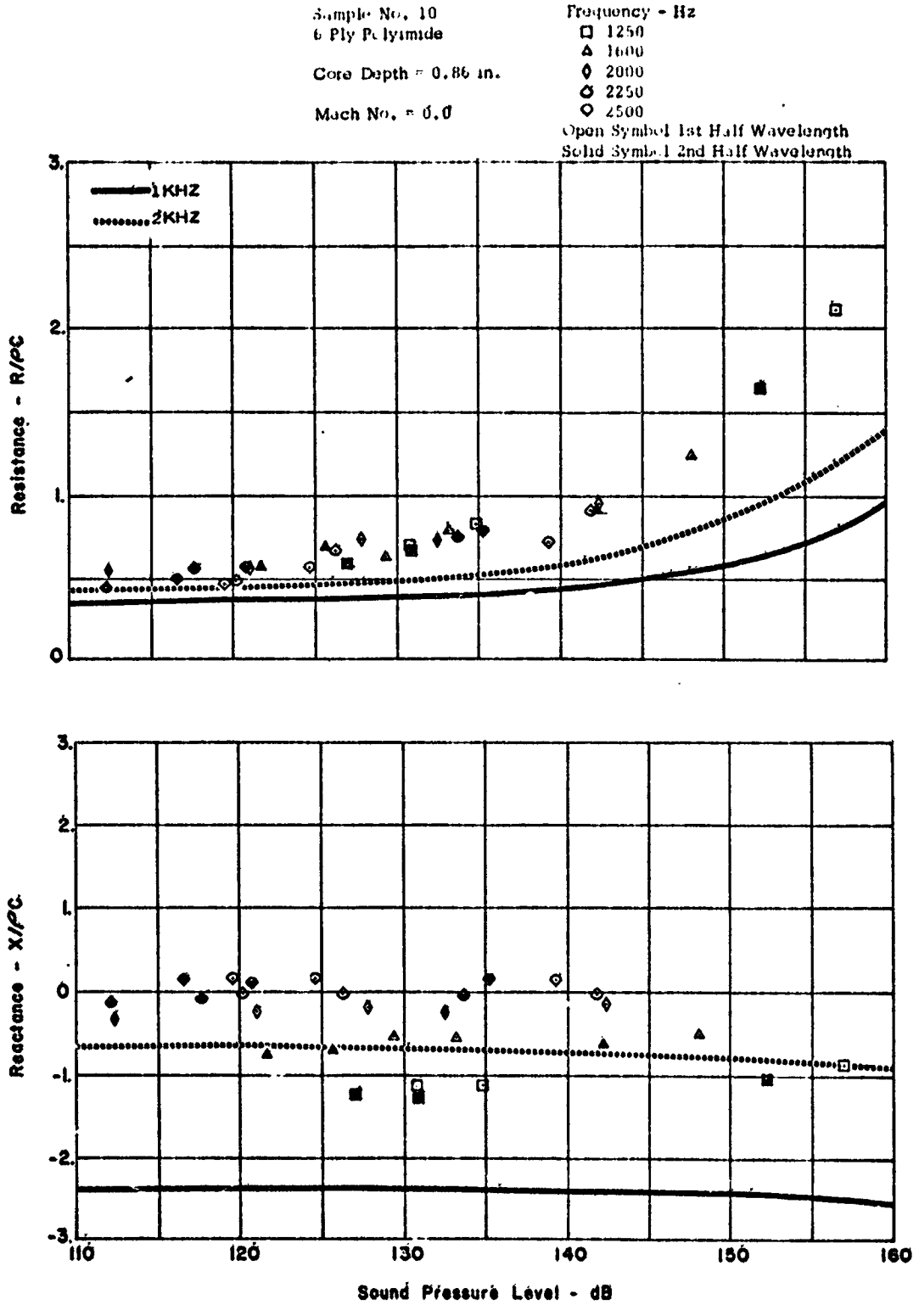

SAMPLE NO. 10, RESISTANCE AND REACTANCE DATA (0.0 MACH)
FIGURE 42

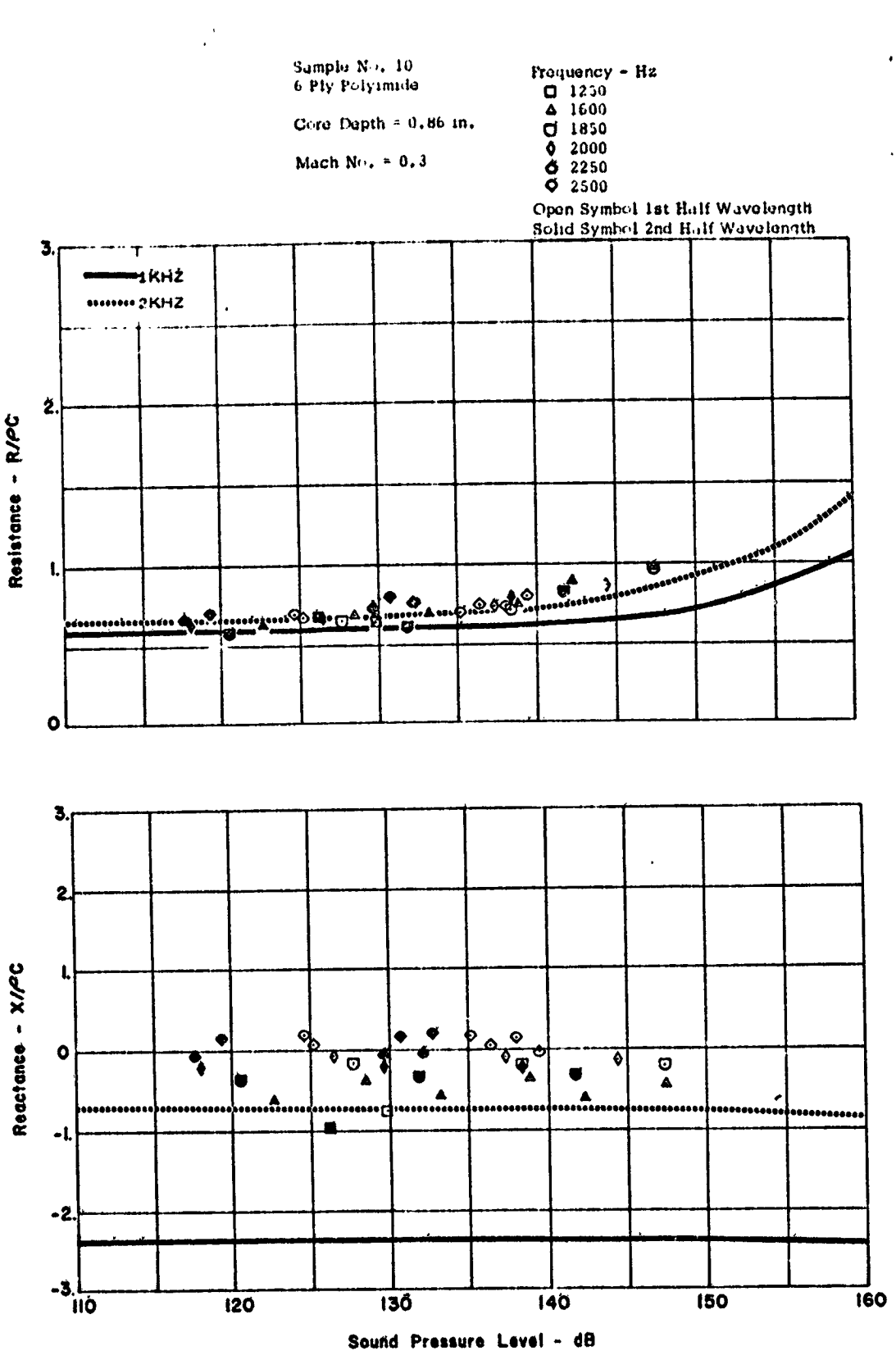

SAMPLE NO. 10, RESISTANCE AND REACTANCE DATA (0.3 MACH)
FIGURE 43

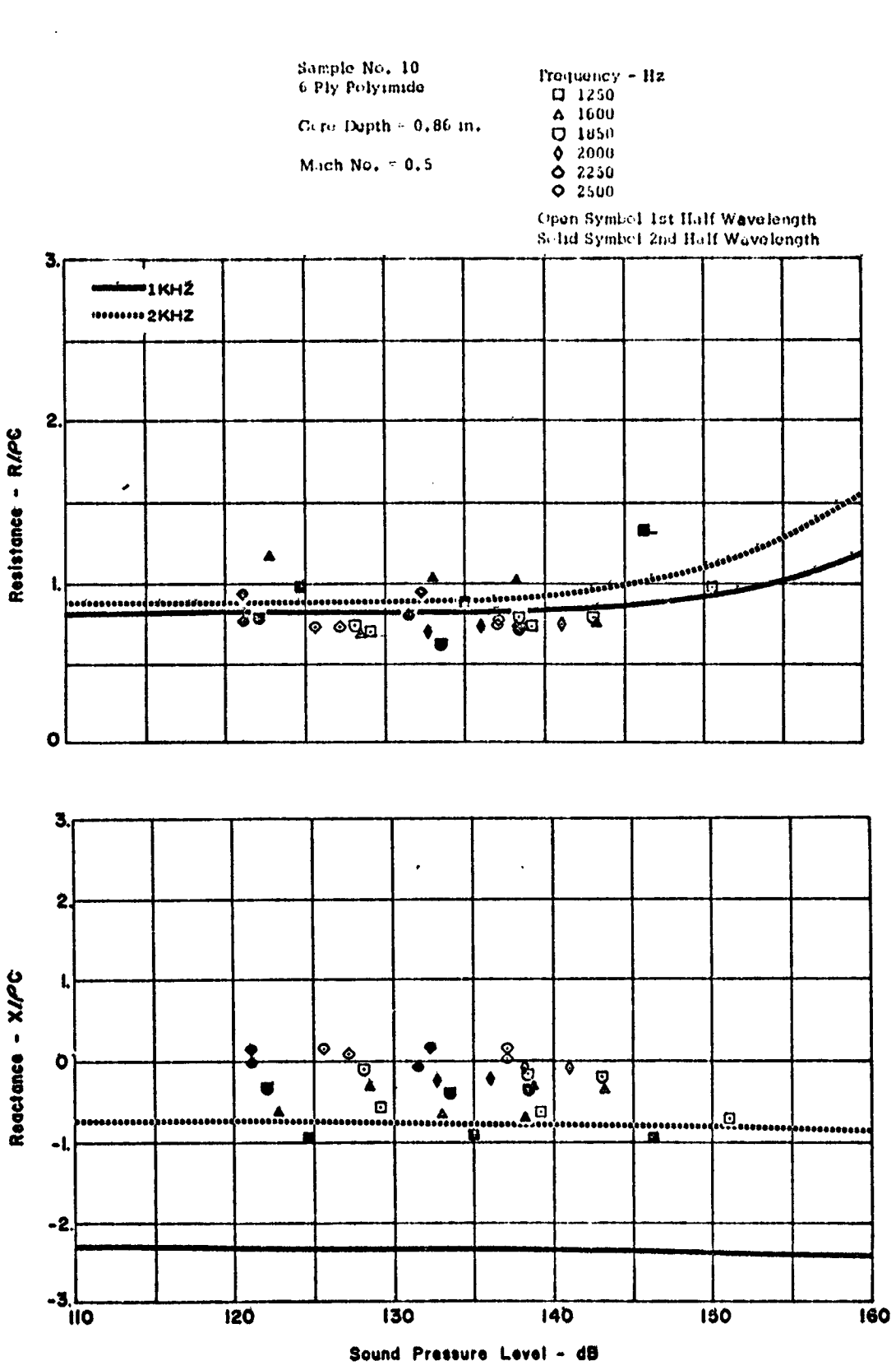

SAMPLE NO. 10, RESISTANCE AND REACTANCE DATA (0.5 MACH)
FIGURE 44

Sample No. 11
6 Ply Polyimide

Core Depth = 1.4 in.

Mach No. = 0.0

Frequency - Hz
- ○ 1000
- □ 1250
- △ 1600
- ▽ 1850
- ◇ 2000

Open Symbol 1st Half Wavelength
Solid Symbol 2nd Half Wavelength

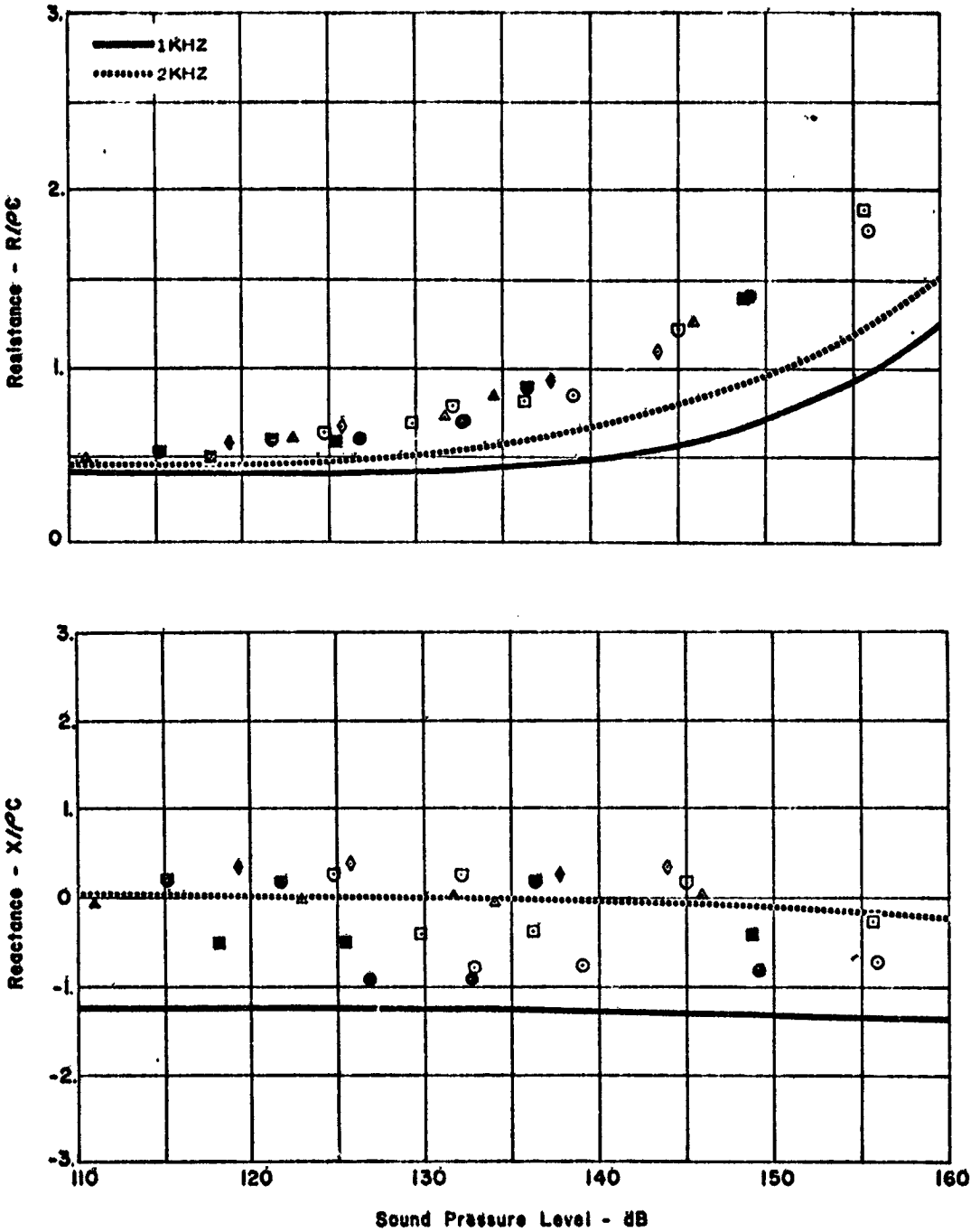

SAMPLE NO. 11, RESISTANCE AND REACTANCE DATA (0.0 MACH)
FIGURE 45

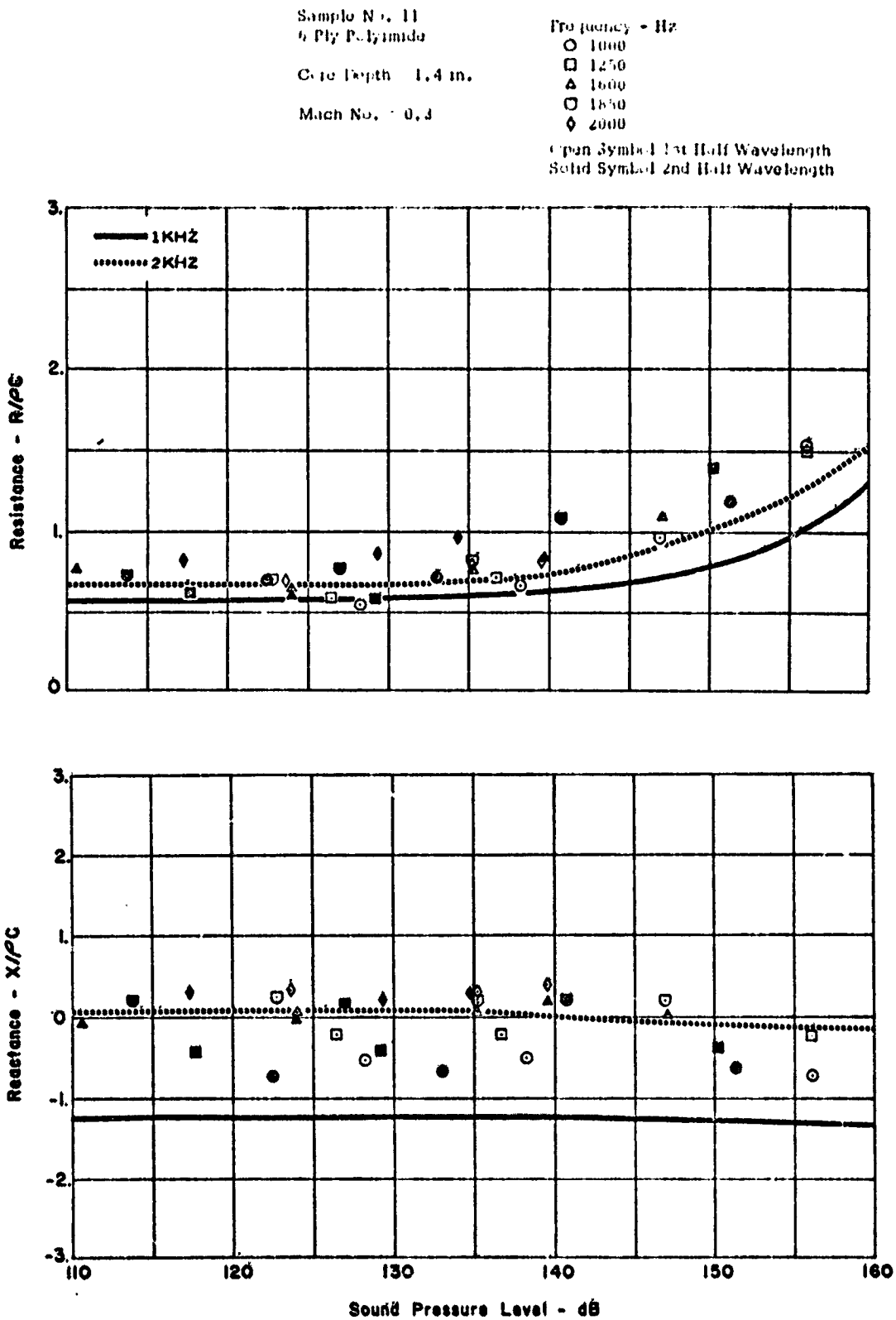

SAMPLE NO. 11, RESISTANCE AND REACTANCE DATA (0.3 MACH)
FIGURE 46

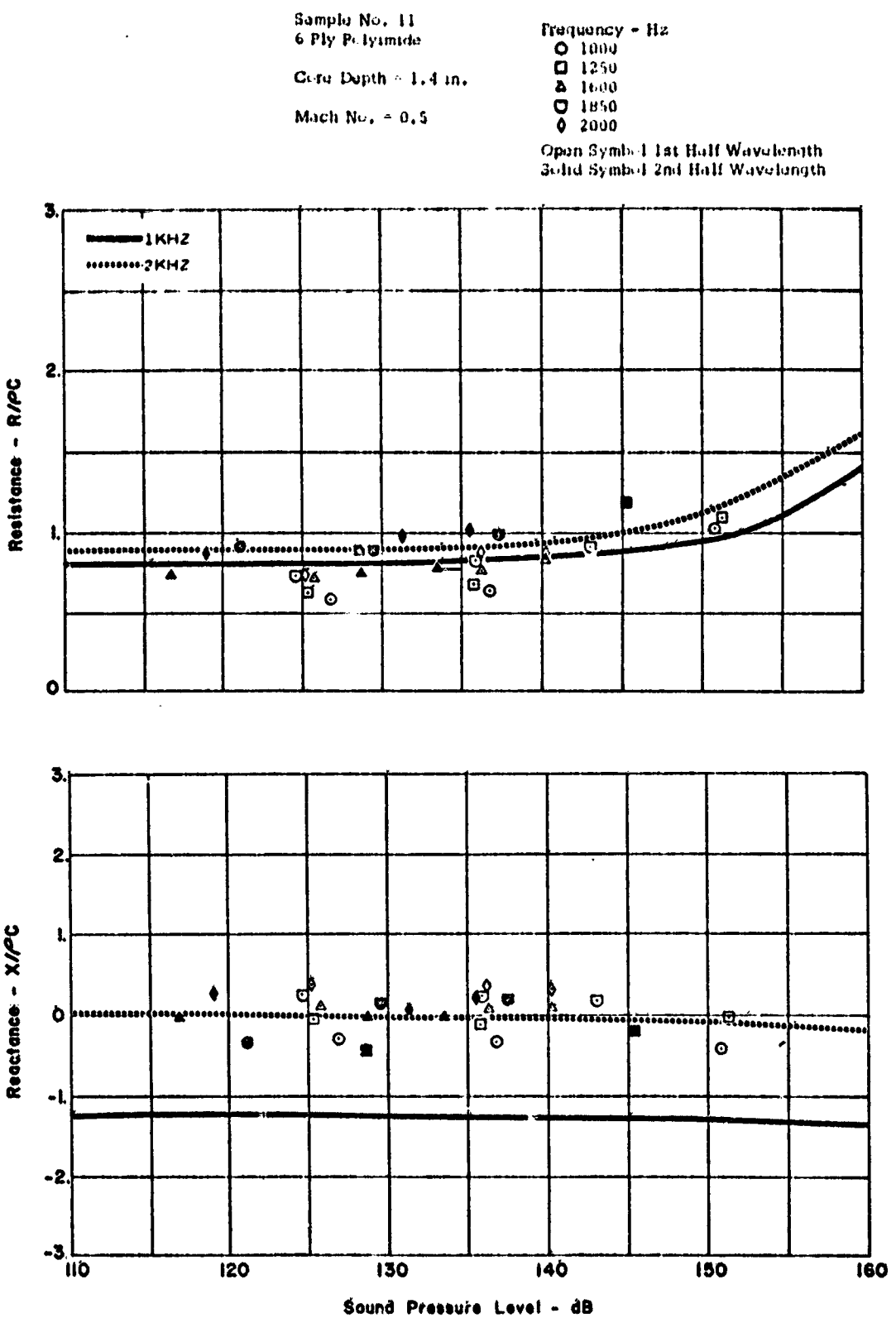

SAMPLE NO. 11, RESISTANCE AND REACTANCE DATA (0.5 MACH)
FIGURE 47

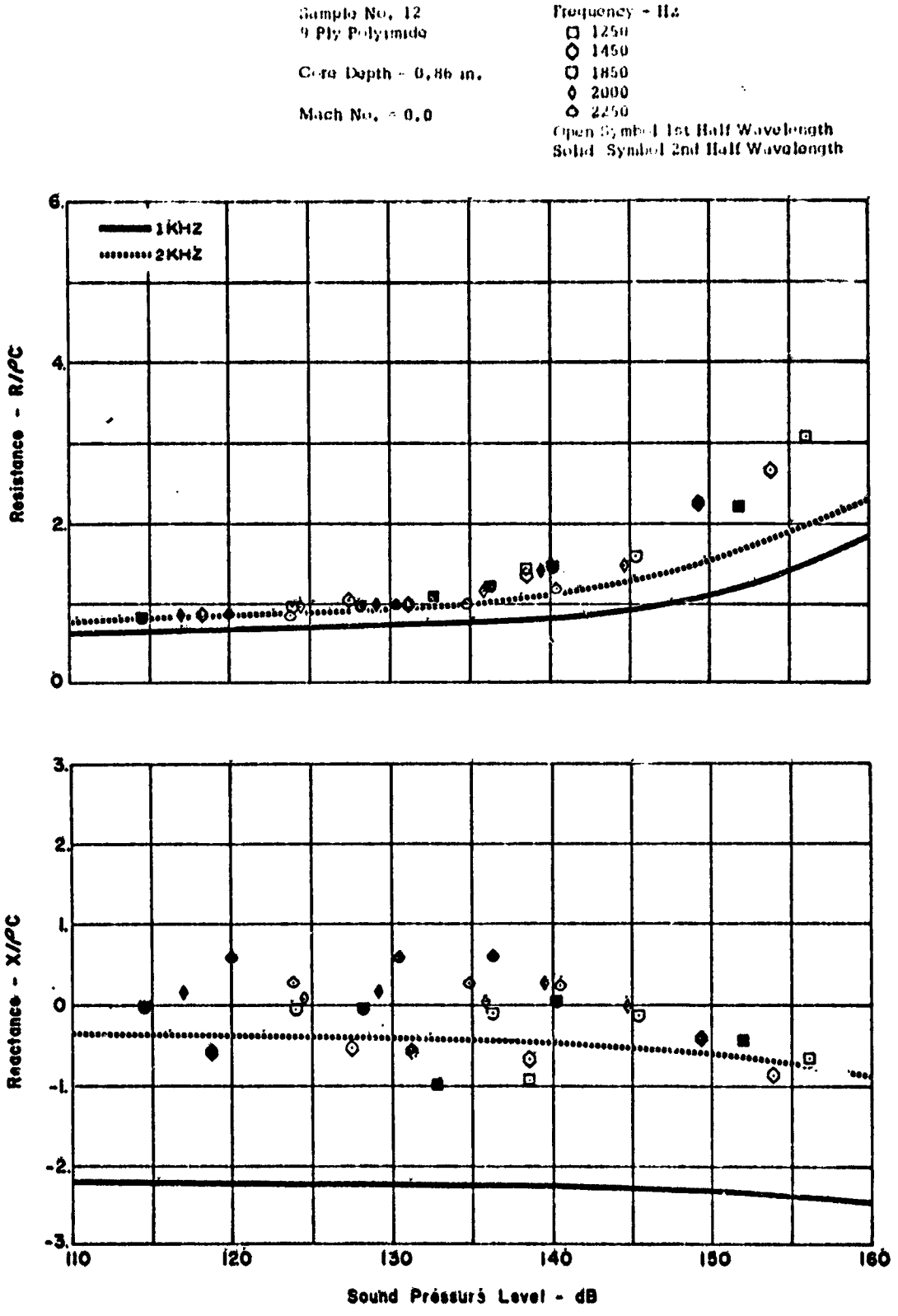

SAMPLE NO. 12, RESISTANCE AND REACTANCE DATA (0.0 MACH)
FIGURE 48

Sample No. 12
9 Ply Polyimide

C to Depth = 0.86 in.

Mach No. = 0.3

Frequency = Hz
- 1450
- 1600
- 1850
- 2000
- 2250

Open Symbol 1st Half Wavelength
Solid Symbol 2nd Half Wavelength

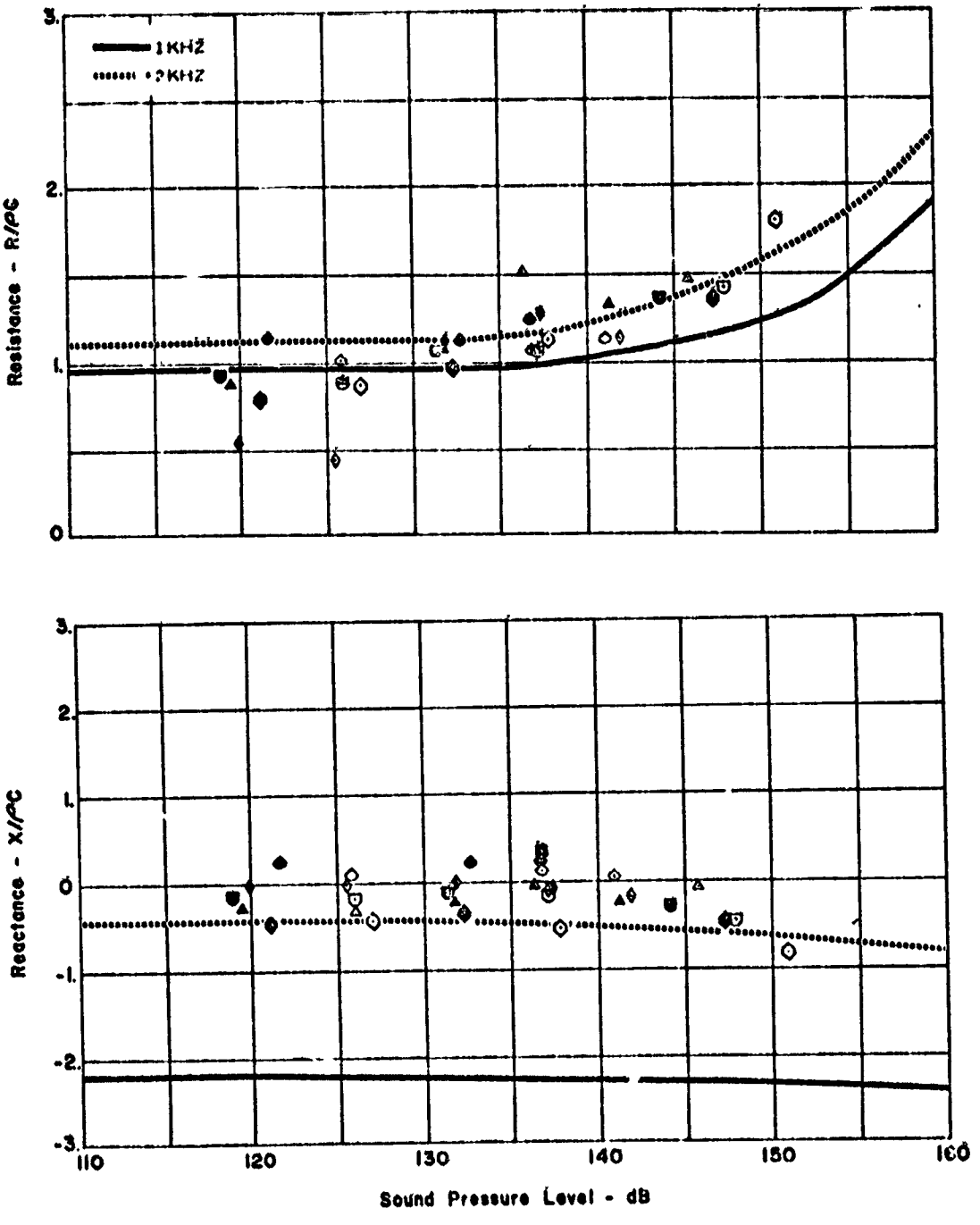

SAMPLE NO. 12, RESISTANCE AND REACTANCE DATA (0.3 MACH)
FIGURE 49

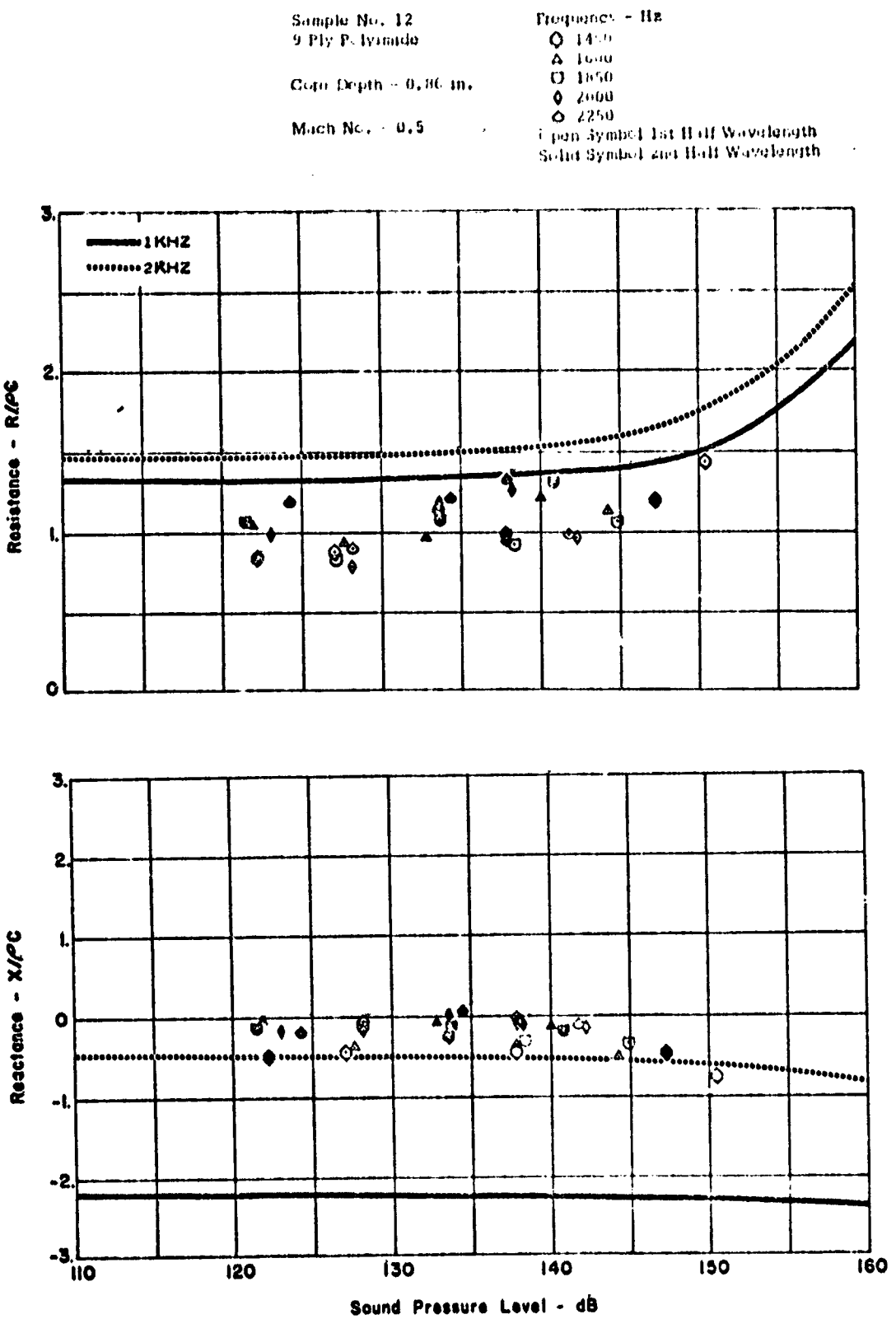

SAMPLE NO. 12, RESISTANCE AND REACTANCE DATA (0.5 MACH)
FIGURE 50

Sample No. 13
9 Ply Polyimide

Core Depth = 1.4 in.

Mach No. = 0.0

Frequency - Hz
- 800
- 1000
- 1250
- 1600
- 1850

Open Symbol 1st Half Wavelength
Solid Symbol 2nd Half Wavelength

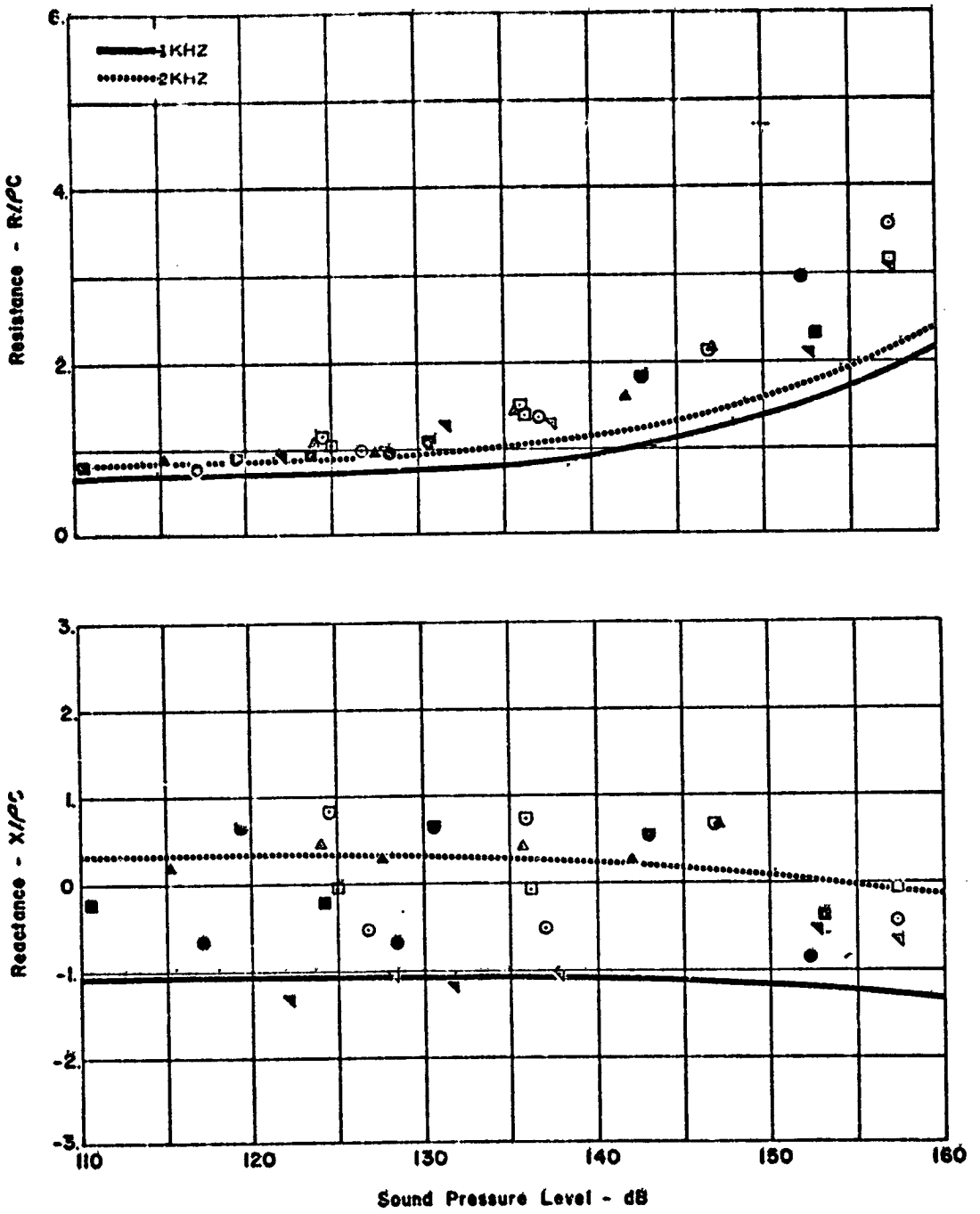

SAMPLE NO. 13, RESISTANCE AND REACTANCE DATA (0.0 MACH)
FIGURE 51

Sample No. 13
9 Pl; Polyimide

Core Depth - 1.4 in.

Mach No. - 0.3

Frequency - Hz
- ○ 1000
- □ 1250
- △ 1600
- ▽ 1750
- ◇ 2000

Open Symbol 1st Half Wavelength
Solid Symbol 2nd Half Wavelength

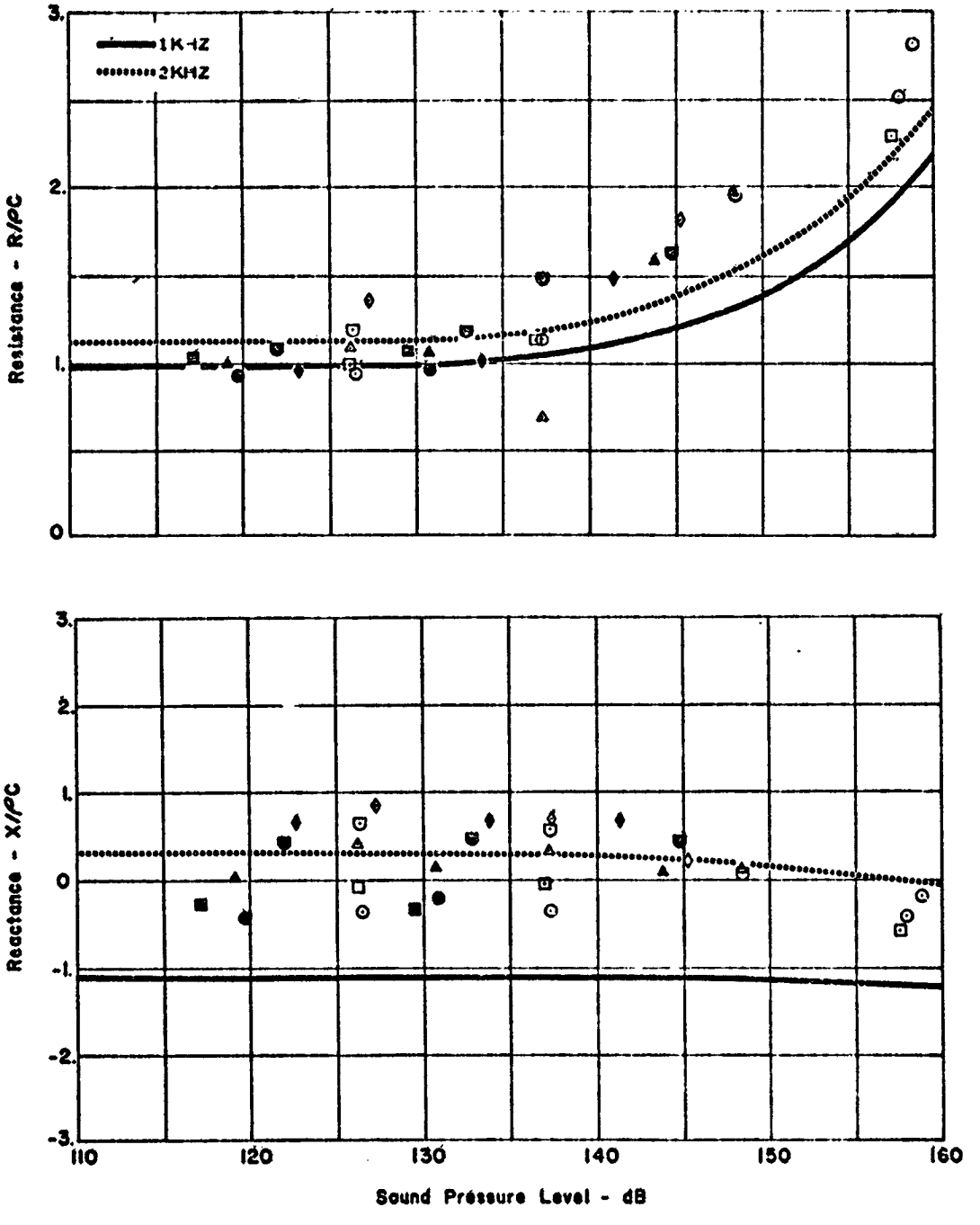

SAMPLE NO. 13, RESISTANCE AND REACTANCE DATA (0.3 MACH)
FIGURE 52

Sample No. 13
9 Ply Polyimide

Core Depth = 1.4 in.

Mach No. = 0.5

Frequency - Hz
- ○ 1000
- □ 1250
- △ 1600
- ⬡ 1850
- ◇ 2000

Open Symbol 1st Half Wavelength
Solid Symbol 2nd Half Wavelength

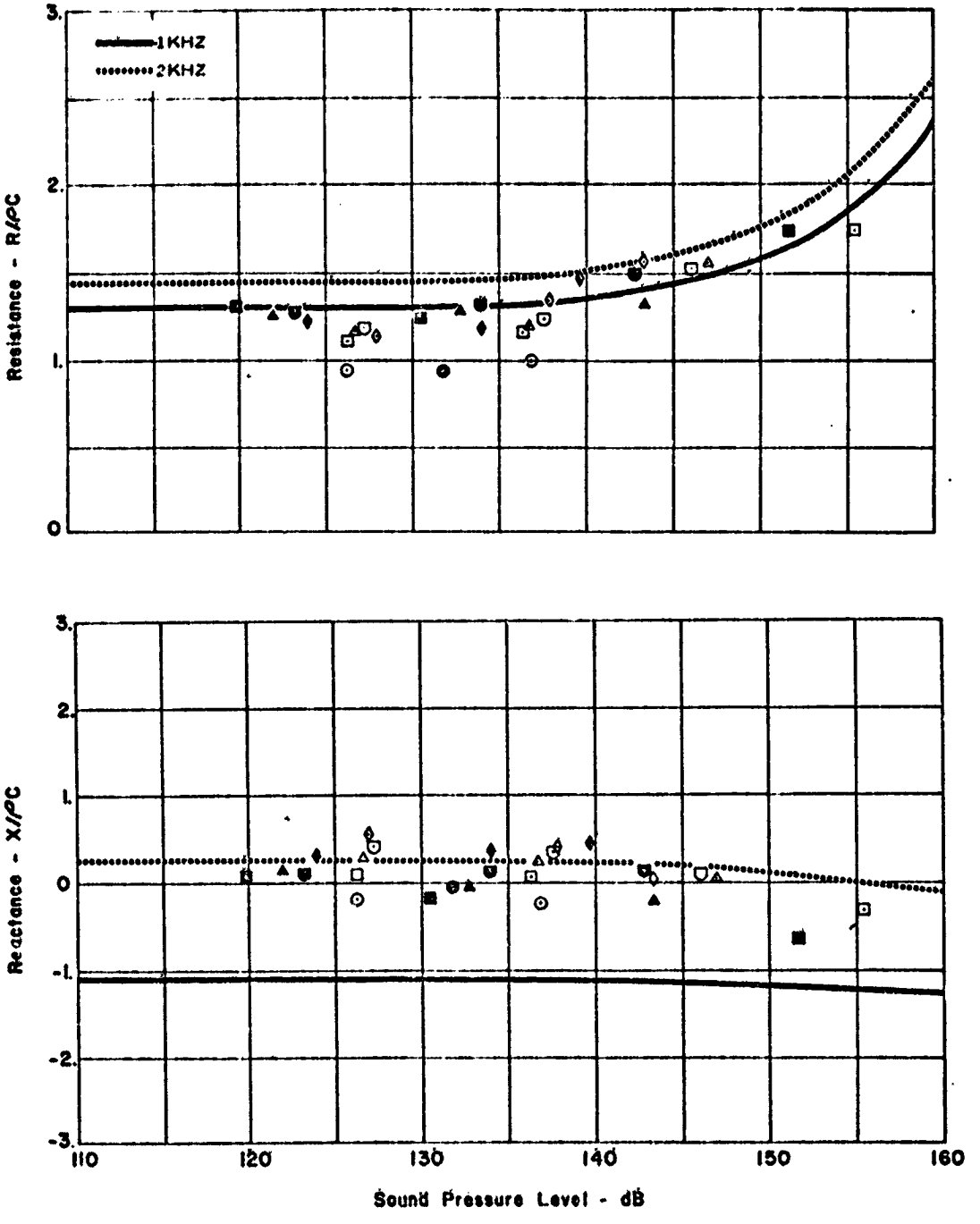

SAMPLE NO. 13, RESISTANCE AND REACTANCE DATA (0.5 MACH)
FIGURE 53

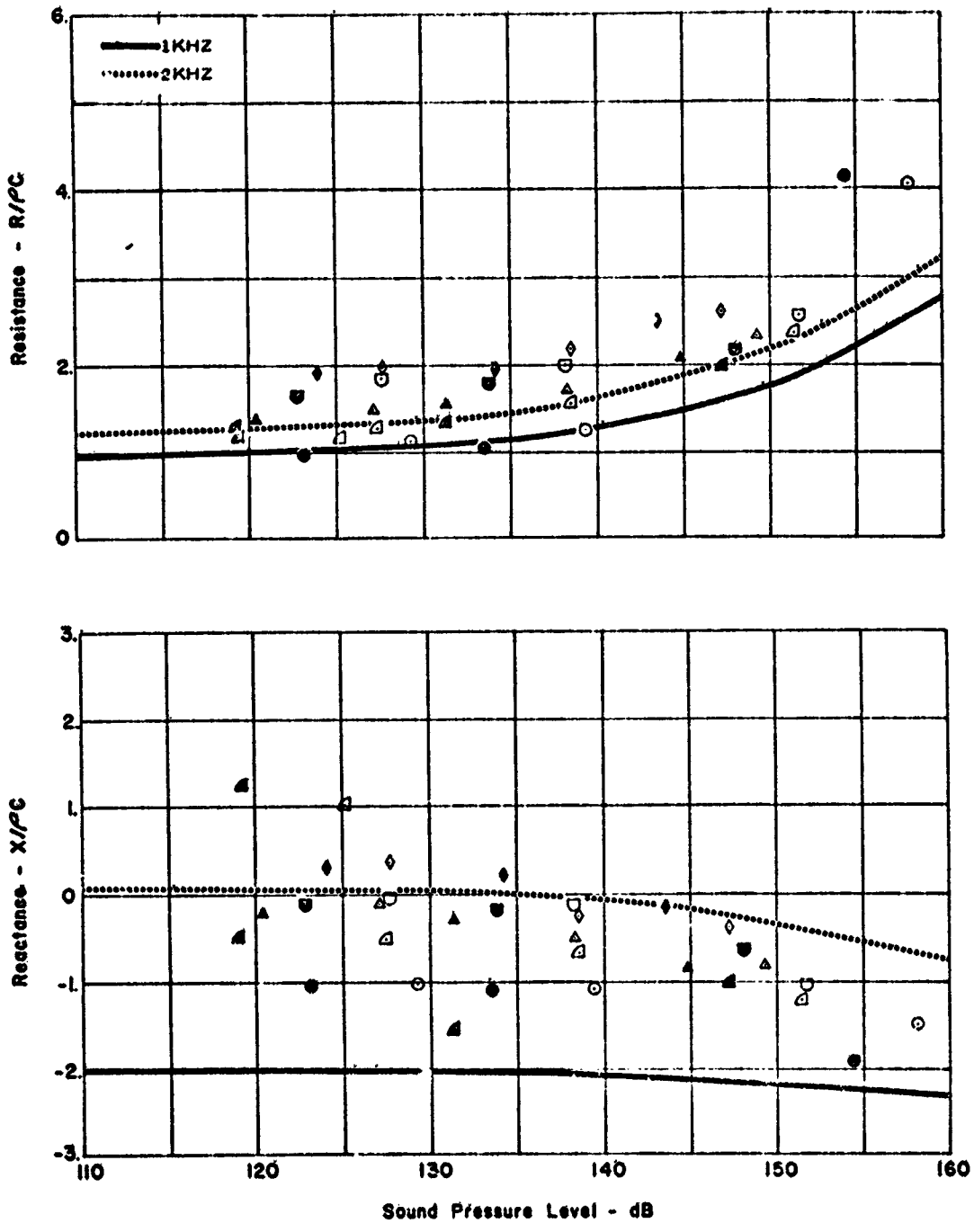

SAMPLE NO. 14, RESISTANCE AND REACTANCE DATA (0.0 MACH)
FIGURE 54

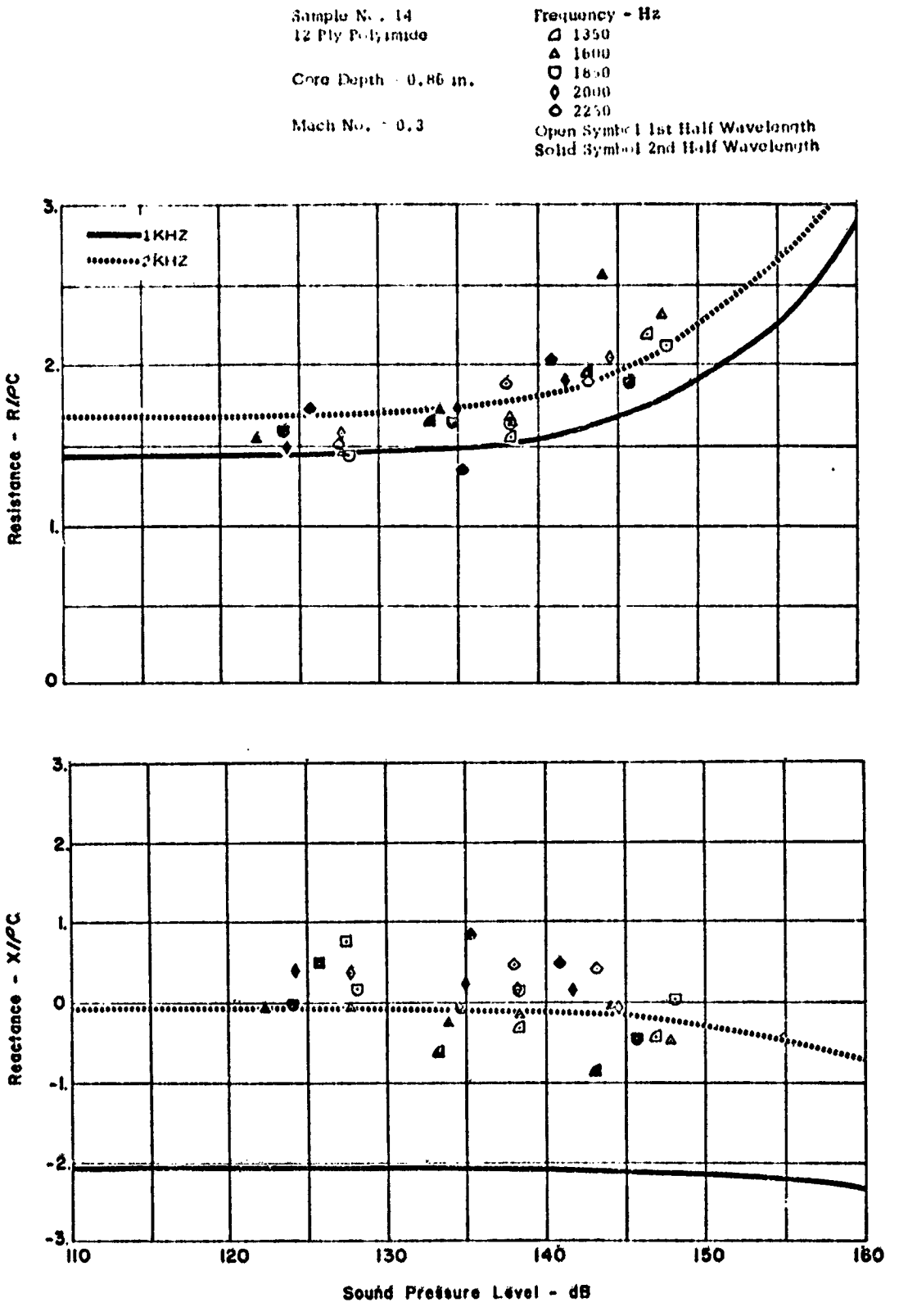

SAMPLE NO. 14, RESISTANCE AND REACTANCE DATA (0.3 MACH)
FIGURE 55

Sample No. 14
12 Ply Polyimide

Core Depth 0.86 in.

Mach No. = 0.5

Frequency - Hz
- 1350
- 1600
- 1850
- 2000
- 2250

Open Symbol 1st Half Wavelength
Solid Symbol 2nd Half Wavelength

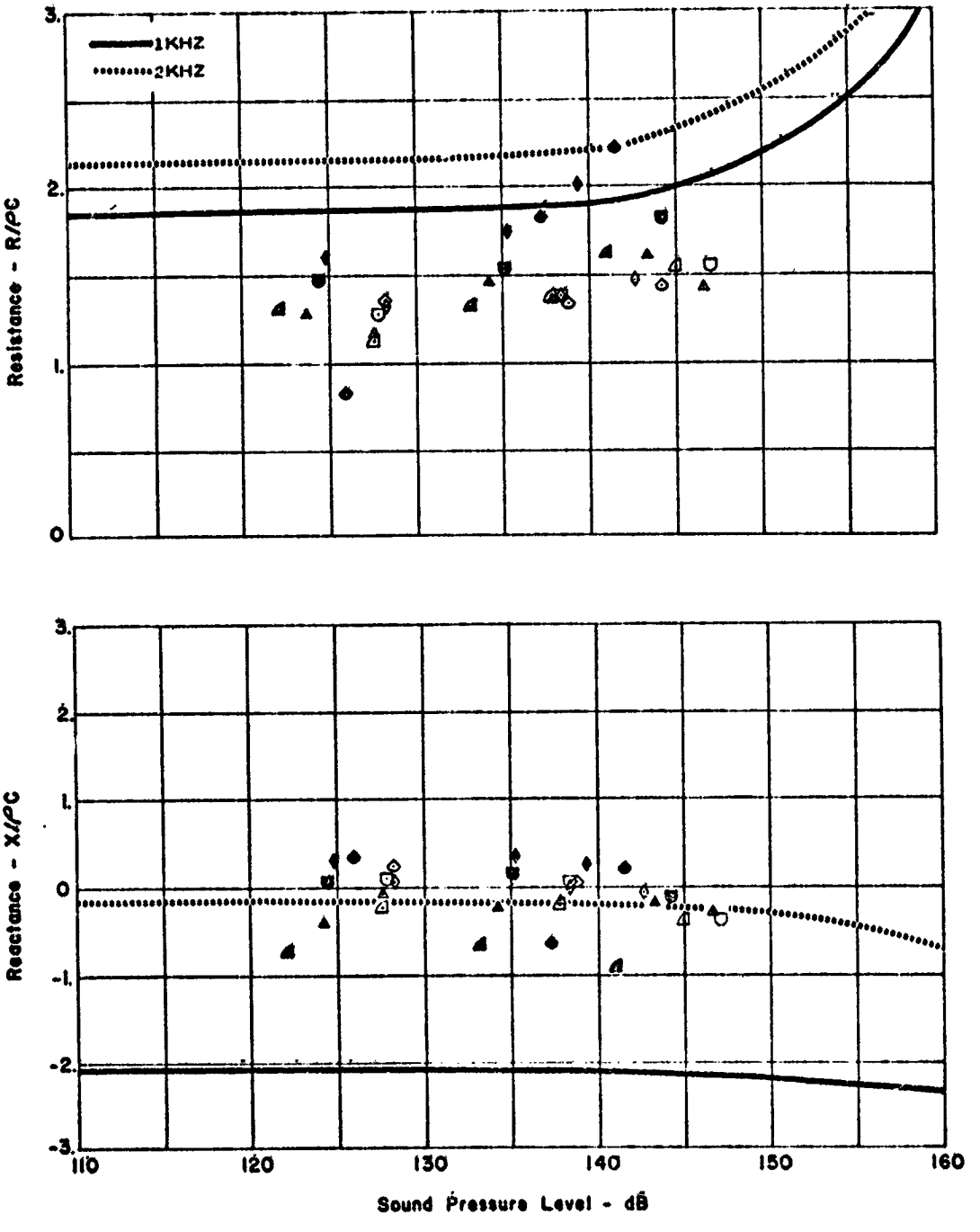

SAMPLE NO. 14, RESISTANCE AND REACTANCE DATA (0.5 MACH)
FIGURE 56

Sample No. 15
12 Ply Polyimide

Core Depth = 1.4 in.

Mach No. = 0.0

Frequency - Hz
800
1000
1250
1600
1850
Open Symbol 1st Half Wavelength
Solid Symbol 2nd Half Wavelength

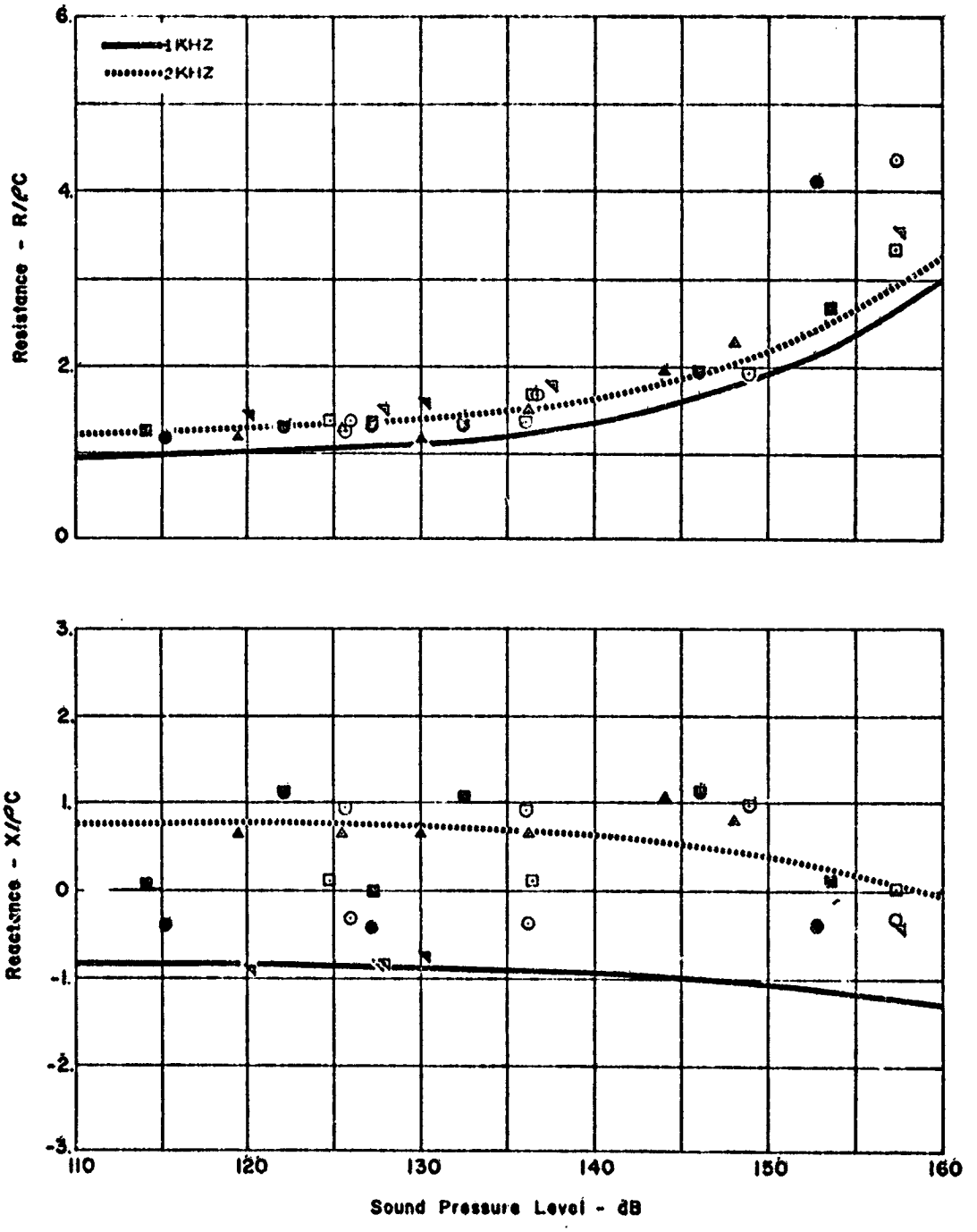

SAMPLE NO. 15, RESISTANCE AND REACTANCE DATA (0.0 MACH)
FIGURE 57

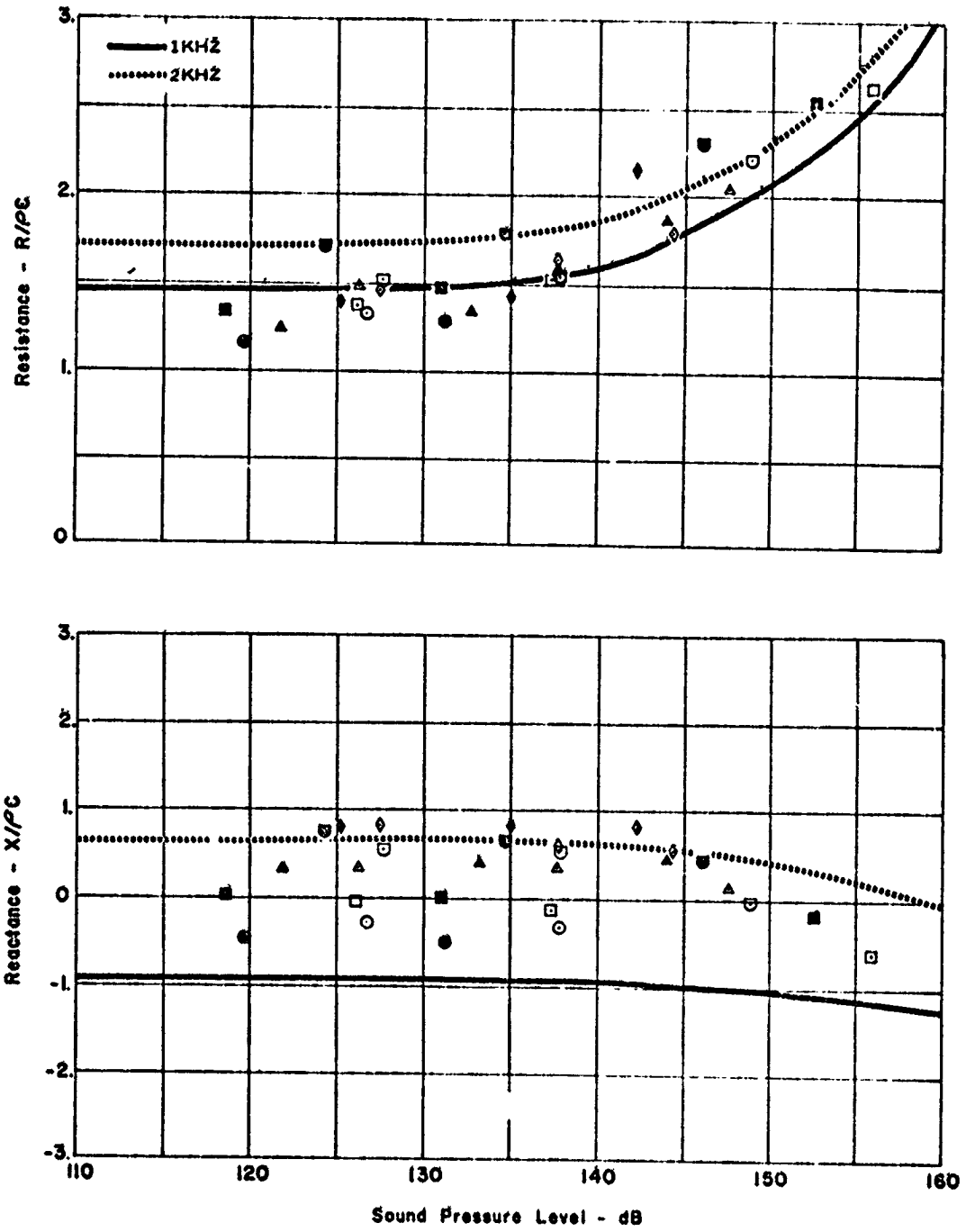

SAMPLE NO. 15, RESISTANCE AND REACTANCE DATA (0.3 MACH)
FIGURE 58

Sample No. 15
12 Ply Polyimide

Core Depth = 1.4 in.

Mach No. = 0.5

Frequency - Hz
○ 1000
□ 1250
△ 1600
⊡ 1850
◊ 2000
Open Symbol 1st Half Wavelength
Solid Symbol 2nd Half Wavelength

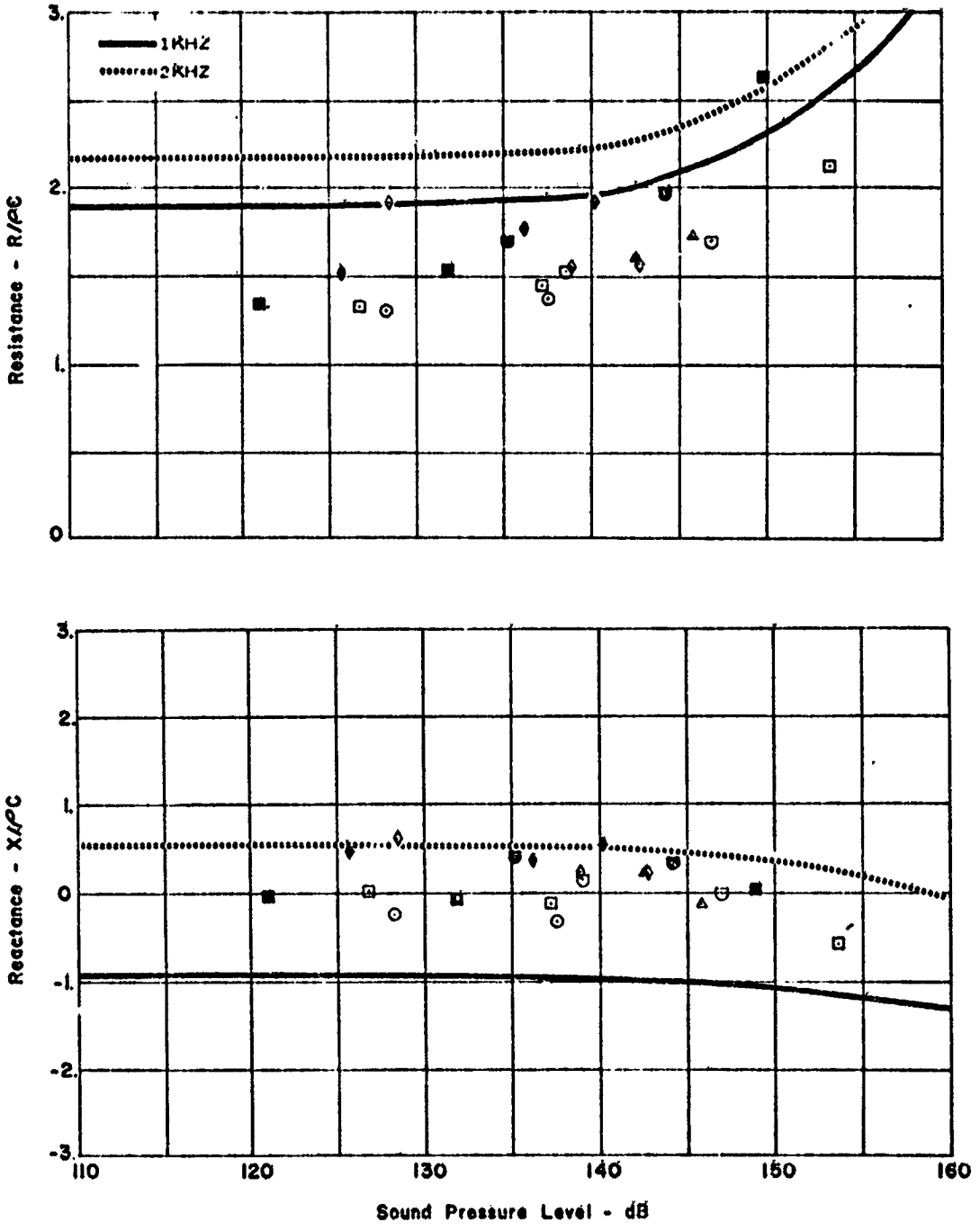

SAMPLE NO. 15, RESISTANCE AND REACTANCE DATA (0.5 MACH)
FIGURE 59

Sample No. 16
15 Ply Polyimide

Core Depth = 0.86 in.

Mach No. = 0.0

Frequency - Hz
800
1000
1350
1650
1850

Open Symbol 1st Half Wavelength
Solid Symbol 2nd Half Wavelength

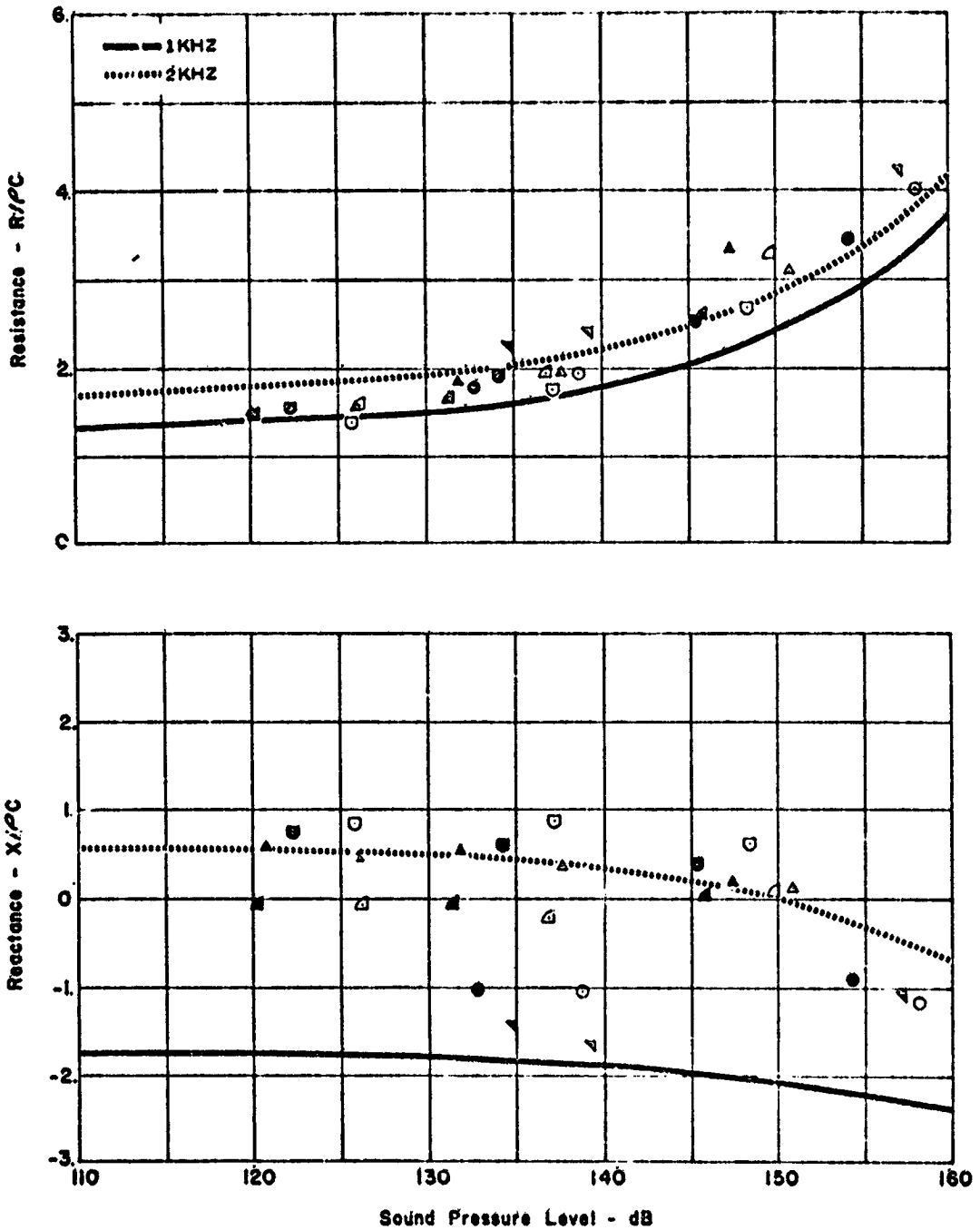

SAMPLE NO. 16, RESISTANCE AND REACTANCE DATA (0.0 MACH)
FIGURE 60

Sample No., 16
15 Ply Polyimide

Core Depth = 0.86 in.

Mach No. = 0.3

Frequency - Hz
- O 1000
- 1350
- 1600
- 1850
- 2000

Open Symbol 1st Half Wavelength
Solid Symbol 2nd Half Wavelength

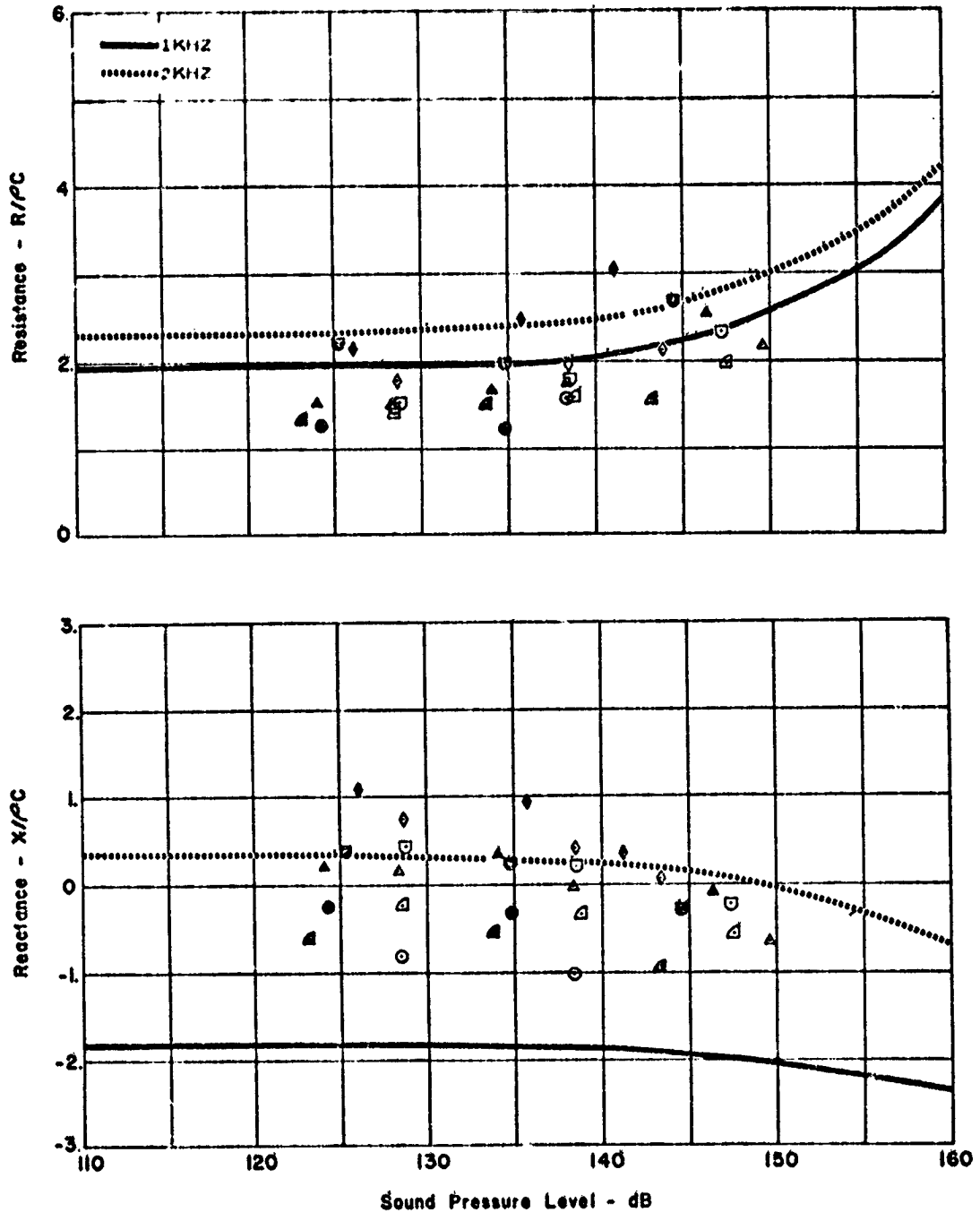

SAMPLE NO. 16, RESISTANCE AND REACTANCE DATA (0.3 MACH)
FIGURE 61

Sample No. 16
16 Ply Polyimide

Core Depth = 0.86 in.

Mach No. = 0.5

Frequency - Hz
- O 1400
- Δ 1450
- △ 1500
- □ 1850
- ◊ 2000

Open Symbol 1st Half Wavelength
Solid Symbol 2nd Half Wavelength

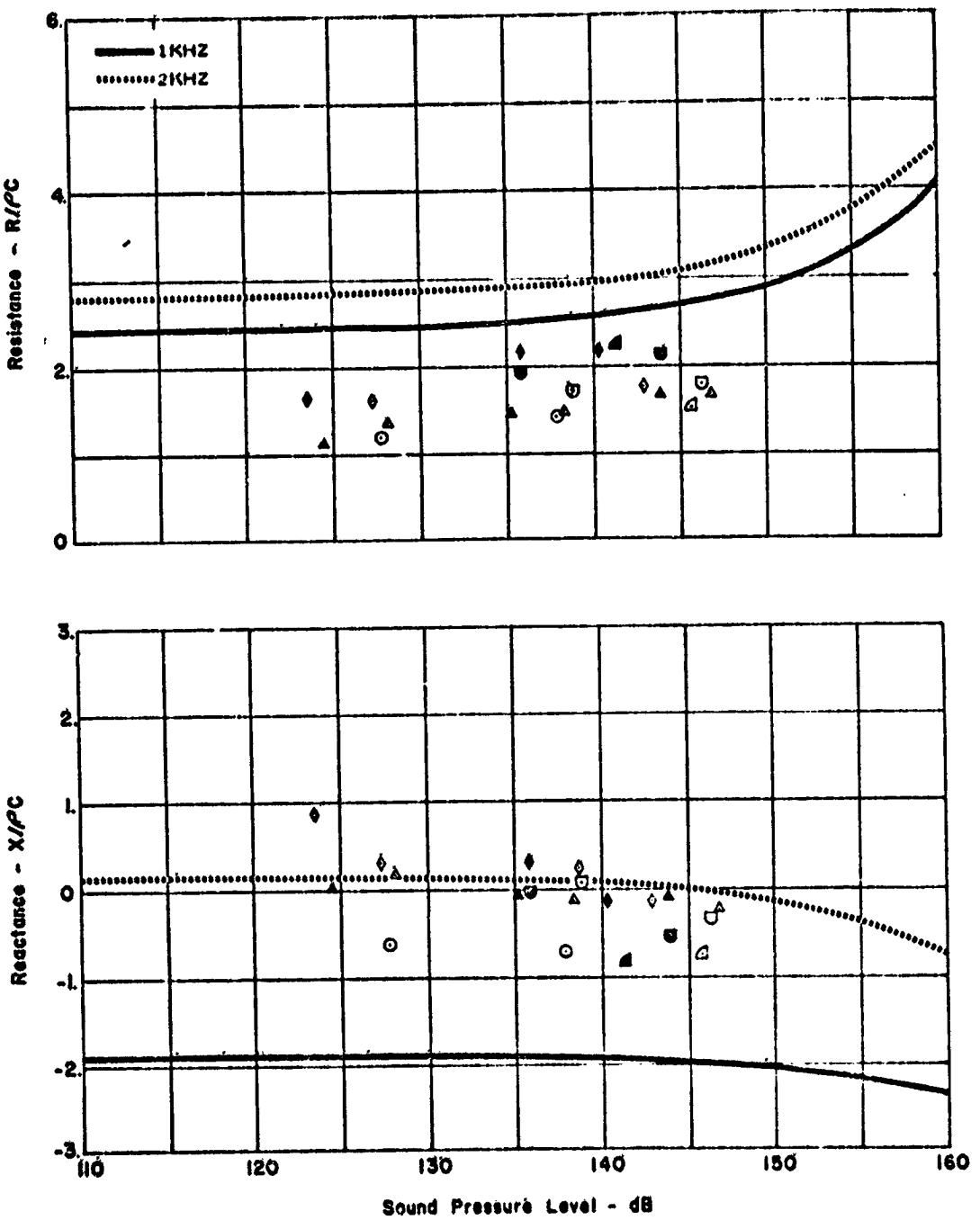

SAMPLE NO. 16, RESISTANCE AND REACTANCE DATA (0.5 MACH)
FIGURE 62

Sample No. 17
15 Pl/ Polyimide

Core Depth = 1.4 in.

Mach No. = 0.0

Frequency - Hz
- 800
- 1000
- 1350
- 1600
- 1850

Open Symbol 1st Half Wavelength
Solid Symbol 2nd Half Wavelength

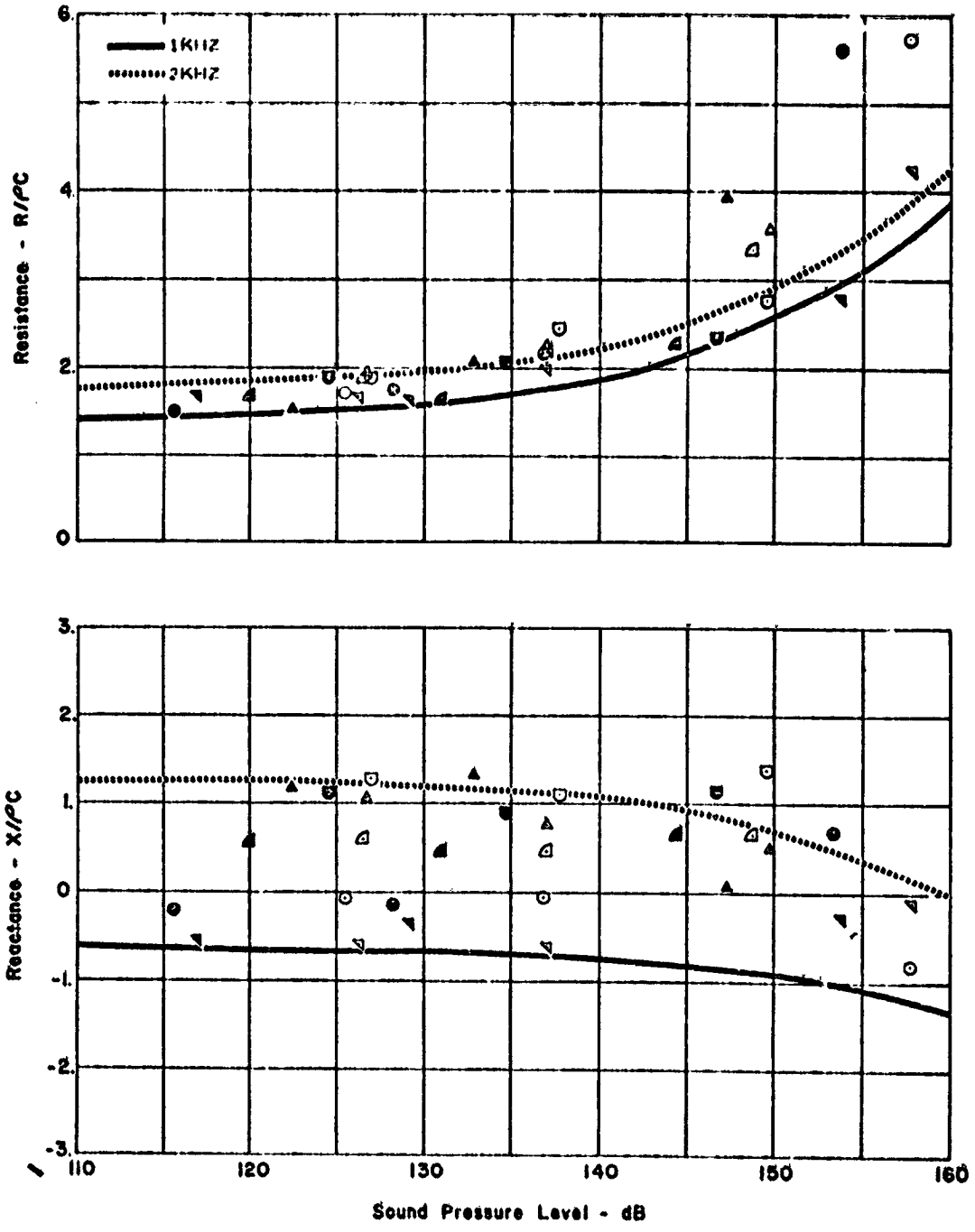

SAMPLE NO. 17, RESISTANCE AND REACTANCE DATA (0.0 MACH)
FIGURE 63

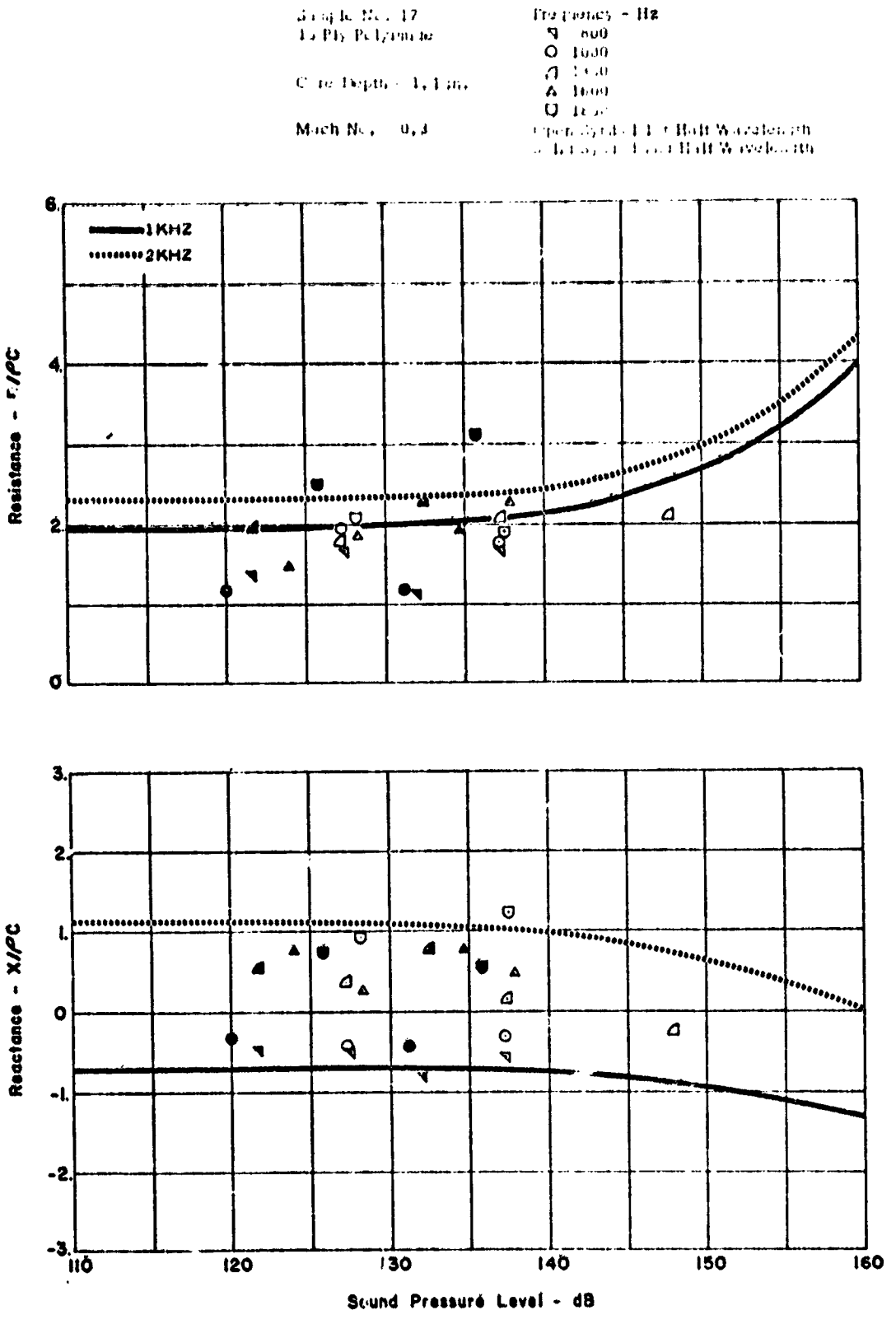

SAMPLE NO. 17, RESISTANCE AND REACTANCE DATA (0.3 MACH)
FIGURE 64

Sample No. 17
15 Ply Polyimide

Core Depth 1.4 in.

Mach No. = 0.5

Frequency - Hz
- 800
- 1000
- 1350
- 1600
- 1850

Open Symbol 1st Half Wavelength
Solid Symbol 2nd Half Wavelength

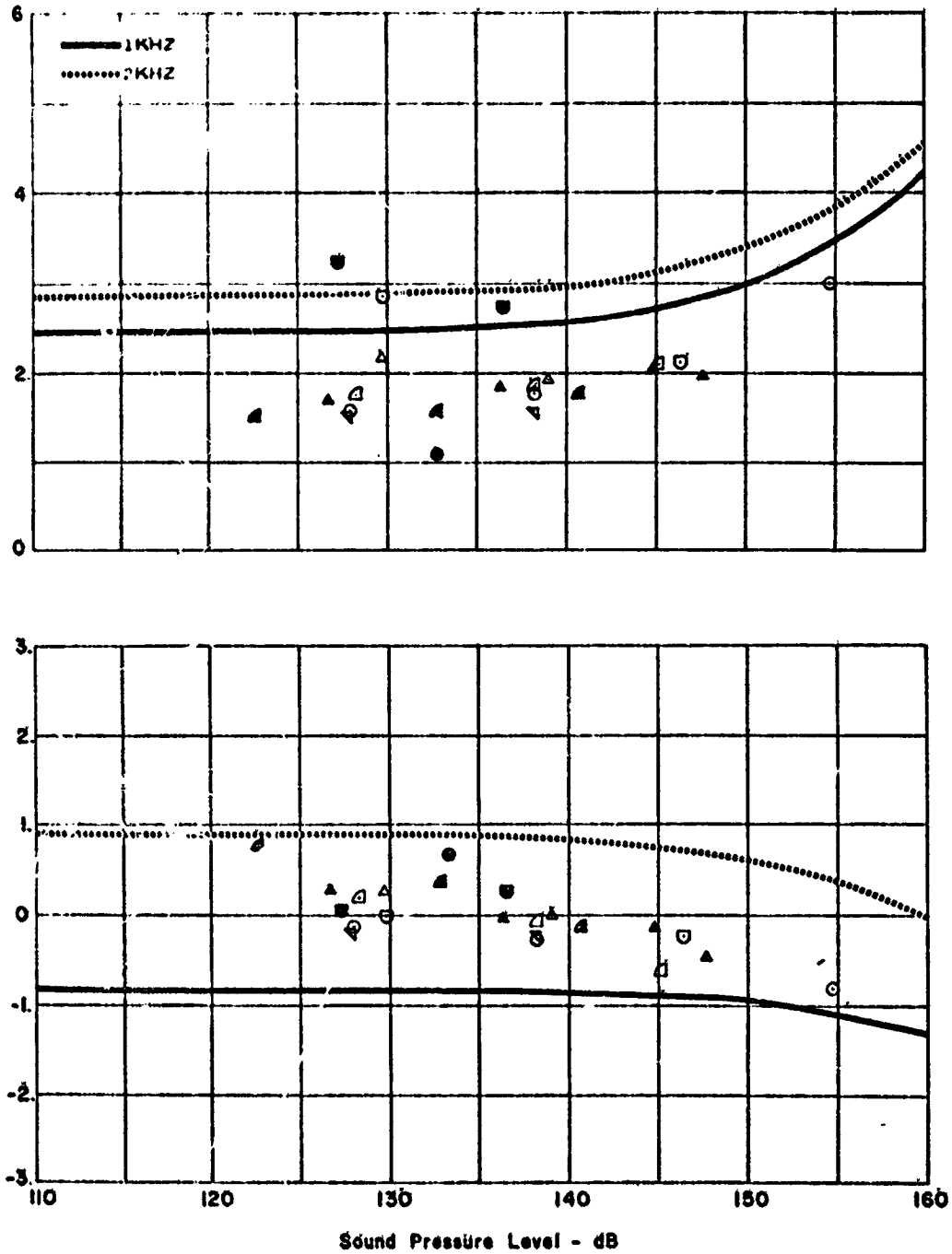

SAMPLE NO. 17, RESISTANCE AND REACTANCE DATA (0.5 MACH)
FIGURE 65